UNIVERSITY OF ALBERTA

A CIRCULAR INCLUSION WITH CIRCUMFERENTIALLY INHOMOGENEOUS IMPERFECT INTERFACE IN PLANE ELASTICITY

BY

LESZEK JOZEF SUDAK

A thesis submitted to the Faculty of Graduate Studies and Research in partial fulfillment of the requirements for the degree of Doctor of Philosophy

Department of Mechanical Engineering

Edmonton, Alberta

Fall 2000

National Library of Canada
Acquisitions and Bibliographic Services
395 Wellington Street
Ottawa ON K1A 0N4
Canada

Bibliothèque nationale du Canada
Acquisitions et services bibliographiques
395, rue Wellington
Ottawa ON K1A 0N4
Canada

Your file Votre référence

Our file Notre référence

The author has granted a non-exclusive licence allowing the National Library of Canada to reproduce, loan, distribute or sell copies of this thesis in microform, paper or electronic formats.

L'auteur a accordé une licence non exclusive permettant à la Bibliothèque nationale du Canada de reproduire, prêter, distribuer ou vendre des copies de cette thèse sous la forme de microfiche/film, de reproduction sur papier ou sur format électronique.

The author retains ownership of the copyright in this thesis. Neither the thesis nor substantial extracts from it may be printed or otherwise reproduced without the author's permission.

L'auteur conserve la propriété du droit d'auteur qui protège cette thèse. Ni la thèse ni des extraits substantiels de celle-ci ne doivent être imprimés ou autrement reproduits sans son autorisation.

0-612-59680-X

Canada

UNIVERSITY OF ALBERTA

LIBRARY RELEASE FORM

Name of Author:	**Leszek Jozef Sudak**
Title of Thesis:	**A Circular Inclusion with Circumferentially Inhomogeneous Imperfect Interface in Plane Elasticity**
Degree:	**Doctor of Philosophy**
Year this Degree Granted:	**2000**

Permission is hereby granted to the University of Alberta Library to reproduce single copies of this thesis and to lend or sell such copies for private, scholarly or scientific research purposes only.

The author reserves all other publication and other rights in association with the copyright in the thesis, and except as herein provided, neither the thesis nor any substantial portion thereof may be printed or otherwise reproduced in any material form whatever without the author's prior written consent.

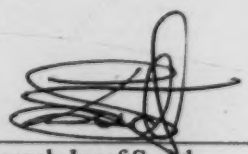

Leszek Jozef Sudak
9408 – 110 Avenue
Edmonton, Alberta
Canada, T5H – 1H1

Date: August 23, 2000

UNIVERSITY OF ALBERTA

FACULTY OF GRADUATE STUDIES AND RESEARCH

The undersigned certify that they have read, and recommend to the Faculty of Graduate Studies and Research for acceptance, a thesis entitled **A Circular Inclusion with Circumferentially Inhomogeneous Imperfect Interface in Plane Elasticity** submitted by Leszek Jozef Sudak in partial fulfillment of the requirements for the degree of Doctor of Philosophy.

Dr. Chongqing Ru, Supervisor

Dr. Peter Schiavone, Co-Supervisor

Dr. Andrew Mioduchowski, Co-Supervisor

Dr. Cornelius O. Horgan

Dr. Robert J. Tait

Dr. Abhijit Bhattacharyya

Dr. Zihui Xia

Date: June 19, 2000

ABSTRACT

Problems involving the mechanical behavior of composite materials, in particular, the effects of *imperfect bonding* at the fiber - matrix boundary, are receiving an increasing amount of attention in the literature. One of the most widely used mechanical models in describing an imperfect bonding condition is based on the premise that the tractions are continuous but displacements are discontinuous across the material interface. More specifically, jumps in the displacement components are assumed to be proportional, in terms of spring - factor type interface parameters, to their respective interface traction components (i.e. an *imperfect interface*).

The concept of imperfect interface has been developed mainly to account for various damages at the fiber - matrix interface, for example, imperfect adhesions, microcracks and voids. In particular, in many composite materials, the actual interface usually exhibits inhomogeneous imperfections. Despite this fact, little attention has been given to study this more general and physically more realistic scenario of inhomogeneous interface damage and imperfection.

The objective of this study is to develop a general method for the rigorous solution of a single isotropic circular inclusion embedded within an infinite homo-

geneous matrix in plane elasticity. The bonding at the inclusion - matrix interface is considered to be imperfect with the assumption that the interface imperfections are circumferentially inhomogeneous (i.e. the extent of damage at the fiber - matrix interface varies pointwise along the interface itself). In fact, for the first time, this dissertation systematically studies two physically significant types of inhomogeneous imperfect interfaces: that being the inhomogeneous spring - layer interface and the inhomogeneous non-slip interface.

Complex variable techniques are used to obtain exact closed - form solutions for the stress fields associated with the inhomogeneous imperfect interfaces. The results from these calculations are compared to the results when the imperfections are circumferentially homogeneous. These comparisons illustrate that replacing the inhomogeneous imperfect interface by its homogeneous counterpart will lead to significant errors in the stresses and even in the calculation of the average stresses induced within the inclusion. Hence, the inhomogeneity of interface damage and imperfection has an essential effect on the stress field and average stresses within the inclusion.

This dissertation is dedicated to the memory of my late father
Jozef Tadeusz Sudak

ACKNOWLEDGMENTS

I would like to extend my deepest gratitude and appreciation to Drs. Chong-qing Ru, Peter Schiavone and Andrew Mioduchowski for their invaluable guidance, support and unwavering confidence throughout my graduate years.

I am especially grateful to my mother Janina and my fiance Elisabeth for their patience, love and support throughout my studies.

I am also grateful to my brother Chris and his wife Kathleen for their everlasting encouragement and advice.

Finally, I owe a debt of gratitude to Dr. Jozef Szymanski for his support and encouragement.

Leszek Sudak

Edmonton, AB

June 2000

TABLE OF CONTENTS

Chapter 1 Introduction **1**

1.1 Background 1

1.1.1 Composite Materials 1

1.1.2 Interphase Layer 5

1.2 Interphase Models 8

1.2.1 Introduction 8

1.2.2 Interphase Layer Model 8

1.2.3 Imperfect Interface Model 13

1.2.3.1 Homogeneous Imperfect Bonding 15

1.2.3.2 Inhomogeneous Imperfect Bonding 16

1.3 Composite Mechanics 20

1.3.1 Introduction 20

1.3.2 Representative Volume Element 21

1.3.3 Determination of Effective Elastic Moduli 23

1.4 Application of Single Inclusion Problem 24

1.5 Overview of Current Study 26

Chapter 2 General Formulation and Subsidiary Results **35**

2.1 General Formulation 35

2.1.1 Preliminaries 35

2.1.2 Representation of Two Analytic Functions-$\Psi_M(z)$ and $\Psi_I(z)$ 38

2.1.3 Basic Boundary Value Problem 40

2.2 Subsidiary Results 43

Chapter 3 Circumferential Inhomogeneous Imperfect Spring - Layer Interface **47**

3.1 Introduction 47

3.2 Spring - Layer Interface 49

3.2.1 The Coupled Differential Equations for $\Phi_I(z)$ and $\Phi_M(z)$ 52

3.3 A Class of Inhomogeneous Spring - Layer Interface 59

3.4 Summary 63

Chapter 4 Examples of the Inhomogeneous Spring - Layer Interface **68**

4.1 Introduction 68

4.2 Inhomogeneous Spring - Layer Interface with Circumferential Number $s = 1$ 69

4.2.1 Average Stress 73

4.3 Inhomogeneous Spring - Layer Interface with Circumferential Number $s = 2$ 77

4.3.1 Average Stress 84

4.4 Summary 89

Chapter 5 Circumferentially Inhomogeneous Non - Slip Interface 98

5.1 Introduction 98

5.2 Inhomogeneous Non - Slipping Interface 99

5.2.1 The Differential Equation for $\Phi_I(z)$ 107

5.3 A Class of Inhomogeneous Non - Slip Interface 114

5.3.1 Case I $\beta < 1$ 117

5.3.2 Case II $\beta > 1$ 118

5.3.3 Case III $\beta = 1$ 119

5.4 Summary 121

Chapter 6 Examples of the Inhomogeneous Non - Slipping Interface 124

6.1 Introduction 124

6.2 Inhomogeneous Non - Slipping Interface with Circumferential Number $s = 1$ 126

6.2.1 Average Stress 127

6.2.2 Interfacial Stress 132

6.3 Inhomogeneous Non - Slipping Interface with Circumferential Number $s = 2$ 139

6.3.1 Average Stress 142

6.4 Summary 146

Chapter 7 Verification of the Solution Procedure 159

7.1 Inhomogeneous Spring-Layer Interface 159

7.1.1 Interface with Circumferential Number $s = 1$ 159

7.1.2 Interface with Circumferential Number $s = 2$ 161

7.2 Inhomogeneous Non - Slipping Interface 163

7.2.1 Interface with Circumferential Number $s = 1$ 163

7.2.2 Interface with Circumferential Number $s = 2$ 165

7.3 Summary 167

Chapter 8 Conclusions and Recommendations for Future Work . 168

8.1 Conclusions 168

8.2 Future Work 175

References 178

Appendix A 190

Appendix B **194**
Appendix C **199**
Appendix D **204**
Appendix E **208**

LIST OF FIGURES

Figure 1-1 *Three Types of Composite Materials* 32

Figure 1-2 *Various Orientations of Fiber Reinforced Composites* 32

Figure 1-3 *Several Weave Patterns for Fibers* 33

Figure 1-4 *Schematic Representation of Fiber Reinforced Laminate Composite* 33

Figure 1-5 *Electron Micrograph of Interphase Region* 34

Figure 1-6 *Schematic Representation of Interphase Region* 34

Figure 2-1 *A Homogeneous Circular Inclusion with Circumferentially Inhomogeneous Imperfect Interface Embedded in an Infinite Elastic Matrix in Plane Elasticity* 46

Figure 3-1 *Schematic Representation of Inhomogeneous Spring - Layer Interface before and after Deformation* 65

Figure 3-2 *Schematic Representation of the Inhomogeneous Spring - Layer Interface* 66

Figure 3-3 *Continuity of* $\Phi_I(z)$ *across Branch Cut:* $\Phi_I(z^+) = \Phi_I(z^-)$ ... 67

Figure 4-1 *Schematic Representation of the Inhomogeneous Spring - Layer Interface have Circumferential Number* $s = 1$ 91

Figure 4-2 *The Effect of the Circumferential Inhomogeneity on the Average Mean Stress inside the Circular Inclusion having Circumferential Number* $s = 1$ 92

Figure 4-3 *The Effect of the Circumferential Inhomogeneity on the Average Deviatoric and Shear Stresses inside the Circular Inclusion having Circumferential Number s = 1* 93

Figure 4-4 *Schematic Representation of the Inhomogeneous Spring - Layer Interface having Circumferential Number s = 2* 94

Figure 4-5 *The Effect of the Circumferential Inhomogeneity on the Average Mean Stress inside the Circular Inclusion having Circumferential Number s = 2 and Loading in x-direction* 95

Figure 4-6 *The Effect of the Circumferential Inhomogeneity on the Average Deviatoric and Shear Stresses inside the Circular Inclusion having Circumferential Number s = 2 and Loading in x-direction* 96

Figure 4-7 *The Effect of the Circumferential Inhomogeneity on the Average Mean Stress inside the Circular Inclusion having Circumferential Number s = 2 and Equal Biaxial Loading* 97

Figure 5-1 *A Homogeneous Circular Inclusion with Circumferentially Inhomogeneous Non - Slip Interface* 122

Figure 5-2 *Schematic Representation of the Inhomogeneous Non - Slipping Interface* 123

Figure 6-1 *Schematic Representation of the Inhomogeneous Non - Slipping Interface having Circumferential Number s = 1* 147

Figure 6-2 *The Effect of the Circumferential Inhomogeneity on the Average Mean Stress inside a Circular Inclusion having Circumferential Number s = 1 and Loading in y-direction* 148

Figure 6-3 *The Effect of the Circumferential Inhomogeneity on the Average Mean Stress inside the Circular Inclusion having Circumferential Number $s = 1$ and Loading in x-direction* ... 149

Figure 6-4 *Non-Uniformity of the Interfacial Stress for various positive Interface Imperfections as a function of Position and Loading in the y-direction* ... 150

Figure 6-5 *Non-Uniformity of the Interfacial Stress for various negative Interface Imperfections as a function of Position and Loading in the y-direction* ... 151

Figure 6-6 *Non-Uniformity of the Interfacial Shear Stress for a particular positive Interface Imperfection as a function of Position and Loading Configuration* ... 152

Figure 6-7 *Non-Uniformity of the Interfacial Shear Stress for a particular negative Interface Imperfection as a function of Position and Loading Configuration* ... 153

Figure 6-8 *The Effect of the Interface Parameter on the Interfacial Shear Stress corresponding to the Maximum Position and Loading in y-direction* ... 154

Figure 6-9 *Schematic Representation of the Inhomogeneous Non - Slipping Interface having Circumferential Number $s = 2$* ... 155

Figure 6-10 *The Effect of the Circumferential Inhomogeneity on the Average Mean Stress inside the Circular Inclusion having Circumferential Number $s = 2$ and Loading in x-direction* ... 156

Figure 6-11 *The Effect of the Circumferential Inhomogeneity on the Average Deviatoric and Shear Stresses inside the Circular Inclusion having Circumferential Number $s = 2$ and Loading in x-direction* 157

Figure 6-12 *The Effect of the Circumferential Inhomogeneity on the Average Deviatoric and Shear Stresses inside a Circular Inclusion for having Circumferential Number $s = 2$ and Equal-Opposite Biaxial Load* 158

CHAPTER 1

Introduction

1.1. BACKGROUND

1.1.1. Composite Materials

The majority of our modern technologies require materials with unusual combinations of properties that cannot be met by conventional metals, ceramics and polymeric materials. This is especially true for materials that are needed for aerospace, underwater, oil and gas production and transportation applications. For instance, aerospace engineers are increasingly searching for structural materials that have low densities, are strong, stiff and impact resistant. However, this is a rather formidable combination of characteristics, since strong materials are relatively dense and by increasing the strength or stiffness generally reduces impact strength. Consequently, material property combinations and ranges have been and are being extended by the development of composite materials.

Composite materials are generally multiphase materials consisting of two or more distinct constituents which are combined to obtain specific properties or performance characteristics. By combining material types, advantageous properties

from each constituent phase can be exploited to create new properties unique to the composite form. Binary (two phase) composite forms are the most common, and typically consist of a dispersed (reinforcement) phase embedded in a continuous (matrix) phase (Figure 1-1(a),(b)). The reinforcement phase should be a material that is strong, stiff and lightweight. Commonly available reinforcement types include continuous and discontinuous short fibers (e.g. glass, kevlar, boron, ceramic), and particles (e.g. Al_2O_3, ThO_2, SiC). Compared with the dispersed phase, the matrix phase must be tough and ductile. Its purpose is to support and allow load to be transmitted to the dispersed phase (only a small proportion of the applied load is sustained by the matrix). It prevents the propagation of brittle cracks from fiber to fiber which could result in catastrophic failure; in other words, the matrix phase serves as a barrier to crack propagation [1]. In addition, the matrix material should also be strong so that it contributes to the overall strength of the composite. Common matrix materials include thermosetting (e.g. epoxies) and thermoplastic (e.g. nylons) polymers, metals (e.g. aluminum, magnesium, copper) and ceramics (e.g. silicon). Hence, the use of a particular binary composite depends on the intended application and the long - term economic savings.

The classification of binary composites, based on the shapes of the materials, is shown in Figure 1-1. The three main divisions are particle reinforced, fiber rein-

forced and laminar composites. Particulate composites are composites where the reinforcement phase is in the form of particles that are embedded in a continuous matrix phase. These composites are generally subdivided into two classes, these being: large - particle composites and dispersed - strengthened composites. The large particle composite, as the name suggests, contain large amounts of coarse particles (e.g. spherical particles) which are harder and stiffer than the matrix. These reinforcing particles tend to restrain deformation of the matrix in the vicinity of each particle. In essence, the matrix transfers some of the applied load to the particles, which bear a fraction of the load. These composites are manufactured to produce specific combinations of properties rather than to improve strength. In order to improve the mechanical behavior or strength of these large - particle composites requires some kind of reinforcement action, such as imposing residual compressive stresses using prestressing or posttensioning techniques.

In the case of dispersion - strengthened composites, the particles are extremely small and the matrix bears the major portion of the applied load. The small particles serve to impede the motion of dislocations in the matrix causing a reduction in plastic deformation thereby increasing the strength of the material. For further details and examples regarding particulate composites see [2].

Fiber reinforced composites, which are two-dimensional analogues of particulate composites (i.e. the particles are aligned as cylinders where each cross section of the cylinder has the same plane geometry), are probably the most predominant composite material in use today. Applications are found in many areas including transportation, aerospace, petrochemical and infrastructure. The fiber reinforced composites improve strength, fatigue, resistance and stiffness by incorporating strong, stiff, brittle fibers into a softer more ductile matrix. The reinforcing materials are also arranged in a variety of orientations from unidirectional arrangements to fibers woven into fabrics (see Figure 1-2 and Figure 1-3). When the fiber is bound together by the matrix material in a parallel orientation, very high stiffness and strength can be achieved in the fiber direction. On the other hand, stiffness and strength transverse to the fiber direction are of matrix order, and thus much lower. These generally low values of stiffness and strength provide the motivation for laminate composites.

Laminate composites consist of thin, planar, unidirectional layers called lamina that have a preferred high - strength direction. The geometry of laminates is defined by the fiber angle orientation of each layer with respect to some loading reference frame. The lamina are stacked and subsequently cemented together such that the orientation of the high strength reinforcing direction varies with

each successive layer (Figure 1.4). Details in design, construction and application of laminate composites can be reviewed in [2] and [3].

The performance of composite materials depends not only on the properties of the constituent phases, their relative amounts and the geometry of the dispersed phase but also on the quality of bonding that exists between the constituent phases. For example, the presence of structural defects such as voids, impurities, imperfect adhesions and microcracks along the fiber/matrix boundary will compromise the effectiveness of load transfer between the matrix and the fiber. Thus, the behavior of composite materials is greatly influenced by the interphase layer existing between matrix and fiber (inclusion).

1.1.2. Interphase Layer

As described in the previous section, the representation of composite materials considers the existence of two phases, namely fiber (inclusion) and matrix. However, in reality, an additional phase exists between the fiber and matrix. This phase, commonly known as the *interphase*, is the juncture that results when the matrix bonds with the fiber surface. Figure 1-5 shows a transmission electron micrograph of an interphase layer [4]. It is evident from this figure that the interphase region is a very complex and non-uniform region consisting of several "interlayers". These

interlayers are illustrated in the schematic diagram (Figure 1-6) and discussed in detail in [5] or [6]. It is within these layers that damage development in the form of interfacial cracking and fiber/matrix debonding can occur. In fact, composite failure is often initiated within the interphase layer [7].

The interphase layer may be the by-product of chemical reactions that occurred between the constituent phases during the fabrication process, or, alternatively, a thin layer, such as functionally graded materials (see [8]), may be introduced in the design stage to improve the performance of the composite material by removing unfavorable residual and thermal stresses along the fiber/matrix boundary, improving the bonding strength or isolating the fiber from severe service or environmental conditions. It should also be noted that the interphase layer may exhibit viscoelastic behavior. Such an interphase would provide relaxation and damping characteristics to an otherwise brittle elastic composite (see [9], [10] for details). In all cases, the *interphase layer* can be defined as a non-uniform, anisotropic region of finite thickness that is either formed as a result of the bonding between the fiber and the matrix, or it may be viewed as a chemical reaction zone, a diffusion zone, a nucleation zone or any combination of the above; it has significantly distinct chemical and mechanical composition as compared to the bulk fiber or matrix [11]. Hence, the properties of the interphase region depend directly on the chemical

and mechanical nature of the bonding process between the matrix and the fiber materials. As a result, the physical characteristics (e.g. Young's Modulus) of the interphase layer are distinct from either the fiber or the matrix. For example, in [12], Metcalfe points out that the interaction compound in boron-titanium composites will posses an elastic modulus different from that of the fiber and matrix. Also, recent experimental investigations on fiber/polymer matrix composites have shown that the interphase region has different mechanical properties than fiber or matrix (see [13] for details). Consequently, the interphase layer has to be characterized in a manner similar to the characterization of the fiber and matrix if it is to be incorporated into any micromechanical analysis. This is essential in accurately predicting the physical and mechanical behavior of composite materials. Note that the characterization of the interphase has to occur at several different levels (i.e. mechanical, chemical and microstructural) for one to fully understand the nature of the bond along the fiber/matrix boundary, but because of the complexity of the interphase layer a thorough thermomechanical characterization of the interphase layer is currently not possible (see [11] for details). However, various approximate (simplifying) models have been proposed to study the physical properties of the interphase layer.

1.2. INTERPHASE MODELS

1.2.1. Introduction

Recognizing the existence of an interphase layer implies that the composite must be regarded, at the least, as a three - phase assemblage. Such a consideration requires the complete knowledge of the physical properties of the interphase, information which is extremely difficult if not impossible to obtain because of the diminutive nature of the interphase (on the order of micrometers), the necessity of making in-situ measurements and the spatial variation of the properties. To overcome this deficiency, approximate models have been developed in an attempt to predict the physical properties of the interphase layer. These interphase models can be broadly classified as an *interphase layer* model and an *imperfect interface* model.

1.2.2. Interphase Layer Model

The interphase layer model (3 - phase model) considers an interphase layer between fiber and matrix having specified thickness and thermoelastic properties (see [7], [14] - [39] among others for details). These interphase layer models can be divided into two classes: the homogeneous (uniform) interphase layer model and the inhomogeneous (non-uniform) interphase layer model.

In [14], Narin considered a 3 - phase model where the interphase properties were assumed to be uniform and identical to that of the matrix material except for the coefficient of thermal expansion which was treated as a variable. Its effect on the stress field was studied using an elasticity based solution method. It was found that increasing the coefficient of thermal expansion of the interphase layer caused a decrease in the residual thermal stresses in the matrix, but at the same time increased the residual stresses in the interphase.

In [16], Vedula et al. used an elasticity solution method based on a 3-phase model to predict the residual thermal stresses in a composite. In their analysis, the Young's modulus of the interphase was treated as a variable (over a range of values above and below the value of the fiber modulus) and the coefficient of thermal expansion and Poisson's ratio were identical to the matrix. It was found that a flexible, soft interphase layer reduced the residual stresses in the matrix.

In [17], [18] and [25], Tandon and Pagano employed an elasticity formulation based on a 3 - phase model. The Young's modulus, coefficient of thermal expansion and the thickness of the interphase layer were treated as variables. Based on their parametric study, they concluded that a judicious choice of interphase thickness and interphase properties can be used to control the constituent stress components.

In [34], Ru neglected the elastic mismatch between the matrix and the interphase (i.e. the elastic constants of the matrix and the interphase are identical) and considered only thermal mismatch induced stresses. Thermal mismatch induced stresses are identified as a major cause of failure in a wide variety of materials and devices, ranging from metal - ceramic composites to passivated interconnect lines in integrated circuits. Using complex variable analysis, Ru derived simple formulas to evaluate the effects of the interphase layers on the thermal stresses within an elliptic inclusion. It is found that the effect of the interphase on the thermal stresses within the inclusion increases with the thickness of the interphase layer. Furthermore, it was found that to reduce the thermal stresses within the inclusion, the optimum thermal expansion coefficient of the interphase is not necessarily between those of inclusion and the matrix. However, if the design objective is to reduce the thermal stresses within the inclusion and the interphase layer, the optimum thermal expansion coefficient of the interphase layer should have a value between that of the fiber and matrix.

In all of these reviews, the thermomechanical properties and/or thickness remain constant throughout the interphase. However, it has been shown that diffusion of material between matrix and fiber may create an elastic moduli profile that smoothly varies from fiber to matrix [29]. Consequently, the interphase ex-

hibits spatially non - uniform properties (i.e. the interphase properties vary from point to point along the thickness of the interphase). For example, in [15], Theocaris developed a hypothetical interphase model for unidirectional glass - reinforced epoxies based on a hypothesis (theory of adhesion) of the mechanism of bonding at the fiber/matrix boundary and calorimetric measurements. In his analysis, the Young's modulus of the interphase varied continuously (non-linear radial variation) between that of the fiber and that of the matrix.

In [21], Sottos et al. assumed that the elastic modulus and thermal expansion coefficient of the interphase varied linearly with the radial distance from the fiber boundary. They used their linear model in a numerical scheme (boundary fitted coordinates technique) to study the effects of the interphase layer on the residual thermal stresses. They concluded, based on parametric studies, that the interphase can be tailored in such a way so as to reduce the local residual stresses.

In [7], Jayaraman and Reifsnider considered several radial variations in the Young's modulus of the interphase, such as power, reciprocal and cubic. They demonstrated how the interphase thickness, fiber volume fraction and functional form of the interphase Young's modulus variation affects the local thermal stress state.

In [31], Jasiuk and Kouider model the inhomogeneity in the elastic constants (i.e. Young's Modulus, Poisson's ratio) of the interphase zone by allowing the elastic properties to change with radial distance from the fiber boundary. They considered two types of variation: a power variation and a linear variation. They concluded that the variation of the elastic constants within the interphase layer has an effect on the elastic properties of the composites. In other words, interphase imperfections influence the overall behavior of the composite material. Furthermore, they report that a homogeneous interphase model may overestimate the overall elastic properties of composites with inhomogeneous interphases.

In the majority of the aforementioned works, the following simplifying assumptions were made:

- the interphase is assumed to be isotropic, linear elastic and perfectly bonded to the fiber and the matrix,
- the perfect bonding requirement implies continuity of tractions and displacements at the fiber - interphase and interphase - matrix boundaries,
- the physical properties are either spatially non - uniform functions of the radius (non - uniform interphase model) or are spatially uniform (uniform model), and

- the degree of damage in the interphase can be simulated by adjusting the elastic properties and thickness of the interphase region.

The main disadvantage of the 3 - phase model is that at least three parameters are required in the analysis, namely the thickness and two elastic parameters (isotropic case) corresponding to the interphase layer. This in turn, makes the analysis of composite materials more complex. To overcome these analytical complications the imperfect interface model was developed.

1.2.3. Imperfect Interface Model

The imperfect interface model assumes a very thin interfacial zone of vanishing thickness existing between fiber and matrix. In other words, when the interphase becomes vanishingly thin it becomes an *interface*. This *interface* is defined as a two-dimensional boundary (a curved plane) separating distinct phases. Thus, it can be assumed that the interface forms a transition zone from matrix material to fiber material through a distribution of discrete contacts. These contacts can transfer load directly, but they offer resistance to local shear and extension (see [40]). In addition, the imperfect bonding model relaxes the classical condition of perfect bonding.

Perfect bonding is a demanding requirement, since it is the desire to weld together materials which by their nature may not be directly welded, for example, certain brittle matrix composites may posses the feature of imperfect adhesion between constituent phases, such as the interface between fiber/interphase and interphase/ matrix. Consequently, the existence of a perfect bond is a convenient idealization of a very complex behavior (see [41] for details). The ability of load transfer between fiber and matrix depends on, and is controlled by, the degree of contact at the interface; thus, a decrease in load transfer, as a result of interfacial damage, gives rise to the concept of *imperfect bonding*. It should be noted that several attempts appear in the literature which incorporate the effect of imperfect bonding in the context of using an interphase layer model (see [42 - 44] for details).

The fundamental premise for the imperfect bonding model lies in the fact that the interphase, in general, is found to be softer/weaker (i.e. compliant, flexible) than both fiber and matrix [45]. In such a representation, the effect of imperfect bonding along the interface is modelled by a continuity of tractions but the displacements are discontinuous. In this context, one of the more useful assumptions is that the normal and tangential displacement jumps are proportional, in terms of spring-factor type interface parameters, to their respective traction components. This type of condition corresponds to modeling the imperfectly bonded interphase

layer by a linear spring - layer of vanishing thickness (i.e. an *imperfect interface*) (see, for example, [46] - [71] among others). Note that these spring-factor type interface parameters characterize the properties of the interphase as well as the fiber/matrix bonding (i.e. spring-factor type interface parameters characterize the strength and the stiffness of the interphase layer). Hence, these parameters can be assumed to be spatially uniform (homogeneous) or spatially non - uniform (inhomogeneous) along the entire length of the fiber/matrix interface.

1.2.3.1. Homogeneous Imperfect Bonding

The concept of a homogeneous imperfect interface implies that the spring - factor interface parameters characterizing the displacement jumps are assumed to be constant. In [52], Hashin used the homogeneous imperfect bonding model to examine the stress fields inside a spherical inclusion. In contrast to the uniform interior stress field associated with a perfectly bonded interface (see, for example, [72] - [77] for details), he found that the stress fields inside the inclusion were no longer uniform. The analogous problem in plane elasticity has been examined in [63] and [68] with similar conclusions.

In [40], [51] and [53], Achenbach and Zhu carried out numerical analyses on a rectangular - array fiber reinforced composite subjected to transverse loading. In addition, they assumed that the spring - factor type interface parameters are

equal. They concluded that the variation of the interfacial stiffness parameters has a pronounced change on the stress fields in the fiber, matrix and interphase, respectively.

In [69], Shen used numerical analyses, based on the homogeneous imperfect interface model, to examine the stress fields associated with an elliptic inclusion in anti-plane and plane elasticity, respectively. In both cases, he showed that the interfacial stresses are non-monotonic functions of the interface parameter. In other words, he is able to identify specific values of the interface parameter which correspond to maximum peak stresses along the material interface.

Unfortunately, the homogeneous imperfect bonding condition implies that the interface imperfections are uniform along the entire material interface, this effectively ignores the more general and physically more realistic scenario of inhomogeneous interface damage in which the extent of bonding at the inclusion-matrix interface varies along the interface itself (i.e. the spring-factor type interface parameters vary pointwise with position along the material interface).

1.2.3.2 Inhomogeneous Imperfect Bonding

Interface imperfections in a composite material are almost always inhomogeneous along the entire length of the material interface. One physical justification comes from the fact that the actual interface usually exhibits behavior that repre-

sents partial debonding, partial sliding and/or partial cracking. In other words, there may exist a region along the interface where failure has taken place and the rest of the interface still remains intact (see [28] and [78] for details). Consequently, interest in these kinds of problems are motivated mainly by a desire to study the physical significance of inhomogeneous interface damage and its subsequent effect on the effective properties of the composite material. Clearly, this raises a challenging topic in the area of elasticity and composite mechanics, however, as of yet, little attention has been given to this area.

In [79], Ru and Schiavone incorporated inhomogeneous interface damage into the model of a circular inclusion subjected to anti-plane shear deformations. Their results show that circumferentially inhomogeneous imperfections in the interface have a significant effect not only on the stress field but also on the average stress induced within the circular inclusion.

In [80], Ru considered a circular inclusion with circumferentially inhomogeneous sliding interface in plane elasticity. In that paper, Ru found that this interface description had virtually no effect on the average stresses induced within the circular inclusion. This result suggests that a homogeneous interface may be used to estimate the average stresses within the inclusion with negligible error. However, it must be noted that more general cases, with respect to circumferential inhomo-

geneous imperfect interfaces in plane elastostatics, have yet to be investigated.

The main drawback of the imperfect bonding model is that the normal displacement continuity condition cannot be negative. In other words, although a positive jump in normal displacement denotes a normal separation between the fiber phase and the matrix phase, a negative jump in the normal displacement corresponds to the interpenetration of the matrix phase into the fiber phase (i.e. material overlapping across the interface) - a physical impossibility. To circumvent this problem one approach would be to require perfect bonding in the area where the normal traction is compressive and consider imperfect bonding in the area where the normal traction is tensile. However, such a condition is cumbersome and technically complicated because in this situation one must identify the contact zone where material overlapping is occurring. Consequently, this approach would transmit into a nonlinear problem. A simpler approach would be to assume some initial thickness of the interphase layer where the normal displacement jumps are defined by the normal deformations of the interphase layer. Then by adjusting the thickness of the compliant interphase layer, for example, moving the interphase - matrix interface inwards by a distance smaller than the initial thickness of the interphase, a small negative normal displacement becomes admissable (see [40] and [52]).

The advantages of using the imperfect interface model over the 3-phase description are:

- the number of unknown parameters are reduced to two (i.e. the thickness, and the elastic constants are combined into two positive spring constants which can be homogeneous or inhomogeneous),
- can simulate intermediate states of bonding (i.e. from perfect bonding to complete debonding),
- the model can be utilized when an interphase cannot be identified or defined, and
- it is more mathematically tractable.

Hence, the imperfect bonding model allows a 3 - phase composite (fiber - interphase - matrix) to be modeled as a two - phase (fiber - interface - matrix) material. Therefore, in this dissertation, the imperfect bonding model is adopted and a systematic analysis of two physically significant inhomogeneous imperfect interfaces will be analyzed, these being: the inhomogeneous imperfect spring - layer interface and the inhomogeneous non-slip imperfect interface, respectively (see [81] - [84]).

1.3. Composite Mechanics

1.3.1. Introduction

Micromechanical analysis of composite materials originates with some of the most renowned names in science. Maxwell in 1873 and Lord Rayleigh in 1892 computed the effective conductivity of composites consisting of a matrix and certain distributions of spherical particles. Albert Einstein, in 1906, computed the effective viscosity of a fluid containing a small amount of spherical particles [9]. Although these works were motivated purely for scientific purposes, it set the stage for the technological advancement of composite materials and mechanics.

Over the last several decades, substantial progress has been made in the micromechanics of composite materials. Typically, the objective of such analysis is to estimate the effective (macroscopic) properties of the composite material given the geometry, bonding characteristics, distribution and properties of the individual phases. To date, numerous micromechanical approaches have been developed, these include: the simple Reuss and Voigt hypotheses, the self-consistent schemes and their generalizations, differential schemes, the Mori-Tanaka method, the Eshelby Equivalent Inclusion method, concentric cylinder models, bounding techniques and approximate or numerical analysis of periodic arrays of inclusions

or fibers in the surrounding matrix phase (see, for example, [9], [85] - [90] for details). The central assumption in the application of the various aforementioned techniques is the existence of a *representative volume element.*

1.3.2. Representative Volume Element

The representative volume element (RVE) is a sample of the composite material that is structurally the same as the whole composite with average properties indistinguishable from those of the statistically homogeneous composite. In other words, the statistical moments, such as average and variance, are the same when taken over any RVE within the composite body (i.e. body averages and representative volume element averages are the same implying statistical homogeneity). Furthermore, the RVE must contain a large number of material phases that are large compared to the scales of microstructure and small compared to the entire body. This implies the RVE is large compared to the typical phase region dimensions (e.g. fiber diameter and spacing) and small compared to the dimensions of the composite body; consequently, it must contain a large number of fibers (inclusions). Therefore, the RVE, as defined, would retain and represent the effective properties of the composite material (in the average sense) and these effective properties would be insensitive to boundary conditions (stress and strain fields)

provided these values are macroscopically homogeneous. On the other hand, in applications with inhomogeneous macroscopic boundary conditions, the prediction of the effective properties of the composite requires a decoupling of the local and global analyses. Such decoupling is based on the assumption that in determining the stress at a given particle, the motion outside an arbitrary neighborhood of that particle can be neglected (i.e. Principle of Local Action). This decoupling limits the range of the classical homogenization technique to composites with small inclusion dimensions (i.e. microstructure). In contrast, composites with relatively large microstructure, the classical homogenization treatment breaks down because of the potentially large gradients in the local field quantities relative to the microstructure of the composite (see [91] for details).

Assuming that the fibers within the RVE are sufficiently spaced apart then all interactions among neighboring inclusions within the RVE can be ignored. Then, based on the known micromechanical theories (e.g. Mori - Tanaka method, Self Consistent method etc.), in any RVE the local field quantities that occur in a neighborhood of inclusions must occur with the same frequency as in the vicinity of a single inclusion. Thus, the RVE of the composite material can be treated as only a single inclusion embedded within some matrix medium. Consequently, the single inclusion model, in conjunction with the known micromechanical models, is a

much simpler model to implement than other available multi - inclusion composite models. Hence, the single inclusion problem becomes of fundamental importance in the mechanics of composite materials.

1.3.3. Determination of Effective Elastic Moduli

The determination of the effective (global) properties of the composite material requires the knowledge of the stress or strain concentration tensors. However, the evaluation of these tensors, via one of the aforementioned micromechanical models, requires the evaluation of the average stress or strain within the single inclusion phase. Consequently, the calculation of the average stress or strain inside the inclusion is of basic importance to composite mechanics (see, for example, [59] among others). In other words, the evaluation of the effective properties of the composite, according to the known micromechanical models, is based on solutions of the single inclusion problem; for example, the basic assumption of the Self Consistent method is that, the average stress or strain in the inclusion phase equals the stress or strain in a single inclusion. This single inclusion is subsequently embedded into an effective medium having an unknown effective moduli tensor C^*. Therefore, in order to have a knowledge of the effective properties of the composite material, the effective moduli tensor C^* needs to be evaluated. In cases where we

have multiphase composite media, such as functionally graded and multilayered interphases, the average stress or strain within the inclusion phase is still of fundamental importance. The only difference lies in a slight modification with respect to the geometry of the embedding configuration in the unknown effective medium (see [92 - 94] for details).

1.4. Application of Single Inclusion Problem

As described in the previous section, the single inclusion problem is of fundamental importance in the prediction of the effective properties of composite materials. There are, however, several other applicable areas for this type of problem. Here we discuss problems associated with prosthetic stability in human bone. This is because the implant - bone interface contributes to a major source of problems, such as implant loosening (see [95 - 96]).

The fixation of an implant to host bone relies primarily upon mechanical interlocking. To achieve this result, some implants are manufactured with a porous coating or with a surface roughened by beads forming cavities. When the implant is inserted and tightly fitted against host bone, the rough interdigitated surface existing between the implant and bone gives rise to an interfacial shear strength that prohibits any relative shear slip, while at the same time, the strong host bone is

allowed to penetrate and interlock with the porous coating (cavities) thereby stabilizing the implant (see [97 - 99] for details). However, the extent of bone ingrowth along the implant - bone interface is not uniform (i.e. bone density is inhomogeneous). One reason for this nonuniformity of bone ingrowth is bone resorption (i.e. bone atrophy). It is generally assumed that this resorptive phenomena is a result of 'stress shielding' (see, for example, [100 - 101] for details). In this process, the implant 'shields' the host bone from loading because it shares the load which is normally taken by the bone itself. As a result, the bone stresses are reduced leading to a reduction in cortical bone density or thickness which ultimately leads to implant loosening (failure). The degree of stress shielding around an implant is affected, first of all, by the bonding conditions at the implant/bone interface and secondly by the implant stiffness (i.e. stem thickness and elastic modulus) [102]. In addition, the formation of soft, fibrous (scar) tissue around the implant-bone interface can be related to that of a debonded interface condition (i.e. there exists gaps between normal bone and implant) (see [95], [98]for details).

Stress shielding is not the only point of concern. High interfacial stress peaks, provoked by high shear stresses, have been shown to appear around interface edges whereas the remainder of the interface may remain unloaded (see, for example [102], [103] and [104]). These stress concentrations are likely another cause of implant

loosening and pain. The stress concentrations indicate that the load transfer is concentrated at the edges and thus poorly distributed [104]. Thus, achieving uniform interfacial stresses by controlling where load transfer is concentrated is essential in maintaining a stable implant.

Designing an implant that minimizes stress shielding while at the same time achieving a more uniform interfacial stress is of great practical interest. However, this leads to potential conflicts because the stiffer the stem, the more load transfer is concentrated distally and the more bone is stress shielded [104]. Clearly, this poses a genuine design conflict. Therefore, the ability to design a stable implant requires a knowledge of the effects of inhomogeneous bone ingrowth patterns on the stress fields existing around human prosthetics. Having an understanding of the behavior of these stress field patterns will lead to a better implant design with the hopes of minimizing the often painful result of implant failure.

1.5. Overview of Current Study

Composite materials are clearly the most predominant material in use today, ranging from aerospace applications to petrochemical, biomechanical and infrastructure use. In the manufacture or fabrication of these composite materials a damage layer containing imperfect adhesions, microcracks and voids inevitably is formed. This

zone of imperfection or interphase layer affects the ability of load transfer between fiber and matrix phases. Consequently, the incorporation of an interphase layer into any micromechanical analysis is critical in describing the physical and mechanical behavior of the composite materials.

The purpose of the current study is to employ the single inclusion model to problems associated with composite mechanics and biomechanics, respectively. From a practical point of view, composite materials with circular cross-sections and for that matter circular holes 'reamed out' in human bone are the most convenient to design and fabricate. This is just one justification for the study of a circular geometry in composites and biomechanics, respectively.

The objective of this research is to consider a single isotropic circular inclusion embedded within an infinite homogeneous matrix in plane elastostatics. The bonding at the inclusion-matrix interface is considered to be imperfect with the assumption that the interface imperfections are circumferentially inhomogeneous. Our aim is to develop a rigorous solution method, using complex variable techniques, to study systematically the effects of two physically significant inhomogeneous imperfect interfaces on the corresponding stress fields: that being the inhomogeneous spring - layer interface and the inhomogeneous non - slip interface, respectively. The knowledge of the influence of an inhomogeneous imperfect inter-

face on the local fields will enable one to calculate the effective (global) properties of composites more accurately which will enhance the design of future structures.

In the following chapters, detailed derivations are given for a circular inclusion with inhomogeneous imperfect interface conditions. Chapter 2 outlines the general formulation for the boundary value problem associated with a single, isotropic circular inclusion embedded within an infinite homogeneous matrix in plane elasticity. It is shown how the basic boundary value problem for four analytic functions is reduced to only two analytic functions. In addition, associated supplementary conditions, such as the average stress induced within a circular inclusion, are derived.

Chapter 3 provides the rigorous derivation of the solution method, corresponding to a particular class of inhomogeneous imperfect interface that describes the circumferential variation in damage, when the spring-factor type interface parameters are inhomogeneous and equal - the so called inhomogeneous spring - layer interface. This interface description has also been studied numerically by Achenbach and Zhu (see [40], [51] and [53]) but under the simplified conditions of homogeneous interface imperfections.

Chapter 4 discusses, in detail, the methodology pertaining to the solution process derived in Chapter 3. In particular, we address two examples arising from

the case when the functional form describing the circumferential variation in damage along the interface take on the specific values $s = 1$ and $s = 2$, respectively. In the former, the equations for the stress potentials are uncoupled and easy to solve. However, in the latter, the equations for the stress potentials are coupled and the solution process is more involved. In addition, we examine the effects of the circumferential variation of the interface parameter on the average stresses induced within the circular inclusion for both cases. In either case, the results demonstrate conclusively how the pointwise variation of the parameter describing the interface imperfections has a pronounced effect on even the average stresses induced within the circular inclusion.

In Chapter 5, the single inclusion problem is extended to deal with problems arising in biomechanics. One major challenge is the development of products with mechanical properties that match those of human bone as closely as possible. For this reason, it is essential for the implants and host bone to combine adequate biocompatible and bioactive (i.e. bone - bonding) behavior. In particular, inhomogeneous bone ingrowth patterns across the implant - bone interface contribute to a major source of problems such as implant loosening. Analysis of retrieved porous-coated implants from humans have shown varying amounts of bone ingrowth into the porous coating [105]. Consequently, a rigorous solution method for the prob-

lem associated with a single isotropic circular inclusion (implant) embedded within an infinite homogeneous matrix (bone) in plane elastostatics is presented. In this instance, the bonding at the inclusion - matrix boundary is circumferentially inhomogeneous as characterized by the non-slip condition $m(\theta)$ finite and $n(\theta) = \infty$ (see [84]). Only a small amount of work has been devoted to non-slip zones in bimaterials having an interface edge crack (see, for example, [106 - 108] for details).

Chapter 6 discusses, in detail, the solution process derived in Chapter 5. In particular, we address two examples arising from the case when the functional form, describing the inhomogeneous non-slipping interface, take on the specific values $s = 1$ and $s = 2$, respectively. Also, we examine the effects of the circumferential variation of the interface parameter on the average stresses induced within the circular inclusion for both cases. In either case, the results demonstrate conclusively how the pointwise variation of the parameter describing the interface imperfections has a significant and pronounced effect on the average stresses induced within the circular inclusion. In addition, the interfacial shear stress is evaluated for the case corresponding to the circumferential number $s = 1$ (see [109]).

Finally, Chapter 7 outlines a method to check the validity of the solutions derived in Chapters 3 - 6. In particular, the general solutions obtained from the inhomogeneous spring - layer interface and the inhomogeneous non - slip interface, respectively, are shown to reduce to the known solutions corresponding to the homogeneous imperfect interface.

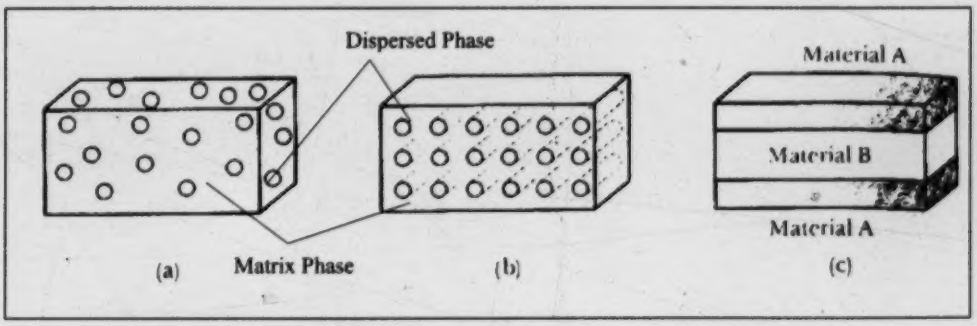

Figure 1-1. Three Types of Composite Materials: (a) Particulate Composite, (b) Fiber-Reinforced Composite, and (c) Laminar Composite

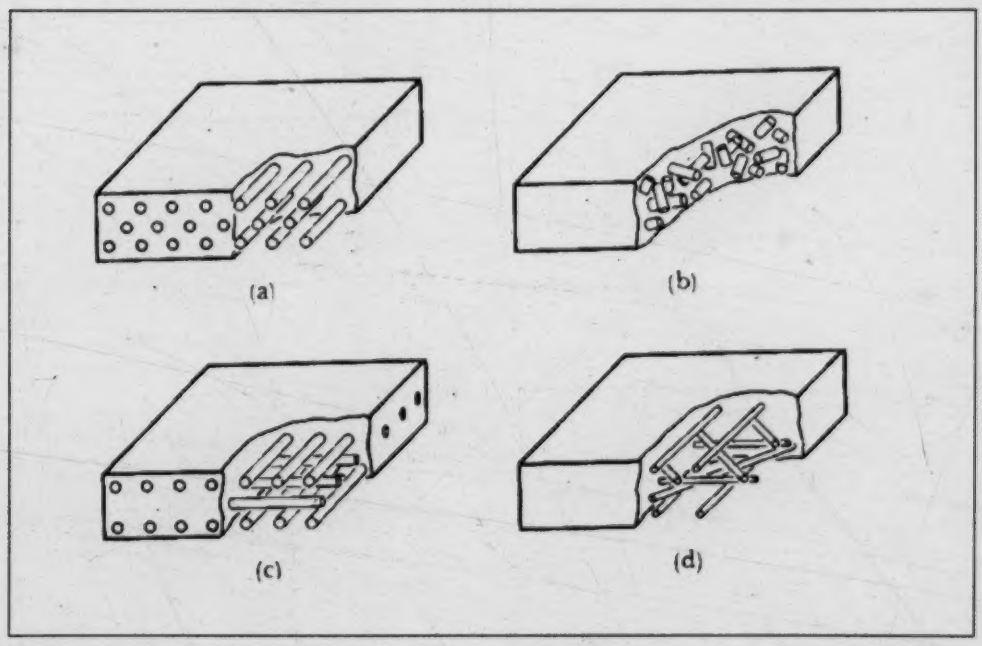

Figure 1-2. Several Orientations of Fiber-Reinforced Composites: (a) Continuous Unidirectional Fibers, (b) Randomly Oriented Short Discontinuous Fibers, (c) Orthogonal Fibers, and (d) Multiple-Ply Fibers (From Donald R. Askeland, *The Science and Engineering of Materials*, Second S.I. Edition, Chapman & Hall 1990)

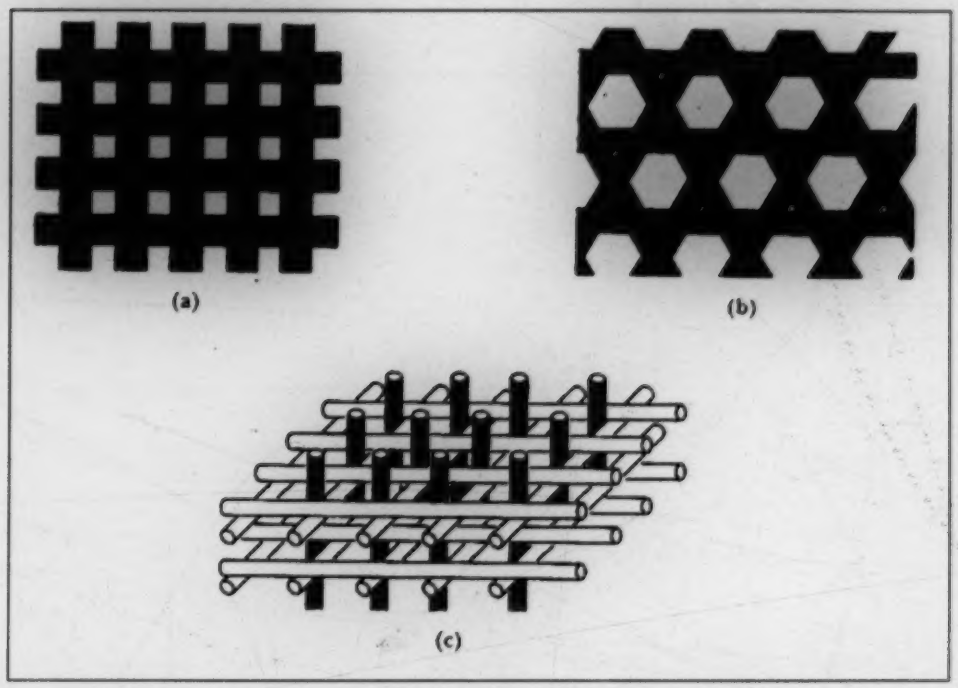

Figure 1-3. Several Weave Patterns for Fibers: (a) Biaxial Weave, (b) Triaxial Weave, and (c) Three-Dimensional Weave (From Donald R. Askeland, *The Science and Engineering of Materials*, Second S.I. Edition, Chapman & Hall, 1990)

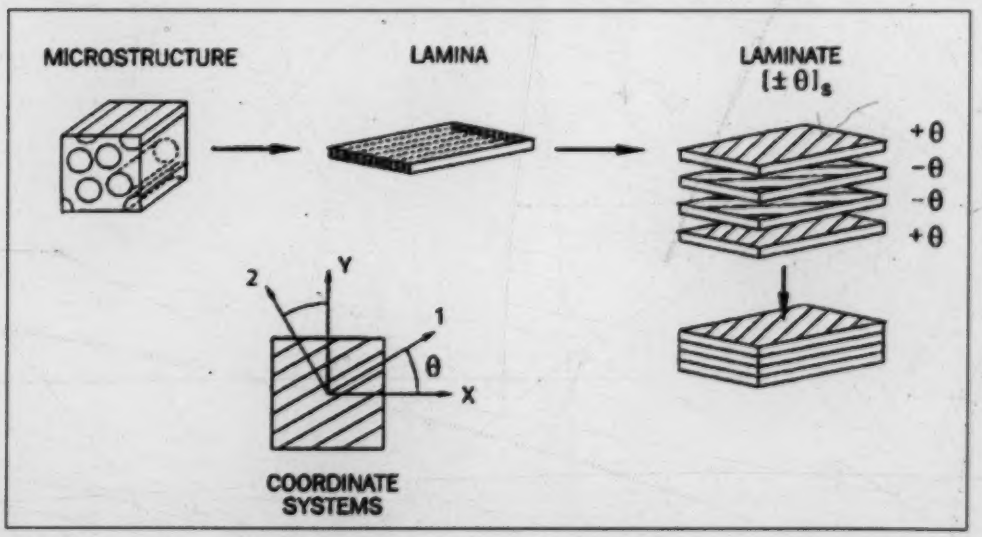

Figure 1-4. Schematic Representation of Fiber-Reinforced Laminate Composite (From John Wolodko, *Biaxial Fatique and Leakage Characteristics of Fiber Reinforced Composite Tubes* Ph. D. Thesis, University of Alberta, 1999)

Figure 1-5. Transmisson Electron Micrograph of Interphase Region. A crack (cr) has formed between the glass layer (g) and the precipitate layer (p). (From Coyle et al. *Proceedings of the Second International Conference on Composite Interfaces*, Elsevier (1988))

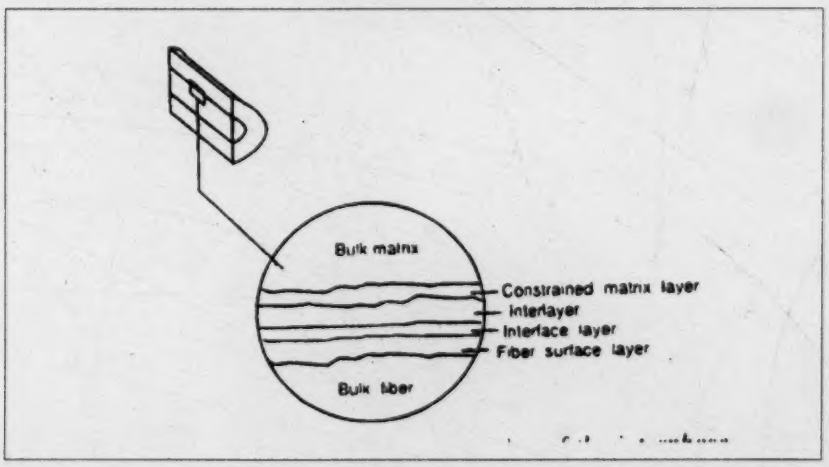

Figure 1-6. Schematic Representation of Interphase Region. (From Yuan et al. *Fiber, Matrix and Interface Properties* ASTM STP 1290, C.J. Spraggs and L.T. Drzal Eds., American Society for Testing and Materials, (1996))

CHAPTER 2

General Formulation and Subsidiary Results

2.1. General Formulation

2.1.1. Preliminaries

Consider a domain in $\mathbb{R}^2$, infinite in extent, containing a single, isotropic circular inclusion with elastic properties different than those of the surrounding matrix. The inclusion, with center at the origin of the coordinate system and radius R, occupies a region denoted by D_I. The matrix occupies a region denoted by D_M and the inclusion - matrix interface is denoted by the curve Γ (see Figure 2-1). Throughout this dissertation, the subscripts and superscripts I and M denote quantities related to the inclusion and matrix, respectively.

For plane deformation, the polar representation of the stresses $(\sigma_{\alpha\beta})$ and the displacements (u, v) can be given in terms of two analytic functions $\Phi(z)$ and $\Psi(z)$ by [110]

$$
\begin{aligned}
2\mu\left(u_r + iu_\theta\right) &= e^{-i\theta}\left[\kappa\Phi(z) - z\overline{\Phi'(z)} - \overline{\Psi(z)}\right] \\
\sigma_r + \sigma_\theta &= 2\left[\Phi'(z) + \overline{\Phi'(z)}\right] \\
\sigma_r - i\sigma_{r\theta} &= \Phi'(z) + \overline{\Phi'(z)} - e^{2i\theta}\left[\overline{z}\Phi''(z) + \Psi'(z)\right],
\end{aligned}
\tag{2.1}
$$

where $z = (x + iy) = re^{i\theta}$ is the complex coordinate, $\kappa = (3 - 4\nu)$ for plane strain and $\kappa = (3 - \nu)/(1 + \nu)$ for plane stress, the prime denotes the derivative with respect to the complex variable z, the overbar denotes the complex conjugate and μ and ν are the shear modulus and Poisson's ratio, respectively.

Assume that the circular inclusion is bonded to the matrix along the curve Γ by an inhomogeneous imperfect interface as described in Chapter 1. Then the interface condition on Γ is given by (see, for example, [80], [82])

$$\|\sigma_r - i\sigma_{r\theta}\| = 0, \quad z \in \Gamma, \tag{2.2}$$

$$\sigma_r = m(\theta)\left[\|u_r\| - u_r^o\right] \qquad \sigma_{r\theta} = n(\theta)\left[\|u_\theta\| - u_\theta^o\right], \quad z \in \Gamma, \tag{2.3}$$

where u^o is the displacement induced by the uniform eigenstrains $\left\{\varepsilon_x^o, \varepsilon_y^o, \varepsilon_z^o\right\}$ prescribed within the inclusion (which might be the result of differences in the thermal expansions of the inclusion and matrix due to temperature change), $\|*\| = (*)_M - (*)_I$ denotes the jump across Γ, m and n are the normal and tangential spring - factor type interface parameters (which are non-negative) and θ is the polar coordinate describing the interface. Clearly, the interface model (2.2 - 2.3) can be realized in practice using an adhesive layer. In doing so, any one of the two interface parameters, $m(\theta)$ and $n(\theta)$, or a combination of them can be specified at will by controlling the thickness or density of the adhesive layer (i.e. the

interface parameters should be inversely proportional to the thickness, or directly proportional to the density of the adhesive layer). For example, to design a circular interface, $m(\theta)$ and $n(\theta)$ must be designed independently. In this case, more than one adhesive material is required. For a detailed discussion regarding interface design see [111].

Remark 1. *When $m(\theta)$ is finite and $n(\theta) = \infty$, (2.2 - 2.3) represent the inhomogeneous non - slipping interface conditions, and if $m(\theta) = n(\theta) = \infty$, (2.2 - 2.3) correspond to a perfectly bonded interface. When $m(\theta) = n(\theta)$, we have the inhomogeneous spring - layer interface.*

The analytic functions $\Phi_M(z), \Psi_M(z), \Phi_I(z)$ and $\Psi_I(z)$, respectively can be represented by a general Laurent series, and since the stresses $\sigma_{\alpha\beta}$ $(\alpha, \beta = 1, 2)$ are always assumed to exist at infinity (i.e. the stresses at infinity are always assumed bounded and finite) and since $\Phi_M'(z)$ and $\Psi_M'(z)$ must have $O(1)$ as $|z| \to \infty$ (from (2.1)) , then the remote loading at infinity can be characterized by the uniform stress field

$$\Phi_M(z) = Az + O(1), \qquad \Psi_M(z) = Bz + O(1), \qquad |z| \to \infty, \tag{2.4}$$

where A is a given real number and B is a given complex number. In addition, the stresses at the origin must also be bounded and finite. Thus, these four analytic

functions admit the following series expansions

$$\Phi_M(z) = Az + \sum_{k=0}^{\infty} A_k z^{-k} \quad , \quad \Psi_M(z) = Bz + \sum_{k=0}^{\infty} B_k z^{-k} \qquad z \in D_M,$$

$$\Phi_I(z) = \sum_{k=0}^{\infty} X_k z^k \quad , \qquad \Psi_I(z) = \sum_{k=0}^{\infty} Y_k z^k \qquad z \in D_I. \tag{2.5}$$

Thus, the goal is to determine the four unknown analytic functions $\Phi_M(z), \Phi_I(z), \Psi_M(z)$ and $\Psi_I(z)$ satisfying conditions (2.2 - 2.4). Once these functions are determined, the complete elastic field distribution for the inclusion - matrix system can be determined via condition (2.1).

2.1.2. Representation of Two Analytic Functions - $\Psi_M(z)$ and $\Psi_I(z)$

To eliminate the possibility of rigid body displacement between inclusion and matrix, the coefficients X_o and Y_o should be properly chosen. Hence, since the inclusion is geometrically symmetric about two mutually perpendicular axes (see Figure 2-1), we have that

$$X_o = Y_o = 0. \tag{2.6}$$

Using condition (2.1), the traction continuity condition (2.2) gives

$$\Phi_M'(z) - \overline{\Phi_I'}\left(\frac{R^2}{z}\right) - z\Phi_M''(z) - \frac{z^2}{R^2}\Psi_M'(z) = \Phi_I'(z) - \overline{\Phi_M'}\left(\frac{R^2}{z}\right) - z\Phi_I''(z) - \frac{z^2}{R^2}\Psi_I'(z), \quad z \in \Gamma. \tag{2.7}$$

Then, in view of (2.5), the right-hand side of (2.7) is analytic in D_I and the left-hand side is analytic in D_M, except at infinity where the left-hand side has the singular behavior

$$A - \frac{Bz^2}{R^2} - \overline{X_1} + \frac{B_1}{R^2}, \qquad |z| \to \infty. \tag{2.8}$$

Using the principle of analytic continuation (see either [110] or [112]), the function, $\Delta(z)$, defined by

$$\Delta(z) \equiv \begin{cases} \Phi_M'(z) - z\Phi_M''(z) - \dfrac{z^2}{R^2}\Psi_M'(z) - \overline{\Phi_I'}\left(\dfrac{R^2}{z}\right) \\ \quad - \left[A - \dfrac{Bz^2}{R^2} - \overline{X_1} + \dfrac{B_1}{R^2}\right], \qquad z \in D_M, \\ \Phi_I'(z) - \overline{\Phi_M'}\left(\dfrac{R^2}{z}\right) - z\Phi_I''(z) - \dfrac{z^2}{R^2}\Psi_I'(z) \\ \quad - \left[A - \dfrac{Bz^2}{R^2} - \overline{X_1} + \dfrac{B_1}{R_2}\right], \qquad z \in D_I \end{cases} \tag{2.9}$$

is analytic and single-valued in the whole complex plane including the point at infinity. Therefore, by Liouville's Theorem, $\Delta(z)$ must be a constant. In fact, since $\Delta(z)$ approaches zero at infinity it must be that the constant is identically equal to zero. Thus, with this condition, integrating (2.9) with respect to the

variable z, expressions for $\Psi_I(z)$ and $\Psi_M(z)$ are obtained and given by

$$\Psi_M(z) = Bz + \frac{AR^2 + B_1 - \overline{X_1}R^2}{z} - \frac{R^2}{z}\Phi_M'(z) + \overline{\Phi_I}\left(\frac{R^2}{z}\right) + C_1, \quad z \in D_M,$$

$$\Psi_I(z) = Bz + \frac{AR^2 + B_1 - \overline{X_1}R^2}{z} - \frac{R^2}{z}\Phi_I'(z) + \overline{\Phi_M}\left(\frac{R^2}{z}\right) + C_2, \quad z \in D_I, \tag{2.10}$$

where B_1 is an unknown coefficient and C_1, C_2 are constants of integration. In fact, substituting (2.5) into (2.10) and equating the coefficients for the powers of z (specifically z^{-1} and z^0) yields the following expressions for the unknown coefficients B_1, C_1 and C_2

$$\frac{B_1}{R^2} = 2\,\mathrm{Re}[X_1] - 2A, \; C_1 = B_o, \; C_2 = 2X_2R^2 - \overline{A_o}. \tag{2.11}$$

Thus, the original problem for four analytic functions has been reduced to finding two unknown analytic functions: Φ_M and Φ_I. To this end, the remaining two displacement interface conditions (2.3) can be written into complex form.

2.1.3. Basic Boundary Value Problem

Since the stresses are continuous across the inclusion-matrix boundary, the two displacement interface conditions, (2.3), can be written as

$$(\sigma_r - i\sigma_{r\theta})_M = \left[mu_r^M - mu_r^I - mu_r^o - inu_\theta^M + inu_\theta^I + inu_\theta^o\right]$$

$$= \left\{\left(\frac{m+n}{2}\right)\left[\left(u_r^M - iu_\theta^M\right) - \left(u_r^I - iu_\theta^I\right)\right] + \right.$$

$$\left.\left(\frac{m-n}{2}\right)\left[\left(u_r^M + iu_\theta^M\right) - i\left(u_r^I + iu_\theta^I\right)\right] - \left[mu_r^o - inu_\theta^o\right]\right\}, \quad z \in \Gamma$$

which, can be simplified to the following

$$(\sigma_r - i\sigma_{r\theta})_M = \left(\frac{m+n}{2}\right)\|u_r - iu_\theta\| + \left(\frac{m-n}{2}\right)\|u_r + iu_\theta\|$$

$$- \left[mu_r^o - inu_\theta^o\right], \quad z \in \Gamma. \tag{2.12}$$

At this stage, it is convenient to express the stress free displacement components u_r^o and u_θ^o, appearing in (2.12), in terms of the eigenstrains themselves. Therefore, from Gao's results [63], the stress free displacement components, on the inclusion-matrix boundary, are given by

$$u_r^o = R\left(\varepsilon_x^o \cos^2\theta + \varepsilon_y^o \sin^2\theta + \varepsilon_{xy}^o \sin 2\theta\right),$$

$$u_\theta^o = R\left[\frac{\varepsilon_y^o - \varepsilon_x^o}{2}\sin 2\theta + \varepsilon_{xy}^o \cos 2\theta\right]. \tag{2.13}$$

Then, with the aid of half-angle formulas, (2.13) is rewritten as follows

$$u_r^o = R\varepsilon_1 + R\varepsilon_2 \cos 2\theta + R\varepsilon_3 \sin 2\theta,$$

$$u_\theta^o = R\varepsilon_3 \cos 2\theta - R\varepsilon_2 \sin 2\theta, \tag{2.14}$$

$$\text{where} \quad \varepsilon_1 = \frac{\varepsilon_x^o + \varepsilon_y^o}{2}, \quad \varepsilon_2 = \frac{\varepsilon_x^o - \varepsilon_y^o}{2}, \quad \varepsilon_3 = \varepsilon_{xy}^o.$$

Hence, in view of (2.14), the stress-free displacements appearing in (2.12) are expressed as

$$\begin{aligned}[mu_r^o - inu_\theta^o] &= mR\varepsilon_1 + mR\varepsilon_2 \cos 2\theta + mR\varepsilon_3 \sin 2\theta - inR\varepsilon_3 \cos 2\theta + inR\varepsilon_2 \sin 2\theta \\ &= mR\varepsilon_1 + R\left(\frac{m+n}{2}\right)\left[(\varepsilon_2 - i\varepsilon_3)\cos 2\theta + i\,(\varepsilon_2 - i\varepsilon_3)\sin 2\theta\right] + \\ &\quad R\left(\frac{m-n}{2}\right)\left[(\varepsilon_2 + i\varepsilon_3)\cos 2\theta - i\,(\varepsilon_2 + i\varepsilon_3)\sin 2\theta\right],\end{aligned}$$

and since $z = \mathrm{R}e^{i\theta}$ on the inclusion-matrix boundary, the above is simplified to the following

$$[mu_r^o - inu_\theta^o] = mR\varepsilon_1 + \left(\frac{m+n}{2R}\right)(\varepsilon_2 - i\varepsilon_3)\,z^2 + \left(\frac{m-n}{2z^2}\right)(\varepsilon_2 + i\varepsilon_3)\,R^3, \quad z \in \Gamma. \tag{2.15}$$

Thus, with conditions (2.1), (2.10), (2.12) and (2.15) the displacement interface

conditions (2.3) are rewritten in terms of $\Phi_I(z)$ and $\Phi_M(z)$ as follows

$$A-\frac{B}{R^2}z^2-\overline{X_1}+\frac{B_1}{R^2}+\overline{\Phi_I'}\left(\frac{R^2}{z}\right)-\left(\frac{m-n}{4}\right)\left[\frac{\kappa_M}{\mu_M}+\frac{1}{\mu_I}\right]\frac{R}{z}\Phi_M(z)$$
$$+\left(\frac{m+n}{4}\right)\left[\frac{\kappa_I}{\mu_I}+\frac{1}{\mu_M}\right]\frac{z}{R}\overline{\Phi_I}\left(\frac{R^2}{z}\right)-\left(\frac{m-n}{4\mu_I}\right)\left[A+\frac{B_1}{R^2}+\frac{\overline{B}R^2}{z^2}-X_1+\frac{\overline{C_2}}{z}\right]R$$
$$+\left(\frac{m-n}{4\mu_M}\right)\left[A+\frac{B_1}{R^2}+\frac{\overline{B}R^2}{z^2}-X_1+\frac{\overline{C_1}}{z}\right]R=\left(\frac{m+n}{4}\right)\left[\frac{\kappa_M}{\mu_M}+\frac{1}{\mu_I}\right]\frac{z}{R}\overline{\Phi_M}\left(\frac{R^2}{z}\right)$$
$$-\overline{\Phi_M'}\left(\frac{R^2}{z}\right)-\left(\frac{m-n}{4}\right)\left[\frac{\kappa_I}{\mu_I}+\frac{1}{\mu_M}\right]\frac{R}{z}\Phi_I(z)-\left(\frac{m+n}{2R}\right)(\varepsilon_2-i\varepsilon_3)z^2$$
$$+\left(\frac{m+n}{4R\mu_I}\right)\left[Bz^2+AR^2+B_1-\overline{X_1}R^2+C_2z\right]-mR\varepsilon_1-\left(\frac{m-n}{2z^2}\right)R^3(\varepsilon_2+i\varepsilon_3)$$
$$-\left(\frac{m+n}{4R\mu_M}\right)\left[Bz^2+AR^2+B_1-\overline{X_1}R^2+C_1z\right],\quad z\in\Gamma. \tag{2.16}$$

Note that the interface parameters m and n appearing in (2.12), (2.15) and (2.16) are all functions of θ.

Hence, the problem has now been reduced to determining two unknown analytic functions $\Phi_M(z)$ and $\Phi_I(z)$ satisfying the interface condition (2.16) and the asymptotic conditions (2.4) for $\Phi_M(z)$.

2.2. Subsidiary Results

As outlined in Chapter 1, the average stress or strain within the single inclusion phase is of basic importance in composite mechanics. Thus, this section will provide the necessary equations for the calculation of the average stresses inside a

circular inclusion.

In view of condition (2.1) and (2.5), the Cartesian components of the stress inside the inclusion can be expressed as

$$\begin{aligned}
\sigma_x + \sigma_y &= 2\left[\sum_{h=0}^{\infty} hX_h z^{h-1} + \sum_{h=0}^{\infty} h\overline{X_h}\,\overline{z}^{h-1}\right], \quad z \in D_l, \\
\sigma_x - i\sigma_{xy} &= \sum_{h=0}^{\infty} h\overline{X_h}\,\overline{z}^{h-1} + \sum_{h=0}^{\infty} hX_h z^{h-1} - \overline{z}\sum_{h=0}^{\infty} h(h-1)X_h z^{h-2} \\
&\quad - \sum_{h=0}^{\infty} hY_h z^{h-1}, \quad z \in D_l.
\end{aligned} \tag{2.17}$$

However, since $z = re^{i\theta}$, where $0 \le r \le R$ and $0 \le \theta \le 2\pi$, then (2.17) is rewritten as

$$\begin{aligned}
\sigma_x + \sigma_y &= 2\left[(X_1 + \overline{X_1}) + \sum_{h=2}^{\infty} hX_h \left(re^{i\theta}\right)^{h-1} + \sum_{h=2}^{\infty} h\overline{X_h}\left(re^{-i\theta}\right)^{h-1}\right], \\
\sigma_x - i\sigma_{xy} &= \left(X_1 + \overline{X_1} - 6r^2X_3 - Y_1\right) + \sum_{h=2}^{\infty} h\overline{X_h}\left(re^{-i\theta}\right)^{h-1} + \sum_{h=2}^{\infty} hX_h\left(re^{i\theta}\right)^{h-1} \\
&\quad - \sum_{h=2}^{\infty} hY_h\left(re^{i\theta}\right)^{h-1} - \sum_{h=4}^{\infty} h(h-1)r^{h-1}X_h e^{i(h-3)\theta}.
\end{aligned} \tag{2.18}$$

Note that the coefficient Y_1, appearing in $(2.18)_2$, needs to be evaluated. This is achieved by substituting (2.5) into $(2.10)_2$ and equating the coefficients corresponding to the power z^1.

Thus, the expression for the coefficient Y_1 is given as

$$Y_1 = B - 3R^2X_3 + \frac{\overline{A_1}}{R^2}. \tag{2.19}$$

Definition 1. *The average value of a function $f(x,y)$ over some region Ω is given by the expression*

$$f_{Avg} = \frac{1}{Area_{\Omega}} \iint_{\Omega} f(x,y)\, dA$$

Therefore, since $x = r\cos\theta$, $y = r\sin\theta$ and $dA = rdrd\theta$, then, with the aid of Definition 1 and noting that the area of the circular inclusion is πR^2 and that term-by-term integration is valid, the average value of (2.18) is given by

$$\begin{aligned} (\sigma_x + \sigma_y)_{Avg} &= 2\left(X_1 + \overline{X_1}\right), \\ (\sigma_x - i\sigma_{xy})_{Avg} &= \left(X_1 + \overline{X_1}\right) - \left(B + \frac{\overline{A_1}}{R^2}\right). \end{aligned} \tag{2.20}$$

where the subscript Avg denotes the average value.

Thus, the equations to calculate the average mean, deviatoric and shear stresses within the inclusion are given by condition (2.20). The advantage of the present formulation is that the exact values for the coefficients X_1 and A_1 can be obtained without the knowledge of the complete solution.

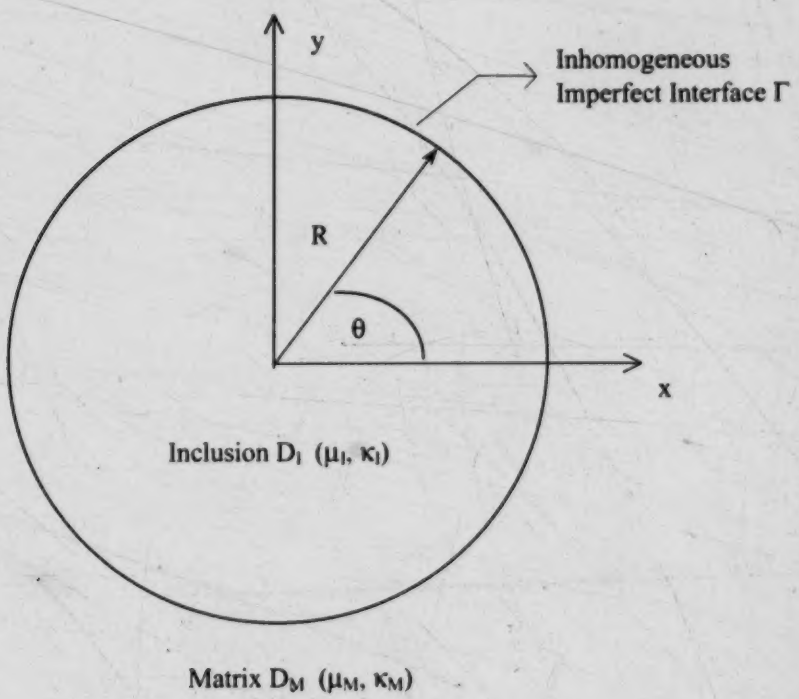

Figure 2-1. A Homogeneous Circular Inclusion with Circumferentially Inhomogeneous Imperfect Interface Embedded in an Infinite Elastic Matrix in Plane Elasticity

CHAPTER 3

Circumferential Inhomogeneous Spring - Layer Interface

3.1. Introduction

In this chapter, the rigorous solution method for the problem associated with the single circular inclusion is presented. The bonding along the inclusion - matrix interface is considered to be circumferentially inhomogeneous and characterized by the condition when the spring-factor interface parameters are equal - the so called inhomogeneous spring - layer interface (i.e. $m(\theta) = n(\theta)$). Note that Achenbach and Zhu (see [40], [51] and [53]) numerically studied this interface description but under the simplified conditions of homogeneous interface imperfections. Physically, this type of imperfect interface corresponds to the case when the jump in the displacement vector across the inclusion - matrix interface is in the same direction as the corresponding interface tractions. For example, prior to any kind of deformation, consider any two points, say A and B, which are very close together (i.e. the points almost coincide), lie on opposite sides of the interface and are connected via a spring. Once deformation has occurred, these two points have moved apart and the jump in the displacement vector across the interface is parallel to

the internal force generated along the spring (see Figure 3-1). This fact can be expressed by setting $m(\theta) = n(\theta)$ in conditions (2.3) which give

$$\frac{\|u_r\| - u_r^o}{\|u_\theta\| - u_\theta^o} = \frac{\sigma_r}{\sigma_{r\theta}}, \quad z \in \Gamma. \tag{3.1}$$

Furthermore, the degree of interface imperfections, although equal, is realized in both the normal and tangential directions. Consequently, in contrast to the case of the radially inhomogeneous interphase discussed by [31], or of the inhomogeneous sliding interface discussed by [80], the interface description discussed in this chapter is practically more significant with respect to the design of interphase layers in composite materials. For example, the ratio $m(\theta)/n(\theta)$ can be assumed to be unity for the spring - layer model (see [40], [51] and [53]), or be a certain constant greater than unity for an elastic interphase layer (see [52]). Consequently, in order to design an interphase layer using a single adhesive material, the design should be carried out under the restriction that the ratio $m(\theta)/n(\theta)$ is a constant not less than one. Note that the scope of this thesis is not the design of interphase layers, rather it is on the effect of interface imperfections on the elastic fields. Thus, in the remainder of this Chapter, we confine our attention to the condition $m(\theta) = n(\theta)$.

3.2. Spring - Layer Interface

As discussed in Section 3.1 of this chapter, a circular inclusion with inhomogeneous imperfect interface characterized by the condition $m(\theta) = n(\theta)$ is considered. This description allows the interface condition (2.16) to be simplified to the following

$$A - \frac{\overline{B}\overline{z}^2}{R^2} - X_1 + \frac{B_1}{R^2} + \Phi_I'(z) + \frac{n(\theta)}{2}\left[\frac{\kappa_I}{\mu_I} + \frac{1}{\mu_M}\right]\frac{\overline{z}}{R}\Phi_I(z) =$$
$$\frac{n(\theta)}{2}\left[\frac{\kappa_M}{\mu_M} + \frac{1}{\mu_I}\right]\frac{\overline{z}}{R}\Phi_M(z) - \Phi_M'(z) - \frac{n(\theta)}{2R\mu_M}\left(\overline{B}\overline{z}^2 + AR^2 + B_1 - X_1R^2 + \overline{C_1}\overline{z}\right)$$
$$+\frac{n(\theta)}{2R\mu_I}\left(\overline{B}\overline{z}^2 + AR^2 + B_1 - X_1R^2 + \overline{C_2}\overline{z}\right) - n(\theta)R\varepsilon_1$$
$$-\frac{n(\theta)\overline{z}^2}{R}(\varepsilon_2 + i\varepsilon_3), \quad z \in \Gamma. \tag{3.2}$$

Note that since $\overline{z}$ is not an analytic function, (3.2) does not appear to be analytic. However, since $z\overline{z} = R^2$ on Γ, then (3.2) can be rewritten as

$$A - \frac{\overline{B}R^2}{z^2} - X_1 + \frac{B_1}{R^2} + \Phi_I'(z) + \frac{n(\theta)}{2}\left[\frac{\kappa_I}{\mu_I} + \frac{1}{\mu_M}\right]\frac{R}{z}\Phi_I(z) =$$
$$\frac{n(\theta)}{2}\left[\frac{\kappa_M}{\mu_M} + \frac{1}{\mu_I}\right]\frac{R}{z}\Phi_M(z) - \Phi_M'(z) - \frac{n(\theta)}{2R\mu_M}\left(\frac{\overline{B}R^4}{z^2} + AR^2 + B_1 - X_1R^2 + \frac{\overline{C_1}R^2}{z}\right)$$
$$+\frac{n(\theta)}{2R\mu_I}\left(\frac{\overline{B}R^4}{z^2} + AR^2 + B_1 - X_1R^2 + \frac{\overline{C_2}R^2}{z}\right) - n(\theta)R\varepsilon_1$$
$$-\frac{n(\theta)R^3}{z^2}(\varepsilon_2 + i\varepsilon_3), \quad z \in \Gamma, \tag{3.3}$$

which is seen to be analytic.

For convenience, let the parameter $\delta(\theta)$ be introduced in place of $n(\theta)$ and defined by

$$\delta(\theta) \equiv \frac{n(\theta) R \left(\frac{\kappa_M}{\mu_M} + \frac{1}{\mu_I} \right)}{2}. \tag{3.4}$$

Furthermore, let

$$1 + f(\theta) = \frac{\delta_o}{\delta(\theta)}, \qquad \delta_o > 0, \qquad f(\theta) > -1, \tag{3.5}$$

where δ_o is a positive real number and $f(\theta)$ is a real periodic function prescribed on Γ. Clearly, $1/\delta(\theta)$ is a non-negative periodic function defined on Γ. Also note that the functional form of $f(\theta)$ describes the circumferential variation in damage along the interface. In addition, as $f(\theta) \to -1$, this is equivalent to $n(\theta) \to \infty$ which corresponds to a perfectly bonded interface.

Since $f(\theta)$ is a periodic function of θ in the space $C_p[0, 2\pi]$, let us represent $f(\theta)$ by the following finite Fourier series

$$f(\theta) = \sum_{k=1}^{s} a_k \sin k\theta + b_k \cos k\theta \tag{3.6}$$

$$a_s^2 + b_s^2 \neq 0 \text{ unless } f(\theta) \equiv 0 \text{ on } \Gamma,$$

where s is a natural number that defines the maximum order of the polynomial and a_k, b_k are some given real coefficients. By noting that

$$\sin k\theta = \frac{e^{ik\theta} - e^{-ik\theta}}{2i}, \qquad \cos k\theta = \frac{e^{ik\theta} + e^{-ik\theta}}{2},$$

(3.6) can be written in terms of the complex variable z as follows

$$f(z) = \frac{1}{2}\sum_{k=1}^{s}\left[ia_k\left(\frac{R^k}{z^k} - \frac{z^k}{R^k}\right) + b_k\left(\frac{z^k}{R^k} + \frac{R^k}{z^k}\right)\right], \quad z \in \Gamma. \tag{3.7}$$

Clearly, it must be that

$$f(z) \equiv f(\theta), \quad z \in \Gamma.$$

Using conditions (3.4), (3.5) and (3.7) the interface condition, (3.3), takes the following form

$$\begin{aligned}[1+f(z)]\,\Phi_I'(z) + \delta_o\beta\frac{\Phi_I(z)}{z} + [1+f(z)]\left[A + \frac{B_1}{R^2} - X_1\right] + \delta_o\eta\left[A + \frac{B_1}{R^2} - X_1\right] \\ + \frac{2\delta_o\varepsilon_1}{\left(\frac{\kappa_M}{\mu_M} + \frac{1}{\mu_I}\right)} = -[1+f(z)]\,\Phi_M'(z) + \delta_o\frac{\Phi_M(z)}{z} + [1+f(z)]\frac{\overline{B}R^2}{z^2} \\ -\delta_o\frac{\overline{B}R^2}{z^2} - \frac{\delta_o}{z}\left[\frac{\frac{\overline{C_1}}{\mu_M} - \frac{\overline{C_2}}{\mu_I}}{\left(\frac{\kappa_M}{\mu_M} + \frac{1}{\mu_I}\right)}\right] - \frac{2\delta_o R^2(\varepsilon_2 + i\varepsilon_3)}{z^2\left(\frac{\kappa_M}{\mu_M} + \frac{1}{\mu_I}\right)}, \quad z \in \Gamma,\end{aligned} \tag{3.8}$$

where

$$\beta \equiv \frac{\left(\frac{\kappa_I}{\mu_I} + \frac{1}{\mu_M}\right)}{\left(\frac{\kappa_M}{\mu_M} + \frac{1}{\mu_I}\right)} > 0, \qquad \eta \equiv \frac{\frac{1}{\mu_M} - \frac{1}{\mu_I}}{\left(\frac{\kappa_M}{\mu_M} + \frac{1}{\mu_I}\right)}. \tag{3.9}$$

It is evident from condition (3.8) that the solutions $\Phi_M(z)$ and $\Phi_I(z)$ will depend on the circumferential variation of imperfections in the interface. As a result of this dependency, the conventional power series method will lead to a coupled infinite

system of algebraic equations for the unknown coefficients X_k and A_k, $k = 1, 2, ...$ Consequently, the exact expressions for even the first few coefficients cannot be determined. To overcome this difficulty, the principle of analytic continuation is used to reduce (3.8) to two *coupled* first order differential equations for $\Phi_M(z)$ and $\Phi_I(z)$. In this way, exact, closed-form solutions can be obtained in the general case of a circumferentially inhomogeneous interface as described by the model given by (3.5, 3.6).

3.2.1. The Coupled Differential Equations for $\Phi_I(z)$ and $\Phi_M(z)$

To derive the differential equations for Φ_I and Φ_M note that, in view of (2.5), the right-hand side of equation (3.8) is analytic in D_M except at infinity where it approaches

$$A(\delta_o - 1) + \frac{\overline{B}}{2}\sum_{k=2}^{s}(b_k - ia_k)\left(\frac{z}{R}\right)^{k-2} + \frac{1}{2}\sum_{k=1}^{s}(b_k - ia_k)\left(\frac{z}{R}\right)^{k}\sum_{p=0}^{k-1}\frac{pA_p}{z^{p+1}}$$
$$-\frac{A}{2}\sum_{k=1}^{s}(b_k - ia_k)\left(\frac{z}{R}\right)^{k}.$$

Similarly, the left-hand side of (3.8) is analytic in D_I except at the origin where it has singular terms

$$\frac{1}{2}\sum_{k=1}^{s}(b_k+ia_k)\left(\frac{R}{z}\right)^k\sum_{r=0}^{k}rX_rz^{r-1}+\frac{1}{2}\left[A+\frac{B_1}{R^2}-X_1\right]\sum_{k=1}^{s}(b_k+ia_k)\left(\frac{R}{z}\right)^k.$$

Denote the sum of the above two expressions by $S(z)$,namely

$$\begin{aligned}S(z)\equiv{}&\frac{1}{2}\sum_{k=1}^{s}(b_k+ia_k)\left(\frac{R}{z}\right)^k\sum_{r=0}^{k}rX_rz^{r-1}+\frac{1}{2}\left[A+\frac{B_1}{R^2}-X_1\right]\sum_{k=1}^{s}(b_k+ia_k)\left(\frac{R}{z}\right)^k\\&+A(\delta_o-1)+\frac{\overline{B}}{2}\sum_{k=2}^{s}(b_k-ia_k)\left(\frac{z}{R}\right)^{k-2}+\frac{1}{2}\sum_{k=1}^{s}(b_k-ia_k)\left(\frac{z}{R}\right)^k\sum_{p=0}^{k-1}\frac{pA_p}{z^{p+1}}\\&-\frac{A}{2}\sum_{k=1}^{s}(b_k-ia_k)\left(\frac{z}{R}\right)^k,\end{aligned}\tag{3.10}$$

and consider the function $\Theta(z)$ defined by

$$\Theta(z)\equiv\begin{cases}[1+f(z)]\,\Phi_I'(z)+\delta_o\beta\dfrac{\Phi_I(z)}{z}+[1+f(z)]\left[A+\dfrac{B_1}{R^2}-X_1\right]\\\quad+\delta_o\eta\left[A+\dfrac{B_1}{R^2}-X_1\right]+\dfrac{2\delta_o\varepsilon_1}{\left(\dfrac{\kappa_M}{\mu_M}+\dfrac{1}{\mu_I}\right)}-S(z),\quad z\in D_I\\-[1+f(z)]\,\Phi_M'(z)+\delta_o\dfrac{\Phi_M(z)}{z}+[1+f(z)]\dfrac{\overline{B}R^2}{z^2}-\delta_o\eta\dfrac{\overline{B}R^2}{z^2}\\-\dfrac{\delta_o}{z}\left[\dfrac{\dfrac{\overline{C_1}}{\mu_M}-\dfrac{\overline{C_2}}{\mu_I}}{\left(\dfrac{\kappa_M}{\mu_M}+\dfrac{1}{\mu_I}\right)}\right]-\dfrac{2\delta_oR^2}{z^2\left(\dfrac{\kappa_M}{\mu_M}+\dfrac{1}{\mu_I}\right)}(\varepsilon_2+i\varepsilon_3)-S(z),\quad z\in D_M.\end{cases}\tag{3.11}$$

In view of the principle of analytic continuation, the function $\Theta(z)$, defined in this way, is analytic and single-valued in both D_I and D_M including the point

of infinity where it approaches zero. Therefore, by Liouville's Theorem $\Theta(z)$ is a constant. In fact, since $\Theta(z)$ approaches zero at infinity it must be that the constant is identically equal to zero. Hence, within the circular inclusion D_I, the governing differential equation is

$$\Phi_I'(z) + \delta_o\beta\frac{\Phi_I(z)}{z[1+f(z)]} = \frac{F(z)}{1+f(z)}, \quad z \in D_I, \tag{3.12}$$

where $F(z)$ is given by

$$F(z) = \dot{S}(z) - [1+f(z)](\overline{X_1} - A) - \delta_o\eta(\overline{X_1} - A) - \frac{2\delta_o\epsilon_1}{\left(\frac{\kappa_M}{\mu_M} + \frac{1}{\mu_I}\right)}. \tag{3.13}$$

Similarly, in the matrix D_M, the governing differential equation is

$$\Phi_M'(z) - \delta_o\frac{\Phi_M(z)}{z[1+f(z)]} = \frac{G(z)}{1+f(z)}, \quad z \in D_M, \tag{3.14}$$

where $G(z)$ is given by

$$G(z) = [1+f(z)]\frac{\overline{B}R^2}{z^2} - S(z) - \delta_o\eta\frac{\overline{B}R^2}{z^2} - \frac{\delta_o}{z}\left[\frac{\frac{\overline{C_1}}{\mu_M} - \frac{\overline{C_2}}{\mu_I}}{\left(\frac{\kappa_M}{\mu_M} + \frac{1}{\mu_I}\right)}\right] - \frac{2\delta_o(\varepsilon_2 + i\varepsilon_3)R^2}{z^2\left(\frac{\kappa_M}{\mu_M} + \frac{1}{\mu_I}\right)}. \tag{3.15}$$

Equations (3.12) and (3.14) are linear first order differential equations with variable coefficients for the unknowns Φ_I and Φ_M, respectively. Hence, the general solution

of (3.12) is given by

$$\Phi_I(z) = C(z)e^{-Q(z)}, \qquad Q(z) = \delta_o\beta \int \frac{dz}{z[1+f(z)]},$$
$$C(z) = \int_{z_I}^{z} \frac{F(z)}{[1+f(z)]} e^{Q(z)}dz + C_o, \quad z \in D_I. \tag{3.16}$$

Similarly, the general solution of (3.14) is given by

$$\Phi_M(z) = H(z)e^{-P(z)}, \qquad P(z) = -\delta_o \int \frac{dz}{z[1+f(z)]},$$
$$H(z) = \int_{z_M}^{z} \frac{G(z)}{[1+f(z)]} e^{P(z)}dz + H_o, \quad z \in D_M. \tag{3.17}$$

Note that z_I and z_M are some arbitrary points in D_I and D_M, respectively and C_o, H_o are arbitrary constants of integration.

The non-homogeneous term $F(z)$ includes s unknown constants $X_k (k = 1, 2, ..., s)$ and $(s-1)$ unknown constants $A_k (k = 1, 2, ..., s-1)$, in view of (2.5), any admissable solution $\Phi_I(z)$ of (3.12) has to satisfy the consistency conditions

$$X_k = \frac{\Phi_I^{'}(z)}{k!}, \qquad k = 1, 2, ..., s. \tag{3.18}$$

To verify (3.18), assume that (3.12) has an analytic solution $\Phi_I(z)$ in D_I which admits a Taylor expansion (i.e. $\Phi_I(z) = \sum_{r=0}^{\infty} Q_r z^r$). Now, substituting this expansion into (3.12) yields

$$\sum_{r=0}^{\infty} rQ_r z^{r-1} + \frac{1}{2}\sum_{k=1}^{s}\left[(b_k + ia_k)\left(\frac{R}{z}\right)^k + (b_k - ia_k)\left(\frac{z}{R}\right)^k\right]\sum_{r=0}^{\infty} rQ_r z^{r-1} +$$

$$\delta_o\beta\sum_{r=0}^{\infty} Q_r z^{r-1} = \frac{1}{2}\sum_{k=1}^{s}(b_k + ia_k)\left(\frac{R}{z}\right)^k \sum_{r=0}^{k} rX_r z^{r-1} + \frac{1}{2}\left(\overline{X_1} - A\right)\sum_{k=1}^{s}(b_k + ia_k)\left(\frac{R}{z}\right)^k$$

$$+\frac{\overline{B}}{2}\sum_{k=2}^{s}(b_k - ia_k)\left(\frac{z}{R}\right)^{k-2} + \frac{1}{2}\sum_{k=1}^{s}(b_k - ia_k)\left(\frac{z}{R}\right)^k \sum_{p=0}^{k-1}\frac{pA_p}{z^{p+1}} - \frac{A}{2}\sum_{k=1}^{s}(b_k - ia_k)\left(\frac{z}{R}\right)^k$$

$$-\left(\overline{X_1} - A\right)\left[1 + \frac{1}{2}\sum_{k=1}^{s}\left[(b_k + ia_k)\left(\frac{R}{z}\right)^k + (b_k - ia_k)\left(\frac{z}{R}\right)^k\right]\right] - \frac{2\delta_o\varepsilon_1}{\left(\frac{\kappa_M}{\mu_M} + \frac{1}{\mu_I}\right)}$$

$$-\delta_o\eta\left(\overline{X_1} - A\right) + A\left(\delta_o - 1\right).$$

Equating the coefficients for all the non-positive powers of z (i.e. $z^{-s}, z^{-s+1}, ..., z^{-1}$) in the above expression gives s conditions that satisfy

$$\frac{1}{2}\sum_{k=1}^{s}(b_k + ia_k)\left(\frac{R}{z}\right)^k \sum_{r=0}^{k} rQ_r z^{r-1} = \frac{1}{2}\sum_{k=1}^{s}(b_k + ia_k)\left(\frac{R}{z}\right)^k \sum_{r=0}^{k} rX_r z^{r-1}$$

which proves that any analytic solution $\Phi_I(z)$ of (3.12) automatically satisfies the consistency condition given by (3.18). On the other hand, no such consistency condition exists for the analytic solution $\Phi_M(z)$ in D_M. However, for completeness, one can show that any admissable analytic solution $\Phi_M(z)$ (say $\Phi_M(z) = Az + \sum_{p=0}^{\infty} T_p z^{-p}$) of (3.14) leads to $(s-1)$ conditions for the unknown coefficients A_i^s. Proceeding in a similar manner as above and noting that the non-homogeneous term $G(z)$ similarly includes s unknown constants $X_k (k = 1, 2, ..., s)$ and $(s-1)$

unknown constants $A_k (k = 1, 2, ..., s-1)$, substituting this expansion into (3.14) yields

$$-A + \sum_{p=0}^{\infty} p\frac{T_p}{z^{p+1}} - \frac{1}{2}\sum_{k=1}^{s}\left[(b_k + ia_k)\left(\frac{R}{z}\right)^k + (b_k - ia_k)\left(\frac{z}{R}\right)^k\right]\left[A - \sum_{p=0}^{\infty} p\frac{T_p}{z^{p+1}}\right] +$$

$$A\delta_o + \delta_o \sum_{p=0}^{\infty} p\frac{T_p}{z^{p+1}} = \frac{1}{2}\sum_{k=1}^{s}(b_k + ia_k)\left(\frac{R}{z}\right)^k \sum_{r=0}^{k} rX_r z^{r-1} + \delta_o \eta \overline{B}\left(\frac{R}{z}\right)^2 +$$

$$A(\delta_o - 1) + \frac{\overline{B}}{2}\sum_{k=2}^{s}(b_k - ia_k)\left(\frac{z}{R}\right)^{k-2} + \frac{1}{2}\sum_{k=1}^{s}(b_k - ia_k)\left(\frac{z}{R}\right)^k \sum_{p=0}^{k-1} p\frac{A_p}{z^{p+1}} -$$

$$\frac{A}{2}\sum_{k=1}^{s}(b_k - ia_k)\left(\frac{z}{R}\right)^k - \overline{B}\left(\frac{R}{z}\right)^2\left[1 + \frac{1}{2}\sum_{k=1}^{s}\left[(b_k + ia_k)\left(\frac{R}{z}\right)^k + (b_k - ia_k)\left(\frac{z}{R}\right)^k\right]\right]$$

$$+\frac{\delta_o}{z}\left[\frac{\dfrac{\overline{C_1}}{\mu_M} - \dfrac{\overline{C_2}}{\mu_I}}{\dfrac{\kappa_M}{\mu_M} + \dfrac{1}{\mu_I}}\right] + 2\delta_o\left(\frac{R}{z}\right)^2\left(\frac{\varepsilon_2 + i\varepsilon_3}{\dfrac{\kappa_M}{\mu_M} + \dfrac{1}{\mu_I}}\right) + \frac{1}{2}(\overline{X_1} - A)\sum_{k=1}^{s}(b_k + ia_k)\left(\frac{R}{z}\right)^k.$$

Equating the coefficients of all positive powers of z including z^0 gives $(s-1)$ conditions that satisfy

$$\frac{1}{2}\sum_{k=1}^{s}(b_k - ia_k)\left(\frac{z}{R}\right)^k \sum_{p=0}^{k-1}\frac{pT_p}{z^{p+1}} = \frac{1}{2}\sum_{k=1}^{s}(b_k - ia_k)\left(\frac{z}{R}\right)^k \sum_{p=0}^{k-1}\frac{pA_p}{z^{p+1}}.$$

In addition, the admissable analytic solution of (3.12) must also satisfy the additional condition

$$X_o = \Phi_I(0) \equiv 0. \tag{3.19}$$

The presence of singular points, such as isolated singular points or branch points of the multi-valued functions appearing in (3.12 - 3.17), means that the solution

of $\Phi_I(z)$ and $\Phi_M(z)$ are, in general, defined only in a simply connected domain obtained by cutting D_I and D_M, respectively, along appropriately chosen lines. However, $\Phi_I(z)$ and $\Phi_M(z)$ given by (3.16) and (3.17), respectively, are in general, not analytic in their respective uncut domains. For example, Φ_I and/or Φ_M can become discontinuous across branch cuts and/or they become unbounded at some or all isolated singular points. Therefore, to ensure the analyticity of Φ_I and Φ_M in their respective uncut domains one must verify the following:

- Φ_I and Φ_M given by (3.16) and (3.17), respectively, must be bounded at all singular points within their respective domains, and
- Φ_I and Φ_M given by (3.16) and (3.17), respectively, must be continuous across all branch cuts within their respective domains.

In summary, the solutions for Φ_I and Φ_M, in general, are *coupled* and are given by (3.16) and (3.17), respectively, include a total of $(2s-1)$ undetermined constants $X_k(k = 1, 2, ..., s)$ and $A_k(k = 1, 2, ..., s-1)$. These constants are determined via the analyticity requirements of Φ_I and Φ_M as well as the consistency condition given by (3.19). In the following section, a particular class of inhomogeneous spring - layer interface will be examined in order to illustrate the method.

3.3. A Class of Inhomogeneous Spring - Layer Interface

As a means of illustrating the method, consider the class of inhomogeneous spring - layer interfaces defined by (3.6) and given as follows (see Figure 3-2)

$$f(\theta) = b_s \cos(s\theta) = \frac{b_s}{2}\left(\frac{z^s}{R^s} + \frac{R^s}{z^s}\right), \qquad -1 < b_s < 1. \tag{3.20}$$

As stated previously, because of the presence of the variable parameter, Φ_I and Φ_M contain variable coefficients. However, by considering the roots of the polynomial $[1 + f(z)]$, the variation is eliminated and a solution can be obtained. Therefore, in view of (3.20), let us consider the roots of the following polynomial in (z/R):

$$\left(\frac{z}{R}\right)^{2s} + \frac{2}{b_s}\left(\frac{z}{R}\right)^{s} + 1 = 0. \tag{3.21}$$

Clearly, it is not difficult to see that if (z^*/R) is a root of (3.21) then it must be that $(R/\overline{z^*})$ is also a root. Furthermore, since $1 + f(z) > 0$ on Γ, the polynomial (3.21) has no roots on Γ. Hence, of the $2s$ roots of the polynomial, s are located inside the circular inclusion and the remaining s roots lie outside the inclusion [79].

Let the s roots located within the inclusion be denoted as

$$\rho_1, \rho_2, \cdots, \rho_s.$$

Similarly, the s roots located outside the inclusion are denoted as

$$\frac{1}{\rho_1}, \frac{1}{\rho_2}, \ldots, \frac{1}{\rho_s}.$$

The s roots within the inclusion can be determined by

$$\left(\frac{z}{R}\right)^s = \rho^s = \rho^*. \tag{3.22}$$

Substituting (3.22) into (3.21) yields the following expression for ρ^*:

$$\rho^* = \begin{cases} -\sqrt{\dfrac{1}{b_s^2} - 1} - \dfrac{1}{b_s} > 0, & \text{if } b_s < 0, \\ \sqrt{\dfrac{1}{b_s^2} - 1} - \dfrac{1}{b_s} < 0, & \text{if } b_s > 0, \end{cases} \tag{3.23}$$

where ρ^* is a real number contained in the open interval $-1 < \rho^* < 1$.

In particular note that

$$-\frac{2}{b_s} = \frac{1 + \rho^{*2}}{\rho^*},$$

from which it follows that

$$b_s^2 \rightarrow 1 \text{ as } \rho^{*2} \rightarrow 1,$$

$$\rho^* \rightarrow -\frac{b_s}{2} \text{ as } b_s \rightarrow 0.$$

Having resolved the issue of how to deal with the variable parameter, the solution for Φ_I and Φ_{AI} can now be obtained, respectively.

Note that (see Appendix A for details)

$$\frac{R\delta_o}{z[1+f(z)]} = \frac{-\lambda\left(\frac{z}{R}\right)^{s-1}}{\left[\left(\frac{z}{R}\right)^s - \rho^s\right]} + \frac{\lambda\left(\frac{z}{R}\right)^{s-1}}{\left[\left(\frac{z}{R}\right)^s - \frac{1}{\rho^s}\right]} \tag{3.24}$$

$$\lambda = -\delta_o\left(\frac{1+\rho^{s2}}{1-\rho^{s2}}\right) < 0$$

and

$$\frac{1}{1+f(z)} = \frac{\left(\frac{2}{b_o}\right)\left(\frac{z}{R}\right)^s}{\left[\left(\frac{z}{R}\right)^s - \rho^s\right]\left[\left(\frac{z}{R}\right)^s - \frac{1}{\rho^s}\right]}. \tag{3.25}$$

Substituting (3.24 - 3.25) into (3.16) and (3.17), the general solutions of Φ_I and Φ_M take the following form, respectively (see Appendix B for details):

$$\Phi_I(z) = \frac{2}{b_o}\left[\left(\frac{z}{R}\right)^s - \rho^s\right]^{\frac{\lambda\varrho}{s}}\left[\left(\frac{z}{R}\right)^m - \frac{1}{\rho^s}\right]^{\frac{-\lambda\varrho}{s}} \tag{3.26}$$
$$\int_{R\rho_1}^{z} F(t)\left(\frac{t}{R}\right)^s\left[\left(\frac{t}{R}\right)^s - \rho^s\right]^{-\left(\frac{\lambda\varrho}{s}+1\right)}\left[\left(\frac{t}{R}\right)^s - \frac{1}{\rho^s}\right]^{\frac{\lambda\varrho}{s}-1} dt \quad , z \in D_I$$

and

$$\Phi_M(z) = \frac{2}{b_o}\left[\left(\frac{z}{R}\right)^s - \rho^s\right]^{\frac{-\lambda}{s}}\left[\left(\frac{z}{R}\right)^s - \frac{1}{\rho^s}\right]^{\frac{\lambda}{s}} \tag{3.27}$$
$$\int_{R/\rho_1}^{z} G(t)\left(\frac{t}{R}\right)^s\left[\left(\frac{t}{R}\right)^s - \rho^s\right]^{\frac{\lambda}{s}-1}\left[\left(\frac{t}{R}\right)^s - \frac{1}{\rho^s}\right]^{-\left(\frac{\lambda}{s}+1\right)} dt \quad , z \in D_M.$$

The solutions Φ_I and Φ_M given by (3.26) and (3.27), respectively, are each well-defined in their respective domains. In each case, the domain is cut along

some non-intersecting straight lines originating from each of the branch points (i.e. $z = R\rho_k$ and $z = \frac{R}{\rho_k}$, $k = 1, 2, ..., s$). In other words, in each domain, branch cuts are made from each of the s branch points of the multi-valued functions appearing in (3.26) and (3.27) with each branch cut running parallel to the real axis in such a way that there is no overlap. Since $\lambda < 0$ and $\beta > 0$ the integrals in (3.26) and (3.27) converge at each of their respective branch points (i.e. the integrals in (3.26) and (3.27) are weakly singular kernels in their respective domains). In addition, to guarantee that $\Phi_I(z)$ and $\Phi_M(z)$ remain bounded at $z = R\rho_1$ and $z = \frac{R}{\rho_1}$, it must be that $C_o = H_o = 0$, respectively. The remaining $2s - 1$ unknown constants X_k $(k = 1, 2, ..., s)$ and $A_k (k = 1, 2, ..., s-1)$ are determined by $2(s-1)$ boundedness conditions given by

$$\int_{R\rho_1}^{R\rho_k} F(t)\left(\frac{t}{R}\right)^s \left[\left(\frac{t}{R}\right)^s - \rho^s\right]^{-\left(\frac{\lambda\beta}{s}+1\right)} \left[\left(\frac{t}{R}\right)^s - \frac{1}{\rho^s}\right]^{\frac{\lambda\beta}{s}-1} dt = 0, \quad k = 2, 3, ..., s \tag{3.28}$$

and

$$\int_{R/\rho_1}^{R/\rho_k} G(t)\left(\frac{t}{R}\right)^s \left[\left(\frac{t}{R}\right)^s - \rho^s\right]^{\frac{\lambda}{s}-1} \left[\left(\frac{t}{R}\right)^s - \frac{1}{\rho^s}\right]^{-\left(\frac{\lambda}{s}+1\right)} dt = 0, \quad k = 2, 3, ..., s \tag{3.29}$$

in addition to condition (3.19).

It remains to prove that $\Phi_I(z)$ and $\Phi_M(z)$ given by (3.26) and (3.27), respectively, are continuous across each of their respective s branch cuts. Consider, first, $\Phi_I(z)$. Following the procedure used in [79], consider the difference $\Phi_I(z^+) - \Phi_I(z^-)$, where $\Phi_I(z^\pm)$ denotes the values of $\Phi_I(z)$ as z approaches the branch cut from above and below, respectively. By taking the integration path along the edges of any one of the s branch cuts made from $z = R\rho_k, k = 1, 2, ...s$ and passing through any one of the s integrable branch points, noting the compensating nature of the terms outside the integral, we obtain $\Phi_I(z^+) = \Phi_I(z^-)$. This implies that $\Phi_I(z)$ is continuous across each of the s branch cuts (see Figure 3-3). A similar procedure can be applied to $\Phi_M(z)$. Hence, both $\Phi_I(z)$ and $\Phi_M(z)$ are continuous across each branch cut in their respective domains.

Remark 1. *Once Φ_I and Φ_M have been determined, the remaining stress potentials Ψ_I and Ψ_M can be determined from condition (2.10).*

3.4. Summary

This chapter has presented the rigorous solution method of a model of a circular inclusion with circumferentially inhomogeneous imperfect damage characterized by the spring - layer interface condition $m(\theta) = n(\theta)$. Our method has been devel-

oped as a consequence of the fact that the circumferential variation of the interface parameter leads to the failure of the conventional power series method. Instead analytic continuation is used to obtain exact closed form solutions, for a particular class of circumferentially inhomogeneous spring - layer interface, in which any of the $(2s-1)$ unknown constants X_k and A_k can be determined from analyticity requirements and certain other supplementary conditions. This method will be illustrated for two specific variations of the interface parameter in Chapter 4.

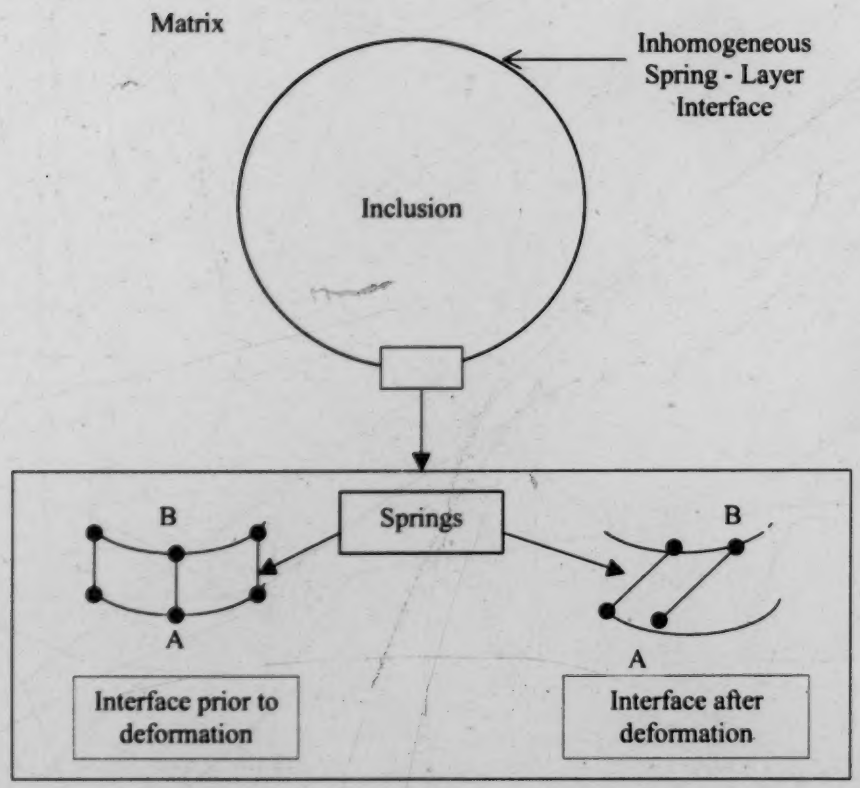

Figure 3-1. Schematic Representation of Inhomogeneous Spring – Layer Interface before and after Deformation

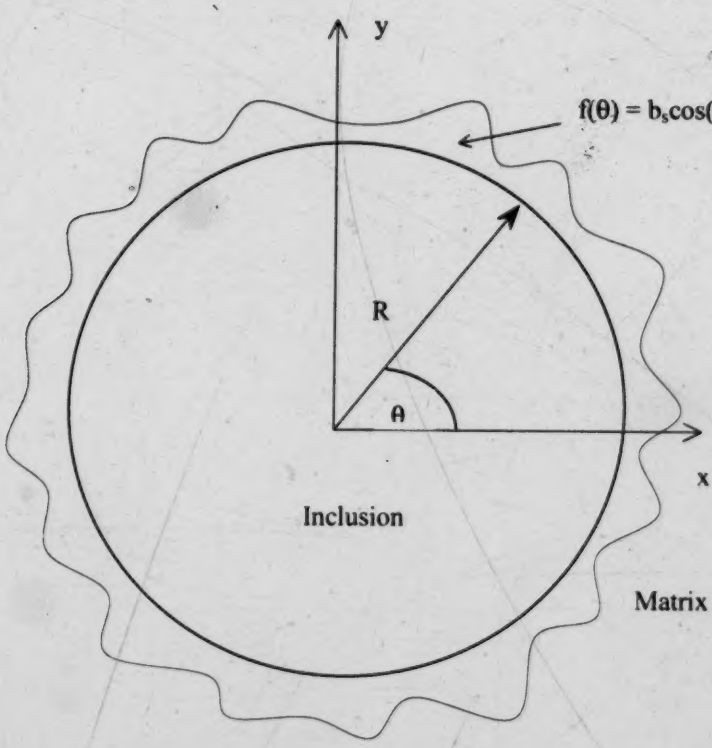

Figure 3-2. Schematic Representation of the Inhomogeneous Spring – Layer Interface

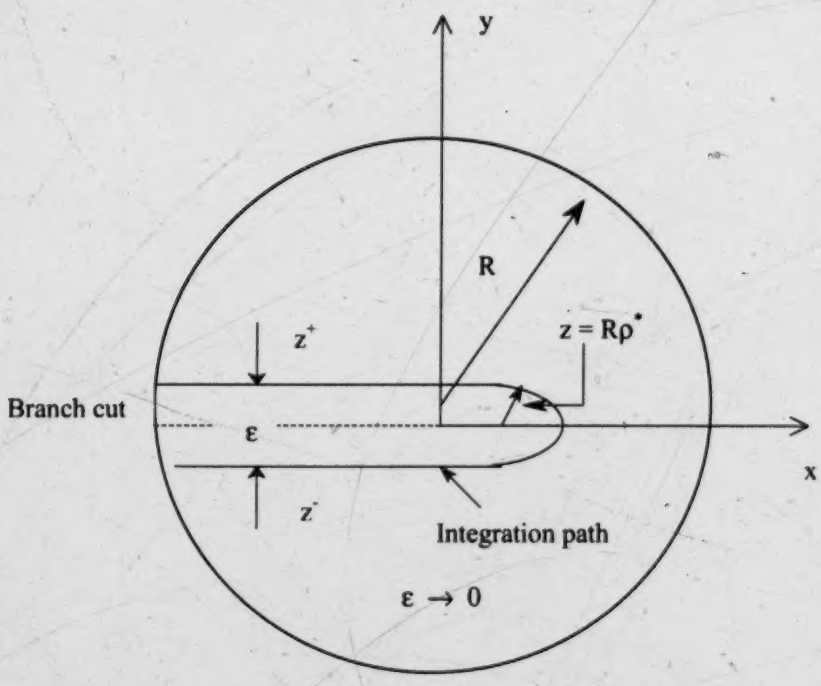

Figure 3-3. Continuity of $\Phi_I(z)$ across the Branch Cut: $\Phi_I(z^+) = \Phi_I(z^-)$

CHAPTER 4

Examples of the Inhomogeneous Spring - Layer Interface

4.1. Introduction

This chapter presents examples illustrating the methodology of the solution process derived in Chapter 3. In particular, two specific examples corresponding to the functional form of the inhomogeneous imperfect interface will be illustrated. In the first case, the equations for the stress potentials, Φ_I and Φ_M, are decoupled and the solution process is relatively straightforward. However, in the more general cases when the variation in interfacial damage becomes larger (i.e. the circumferential number $s > 1$) the equations for the stress potentials, Φ_I and Φ_M, are coupled and the solution process becomes more involved. Thus, in the second case, the solution method is extended to deal with the more general coupling problem. Note that the variation or distribution in interface imperfections depends on the specific value of the circumferential parameter s. Therefore, if the maximum order of the polynomial that describes the inhomogeneous interface takes on the value $s = 2$, the distribution of imperfections along the material interface corresponding to this

case is greater than that corresponding to a distribution of imperfections given by say $s = 1$. Hence, the larger the order of the polynomial (i.e. circumferential number), describing the inhomogeneous interface, the greater the distribution of interface imperfection.

In addition, the effects of the circumferential inhomogeneous interface parameter on the average mean, deviatoric and shear stresses induced within the inclusion will be examined for both the coupled and decoupled case, respectively.

4.2. Inhomogeneous Spring - Layer Interface with Circumferential Number $s = 1$

In this situation, the functional form of the inhomogeneous imperfect interface takes the form (see Figure 4-1)

$$f(z) = \frac{b_1}{2}\left(\frac{z}{R} + \frac{R}{z}\right), \quad -1 < b_1 < 1, \tag{4.1}$$

and by confining ourselves to the case $\beta = 1$ with $s = 1$ the equations for Φ_I and Φ_M [see equations (3.26) and (3.27)] are respectively given by

$$\Phi_I(z) = \frac{2}{b_1}\left[\frac{z}{R} - \rho^*\right]^{\lambda}\left[\frac{z}{R} - \frac{1}{\rho^*}\right]^{-\lambda} \times$$

$$\int_{R\rho^*}^{z} F(t)\left(\frac{t}{R}\right)\left[\frac{t}{R} - \rho^*\right]^{-(\lambda+1)}\left[\frac{t}{R} - \frac{1}{\rho^*}\right]^{\lambda-1} dt, \quad z \in D_I, \tag{4.2}$$

and

$$\Phi_M(z) = \frac{2}{b_1}\left[\frac{z}{R} - \rho^*\right]^{-\lambda}\left[\frac{z}{R} - \frac{1}{\rho^*}\right]^{\lambda} \times$$

$$\int_{R/\rho^*}^{z} G(t)\left(\frac{t}{R}\right)\left[\frac{t}{R} - \rho^*\right]^{\lambda-1}\left[\frac{t}{R} - \frac{1}{\rho^*}\right]^{-(\lambda+1)} dt, \quad z \in D_M. \tag{4.3}$$

The non-homogeneous terms $F(t)$ and $G(t)$, as determined by conditions (3.13) and (3.15), are respectively given by

$$F(t)\left(\frac{t}{R}\right) = \frac{b_1 X_1}{2} - \frac{b_1 \overline{X_1}}{2}\left(\frac{t}{R}\right)^2 -$$

$$\left[\overline{X_1}(1+\delta_o\eta) - A\delta_o(1+\eta) + \frac{2\delta_o\varepsilon_1}{\left(\frac{\kappa_M}{\mu_M} + \frac{1}{\mu_I}\right)}\right]\left(\frac{t}{R}\right) \tag{4.4}$$

and

$$G(t)\left(\frac{t}{R}\right) = \overline{B}\frac{b_1}{2}\left(\frac{R}{t}\right)^2 + A\frac{b_1}{2}\left(\frac{t}{R}\right)^2 + \left[(1-\delta_o\eta)\overline{B} - \frac{2\delta_o(\varepsilon_2 + i\varepsilon_3)}{\left(\frac{\kappa_M}{\mu_M} + \frac{1}{\mu_I}\right)}\right]\left(\frac{R}{t}\right) \tag{4.5}$$

$$+ \left[\frac{b_1}{2}(A+\overline{B}) - \frac{b_1}{2}(X_1 + \overline{X_1}) - \frac{\delta_o}{R}\left(\frac{\frac{\overline{C_1}}{\mu_M} - \frac{\overline{C_2}}{\mu_I}}{\frac{\kappa_M}{\mu_M} + \frac{1}{\mu_I}}\right)\right] + A(1-\delta_o)\left(\frac{t}{R}\right).$$

Having the expressions for Φ_I and Φ_M, the solution procedure reduces to finding the solution for the unknown coefficient X_1. The coefficient X_1 is evaluated from the supplementary condition (3.19) which yields

$$0 = \frac{2}{b_1}(-\rho^*)^{\lambda}\left(-\frac{1}{\rho^*}\right)^{-\lambda} \times \tag{4.6}$$

$$\int_{R\rho^*}^{0} \frac{-\frac{b_1}{2}\overline{X_1}\left(\frac{t}{R}\right)^2 + \left[A\delta_o(1+\eta) - \overline{X_1}(1+\delta_o\eta) - \frac{2\delta_o\varepsilon_1}{\frac{\kappa_M}{\mu_M}+\frac{1}{\mu_I}}\right]\left(\frac{t}{R}\right) + \frac{b_1}{2}X_1}{\left[\frac{t}{R}-\rho^*\right]^{\lambda+1}\left[\frac{t}{R}-\frac{1}{\rho^*}\right]^{1-\lambda}} dt.$$

For example, if $\lambda = -1$, then by integrating (4.6), the general expression for X_1 is found to be

$$X_1\rho^{*4} + \overline{X_1}\left[\rho^{*4}(2+\delta_o\eta) - \rho^{*2}(1-\delta_o\eta)\right.$$

$$\left.+(1-\rho^{*2})\ln\left(\frac{1}{1-\rho^{*2}}\right)\left(1-\rho^{*2}-\delta_o\eta(1+\rho^{*2})\right)\right] = \left[A\delta_o(1+\eta) - \frac{2\delta_o\varepsilon_1}{\frac{\kappa_M}{\mu_M}+\frac{1}{\mu_I}}\right] \times$$

$$\left[(1+\rho^{*2})\left(\rho^{*2} - (1-\rho^{*2})\ln\left(\frac{1}{1-\rho^{*2}}\right)\right)\right] \quad ; \tag{4.7}$$

Having established the expression for the coefficient X_1, the solutions for the stress potentials Φ_I and Φ_M are obtained by integrating (4.2) and (4.3), respectively. The resulting expressions for Φ_I and Φ_M are respectively given by

$$\Phi_I(z) = \overline{X_1}\left[\begin{array}{c} R\left(\dfrac{2-\rho^{*2}}{\rho^*(1-\rho^{*2})}+\dfrac{2(1+\delta_o\eta)}{b_1(1-\rho^{*2})}\right)- \\ 2R\left(\dfrac{1}{\rho^*}+\dfrac{(1+\delta_o\eta)}{b_1}\right)\ln\left(\dfrac{1-\rho^*\left(\frac{z}{R}\right)}{1-\rho^{*2}}\right)\left(\dfrac{\frac{z}{R}-\frac{1}{\rho^*}}{\frac{z}{R}-\rho^*}\right)-z \end{array}\right]-$$

$$X_1R\left(\frac{\rho^*}{1-\rho^{*2}}\right)+\frac{2R}{b_1}\left(A\delta_o(1+\eta)-\frac{2\delta_o\varepsilon_1}{\dfrac{\kappa_M}{\mu_M}+\dfrac{1}{\mu_I}}\right)\times$$

$$\left[\ln\left(\frac{1-\rho^*\left(\frac{z}{R}\right)}{1-\rho^{*2}}\right)\left(\frac{\frac{z}{R}-\frac{1}{\rho^*}}{\frac{z}{R}-\rho^*}\right)-\frac{1}{1-\rho^{*2}}\right],\quad z\in D_I \tag{4.8}$$

and

$$\Phi_M(z) = Az+\left[\frac{\overline{B}R}{\rho^{*3}}(1+\eta)(1-\rho^{*2})+\frac{2R(1-\rho^{*2})(\varepsilon_2+i\varepsilon_3)}{\rho^{*3}\left(\dfrac{\kappa_M}{\mu_M}+\dfrac{1}{\mu_I}\right)}\right]\left[\frac{\frac{z}{R}-\rho^*}{\frac{z}{R}-\frac{1}{\rho^*}}\right]\log\left[\frac{1-\rho^{*2}}{1-\frac{R}{z}\rho^*}\right]$$

$$+\frac{\overline{B}R}{\left(\frac{z}{R}-\frac{1}{\rho^*}\right)}\left[\frac{R}{z\rho^*}-\frac{\rho^*\left(\frac{z}{R}-\rho^*\right)}{1-\rho^{*2}}\right]+\frac{\overline{B}R}{\rho^*(1-\rho^{*2})}\left[(1+\eta)(1+\rho^{*4})-2\eta\rho^{*2}\right]$$

$$+\frac{R\rho^*}{1-\rho^{*2}}\left(\overline{B}-2\,\mathrm{Re}[X_1]\right)+\frac{2R(\varepsilon_2+i\varepsilon_3)}{\rho^*\left(\dfrac{\kappa_M}{\mu_M}+\dfrac{1}{\mu_I}\right)}+\frac{\frac{\overline{B_o}}{\mu_M}-\frac{2\overline{X_2}R^2-A_o}{\mu_I}}{\left(\dfrac{\kappa_M}{\mu_M}+\dfrac{1}{\mu_I}\right)},\quad z\in D_M. \tag{4.9}$$

Note that the last term, containing the constants A_o, B_o and X_2 appearing in (4.9), need not be evaluated explicitly and in fact can be neglected. This is because it merely reflects a rigid body translation and as such has no physical influence on the corresponding stress fields. Furthermore, despite their relatively simple form, the solutions (4.8) and (4.9) cannot be obtained via the power series method since their series expansions are infinite sums.

Hence, equations (4.7 - 4.9) as well as equations (2.10) constitute the complete solution for a homogeneous elastic inclusion embedded within an infinite elastic matrix having a circumferentially inhomogeneous imperfect interface characterized by the spring - layer interface condition $m(\theta) = n(\theta)$ and the parameters $s = 1, \beta = 1$ and $\lambda = -1$. Having these expressions (i.e. Φ_I, Φ_M, Ψ_I and Ψ_M) the evaluation of the elastic field distributions can be obtained via (2.1). In particular, the average stress inside the circular inclusion can be determined, which, in turn, leads to the estimation the effective properties of the composite material through the known micromechanical models.

4.2.1. Average Stress

The calculation of the average stress inside an inclusion gives important information regarding the overall understanding and behavior of the composite material (see Chapter 1). In what follows, we examine the effects of the circumferential inhomogeneity of an imperfect interface on the average stress field induced within the circular inclusion when the inhomogeneous imperfect interface is characterized by the condition $m(\theta) = n(\theta)$ and the parameters $s = 1, \beta = 1$ and $\lambda = -1$. To do this, we compare the inhomogeneous spring - layer interface described by

$$\frac{1}{n(\theta)} = \frac{R\left(\frac{\kappa_M}{\mu_M} + \frac{1}{\mu_I}\right)}{2\delta_o}\left[1 + b_1\cos\theta\right], \qquad -1 < b_1 < 1,$$

$$\delta_o = \frac{1-\rho^{*2}}{1+\rho^{*2}}, \tag{4.10}$$

with the corresponding homogeneous spring - layer interface under otherwise identical conditions

$$\frac{1}{n} = \frac{R\left(\frac{\kappa_M}{\mu_M} + \frac{1}{\mu_I}\right)}{2\delta_o}, \qquad \delta_o = \frac{1-\rho^{*2}}{1+\rho^{*2}}. \tag{4.11}$$

The exact average stresses within the circular inclusion have been derived in Chapter 2 and are given by equations (2.20). Thus, for the average stress corresponding to a homogeneous spring - layer interface, the coefficients X_1 and A_1 need to be evaluated. This is achieved when the circumferential inhomogeneous interface parameter is zero (i.e. $\rho^* = 0$) (see Appendix C). Therefore, assuming zero eigenstrains, the average mean, deviatoric and shear stresses corresponding to a homogeneous spring - layer interface are given by

$$(\sigma_x + \sigma_y)^H_{Avg} = \frac{4A(1+\eta)(1-\rho^{*2})}{3+\eta+\rho^{*2}(3-\eta)},$$

$$\left(\frac{\sigma_y - \sigma_x}{2} + i\sigma_{xy}\right)^H_{Avg} = \frac{B}{2}(1+\eta)(1-\rho^{*2}). \tag{4.12}$$

Here the superscript H denotes stresses associated with a homogeneous interface.

Similarly, the average mean, deviatoric and shear stresses associated with the inhomogeneous spring - layer interface are given by

$$(\sigma_x+\sigma_y)_{Avg}=\frac{4A(1+\eta)\left[\rho^{*2}(1-\rho^{*2})-(1-\rho^{*2})^2\ln\left(\frac{1}{1-\rho^{*2}}\right)\right]}{\rho^{*4}(3-\eta)-(1-\eta)\left[\rho^{*2}-(1-\rho^{*2})^2\ln\left(\frac{1}{1-\rho^{*2}}\right)\right]},$$

$$\left(\frac{\sigma_y-\sigma_x}{2}+i\sigma_{xy}\right)_{Avg}=B\left[\frac{(1+\eta)\left[\rho^{*2}(1-\rho^{*2})+(1-\rho^{*2})^2\ln(1-\rho^{*2})\right]}{\rho^{*4}}\right]. \tag{4.13}$$

It follows that the ratios $q(\eta,\rho^*)$ and $\omega(\rho^*)$ of the average stresses (i.e. the ratio of each of the expressions in (4.13) to the corresponding expressions in (4.12)) is given by

$$(\sigma_x+\sigma_y)_{Avg}=q(\eta,\ \rho^*)\,(\sigma_x+\sigma_y)^H_{Avg},$$

$$q(\eta,\rho^*)=\frac{(3+\eta+\rho^{*2}(3-\eta))\left[\rho^{*2}-(1-\rho^{*2})\ln\left(\frac{1}{1-\rho^{*2}}\right)\right]}{\rho^{*4}(3-\eta)-(1-\eta)\left[\rho^{*2}-(1-\rho^{*2})^2\ln\left(\frac{1}{1-\rho^{*2}}\right)\right]} \tag{4.14}$$

and

$$\left(\frac{\sigma_y-\sigma_x}{2}+i\sigma_{xy}\right)_{Avg}=w(\rho^*)\left(\frac{\sigma_y-\sigma_x}{2}+i\sigma_{xy}\right)^H_{Avg},$$

$$w(\rho^*)=2\left[\frac{\rho^{*2}+(1-\rho^{*2})\ln(1-\rho^{*2})}{\rho^{*4}}\right]. \tag{4.15}$$

Note that both $q(\eta,\rho^*)$ and $\omega(\rho^*)$ are even functions.

The effects of the circumferential inhomogeneity of the interface, as represented by the functions $q(\eta, \rho^*)$ and $w(\rho^*)$ are given in Figures 4-2 and 4-3, respectively. These results show that replacing the inhomogeneous spring - layer interface by its homogeneous counterpart has a significant effect on the estimation of the average stresses induced within the inclusion. For example, by neglecting the inhomogeneity of interface imperfections (i.e. replacing the inhomogeneous spring - layer interface by its homogeneous counterpart), the relative error in the average mean stress approaches 200 % (Figure 4-2). Alternatively, the relative error in the average deviatoric and shear stresses approaches 100% (Figure 4-3). By comparison, in [80], Ru found that the circumferentially inhomogeneous imperfect interface in the case of the sliding interface has an negligible effect on the average stresses induced within the inclusion. Hence, for the first time in plane elasticity, our results demonstrate conclusively the significant effect of a varying pointwise inhomogeneous imperfect interface on the average stress field induced within a circular inclusion. Hence, replacing an inhomogeneous interface by its homogeneous counterpart will lead to significant errors in even the calculation of the average stresses.

4.3. Inhomogeneous Spring - Layer Interface with Circumferential Number $s = 2$

In this case, the functional form of the inhomogeneous imperfect interface takes the form (see Figure 4-4)

$$f(z) = \frac{b_2}{2}\left[\left(\frac{z}{R}\right)^2 + \left(\frac{R}{z}\right)^2\right], \quad -1 < b_2 < 1 \tag{4.16}$$

then the equations for the stress potentials, $\Phi_I(z)$ and $\Phi_M(z)$ (see equations (3.26) and (3.27)) are respectively given by

$$\Phi_I(z) = \frac{2}{b_2}\left[\left(\frac{z}{R}\right)^2 - \rho^*\right]^{\frac{\lambda\beta}{2}}\left[\left(\frac{z}{R}\right)^2 - \frac{1}{\rho^*}\right]^{-\frac{\lambda\beta}{2}} \times$$
$$\int_{R\rho_1}^{z} F(t)\left(\frac{t}{R}\right)^2\left[\left(\frac{t}{R}\right)^2 - \rho^*\right]^{-\left(\frac{\lambda\beta}{2}+1\right)}\left[\left(\frac{t}{R}\right)^2 - \frac{1}{\rho^*}\right]^{\frac{\lambda\beta}{2}-1} dt, \quad z \in D_I, \tag{4.17}$$

and

$$\Phi_M(z) = \frac{2}{b_2}\left[\left(\frac{z}{R}\right)^2 - \rho^*\right]^{-\frac{\lambda}{2}}\left[\left(\frac{z}{R}\right)^2 - \frac{1}{\rho^*}\right]^{\frac{\lambda}{2}} \times$$
$$\int_{R/\rho_1}^{z} G(t)\left(\frac{t}{R}\right)^2\left[\left(\frac{t}{R}\right)^2 - \rho^*\right]^{\frac{\lambda}{2}-1}\left[\left(\frac{t}{R}\right)^2 - \frac{1}{\rho^*}\right]^{-\left(\frac{\lambda}{2}+1\right)} dt, \quad z \in D_M. \tag{4.18}$$

As in the previous case, the non-homogeneous terms $F(t)$ and $G(t)$ are determined via conditions (3.13) and (3.15) and are respectively given by

$$F(t)\left(\frac{t}{R}\right)^2 = \frac{b_2}{2}\left[\frac{A_1}{t^2} - \overline{X_1}\right]\left(\frac{t}{R}\right)^4 + \left[A\delta_o(1+\eta) + \frac{b_2}{2}\overline{B} - \overline{X_1}(1+\delta_o\eta) - \frac{2\delta_o\varepsilon_1}{\frac{\kappa_M}{\mu_M}+\frac{1}{\mu_I}}\right]\left(\frac{t}{R}\right)^2 + \frac{b_2}{2}\left[X_1 + 2X_2 t\right], \tag{4.19}$$

and

$$G(t)\left(\frac{t}{R}\right)^2 = \frac{b_2}{2}A\left(\frac{t}{R}\right)^4 - \left[\frac{b_2}{2}\frac{A_1}{R^2} + A(\delta_o - 1)\right]\left(\frac{t}{R}\right)^2 - \frac{\delta_o}{R}\left[\frac{\frac{\overline{C_1}}{\mu_M} - \frac{\overline{C_2}}{\mu_I}}{\frac{\kappa_M}{\mu_M}+\frac{1}{\mu_I}}\right]\left(\frac{t}{R}\right) + \left[\overline{B}(1-\delta_o\eta) - \frac{2\delta_o(\varepsilon_2 + i\varepsilon_3)}{\frac{\kappa_M}{\mu_M}+\frac{1}{\mu_I}} - \frac{b_2}{2}\left(X_1 + \overline{X_1} - A\right)\right] + \frac{b_2}{2}\overline{B}\left(\frac{t}{R}\right)^2. \tag{4.20}$$

Note that unlike the case corresponding to the circumferential number $s = 1$, where Φ_I can be evaluated independently from Φ_M (i.e. Φ_I depends on the coefficient X_1 only). The case corresponding to the circumferential number $s = 2$ requires the evaluation of 3 coefficients (i.e. X_1, X_2 and A_1) in order to evaluate the stress potentials explicitly. The evaluation of the 3 unknown constants is achieved via the supplementary condition (3.19) and the boundedness conditions (3.28 - 3.29).

Therefore, the 3 unknown constants (X_1, X_2 and A_1) can be expressed in terms of definite integrals of known power functions. Hence, in view of (4.19) and (4.20), conditions (3.19) and (3.28 - 3.29) yield the following

$$\left[A\delta_o(1+\eta) + \overline{B}\frac{b_2}{2} + A_1\frac{b_2}{2R^2} - \overline{X_1}(1+\delta_o\eta) - \frac{2\delta_o\varepsilon_1}{\frac{\kappa_M}{\mu_M}+\frac{1}{\mu_I}}\right] I_{02} + b_2X_2RI_{01} + \frac{b_2}{2}X_1I_{00} - \frac{b_2}{2}\overline{X_1}I_{01} = 0, \tag{4.21}$$

$$\left[A\delta_o(1+\eta) + \overline{B}\frac{b_2}{2} + A_1\frac{b_2}{2R^2} - \overline{X_1}(1+\delta_o\eta) - \frac{2\delta_o\varepsilon_1}{\frac{\kappa_M}{\mu_M}+\frac{1}{\mu_I}}\right] I_{12} + b_2X_2RI_{11} + \frac{b_2}{2}X_1I_{10} - \frac{b_2}{2}\overline{X_1}I_{14} = 0 \tag{4.22}$$

and

$$A\frac{b_2}{2}M_{14} - \left[A_1\frac{b_2}{2R^2} + A(\delta_o - 1)\right] M_{12} - \frac{\delta_o}{R}\left[\frac{\frac{\overline{C_1}}{\mu_M} - \frac{\overline{C_2}}{\mu_I}}{\frac{\kappa_M}{\mu_M}+\frac{1}{\mu_I}}\right] M_{11} + \overline{B}\frac{b_2}{2}M_{12} + \left[\overline{B}(1-\delta_o\eta) - \frac{2\delta_o(\varepsilon_2+i\varepsilon_3)}{\frac{\kappa_M}{\mu_M}+\frac{1}{\mu_I}} - \frac{b_2}{2}\left(X_1 + \overline{X_1} - A\right)\right] M_{10} = 0. \tag{4.23}$$

Here,

$$I_{0k} = \frac{2}{b_2}(-\rho^*)^{\frac{\lambda\beta}{2}}\left(-\frac{1}{\rho^*}\right)^{-\frac{\lambda\beta}{2}}\int_{R\rho_1}^{0}\left(\frac{t}{R}\right)^k\left[\left(\frac{t}{R}\right)^2-\rho^*\right]^{-\left(\frac{\lambda\beta}{2}+1\right)}\left[\left(\frac{t}{R}\right)^2-\frac{1}{\rho^*}\right]^{\frac{\lambda\beta}{2}-1}dt,$$

$$I_{1k} = \int_{R\rho_1}^{R\rho_2}\left(\frac{t}{R}\right)^k\left[\left(\frac{t}{R}\right)^2-\rho^*\right]^{-\left(\frac{\lambda\beta}{2}+1\right)}\left[\left(\frac{t}{R}\right)^2-\frac{1}{\rho^*}\right]^{\frac{\lambda\beta}{2}-1}dt$$

$$k = 0, 1, 2 \text{ and } 4 \qquad (4.24)$$

and

$$M_{1k} = \int_{R/\rho_1}^{R/\rho_2}\left(\frac{t}{R}\right)^k\left[\left(\frac{t}{R}\right)^2-\rho^*\right]^{\frac{\lambda}{2}-1}\left[\left(\frac{t}{R}\right)^2-\frac{1}{\rho^*}\right]^{-\left(\frac{\lambda}{2}+1\right)}dt, \quad k = -2, 0, 1, 2 \text{ and } 4.$$

(4.25)

Note that M_{1k} has a singular point at $t = 0$ when the index $k = -2$. However, since M_{1k} can be regarded as a contour integral, it only depends on the end points and not the path of integration. In other words, since M_{1k} is defined only in the matrix, the value of M_{1k} must be independent of any contour C as long as C extends from R/ρ_1 to R/ρ_2, does not pass through the singular points of M_{1k} and lies entirely in D_M. In this way, the value of M_{1k} is assured.

Further, for $s = 2$, condition (3.22) gives

$$\rho^2 = \rho^*,$$

or by taking square roots we can choose

$$\begin{aligned} &\rho_2 = \sqrt{\rho^*}, \qquad \rho_1 = \sqrt{\rho^*}, \\ &\Longleftrightarrow \rho_2 = -\rho_1, \\ &\Longleftrightarrow \rho_2^2 = \rho_1^2 = \rho^*. \end{aligned} \tag{4.26}$$

Therefore, using condition (4.26) and the property of integrals of symmetric functions, $(4.24)_2$ and (4.25), for index $k = 1$, respectively yield

$$I_{11} = 0, \qquad M_{11} = 0. \tag{4.27}$$

In addition, for indexes $k = 0, 2$ and 4, (4.24) gives

$$\frac{I_{02}}{I_{00}} \equiv \frac{I_{12}}{I_{10}}, \qquad \frac{I_{04}}{I_{00}} \equiv \frac{I_{14}}{I_{10}}. \tag{4.28}$$

Hence, in view of conditions (4.27 - 4.28), equations (4.21 - 4.22) can be solved for X_2 to give

$$b_2 X_2 R\left(\frac{I_{01}}{I_{00}}\right) = 0,$$

and since $b_2\left(\frac{I_{01}}{I_{00}}\right) R \neq 0$, it must be that

$$X_2 = 0. \tag{4.29}$$

The remaining two coefficients, X_1 and A_1, can now be obtained from (4.22 - 4.23) and are given by

$$X_1\left[\frac{b_2}{2}\left(\frac{M_{10}}{M_{12}}-\frac{I_{10}}{I_{12}}\right)\right]+\overline{X_1}\left[\frac{b_2}{2}\left(\frac{M_{10}}{M_{12}}+\frac{I_{14}}{I_{12}}\right)+(1+\delta_o\eta)\right]= \tag{4.30}$$
$$A\left[\frac{b_2}{2}\left(\frac{M_{14}+M_{10}}{M_{12}}\right)+(1+\delta_o\eta)\right]+\overline{B}\left[\frac{b_2}{2}\left(1+\frac{M_{1-2}}{M_{12}}\right)+(1-\delta_o\eta)\frac{M_{10}}{M_{12}}\right]-$$
$$\frac{2\delta_o}{\frac{\kappa_M}{\mu_M}+\frac{1}{\mu_I}}\left[\varepsilon_1+(\varepsilon_2+i\varepsilon_3)\frac{M_{10}}{M_{12}}\right],$$

and

$$A_1\frac{b_2}{2R^2}=A\frac{b_2}{2}\left(\frac{M_{14}}{M_{12}}\right)+\overline{B}\frac{b_2}{2}\left(\frac{M_{1-2}}{M_{12}}\right) \tag{4.31}$$
$$+\left[\overline{B}(1-\delta_o\eta)-\frac{2\delta_o(\varepsilon_2+i\varepsilon_3)}{\frac{\kappa_M}{\mu_M}+\frac{1}{\mu_I}}-\frac{b_2}{2}\left(X_1+\overline{X_1}-A\right)\right]\left(\frac{M_{10}}{M_{12}}\right)+A(1-\delta_o),$$

respectively. In particular, if $\beta = 1$ and $\lambda = -2$, the relations (4.24) and (4.25) can be integrated to give the following expressions

$$\frac{I_{10}}{I_{12}} = \rho^* \left[\frac{\dfrac{2\rho^*}{1-\rho^{*2}} + \ln\left(\dfrac{1+\rho^*}{1-\rho^*}\right)}{\dfrac{2\rho^*}{1-\rho^{*2}} - \ln\left(\dfrac{1+\rho^*}{1-\rho^*}\right)} \right], \quad \frac{I_{14}}{I_{12}} = \frac{1}{\rho^*} \left[\frac{\dfrac{6\rho^* - 4\rho^{*3}}{1-\rho^{*2}} - 3\ln\left(\dfrac{1+\rho^*}{1-\rho^*}\right)}{\dfrac{2\rho^*}{1-\rho^{*2}} - \ln\left(\dfrac{1+\rho^*}{1-\rho^*}\right)} \right],$$

$$\frac{M_{10}}{M_{12}} = \frac{1}{\rho^*} \left[\frac{\dfrac{2\rho^*}{1-\rho^{*2}} - \ln\left(\dfrac{1+\rho^*}{1-\rho^*}\right)}{\dfrac{2\rho^*}{1-\rho^{*2}} + \ln\left(\dfrac{1+\rho^*}{1-\rho^*}\right)} \right], \quad \frac{M_{14}}{M_{12}} = \rho^* \left[\frac{\dfrac{6\rho^{*2} - 4}{\rho^*(1-\rho^{*2})} + 3\ln\left(\dfrac{1+\rho^*}{1-\rho^*}\right)}{\dfrac{2\rho^*}{1-\rho^{*2}} + \ln\left(\dfrac{1+\rho^*}{1-\rho^*}\right)} \right],$$

(4.32)

$$\frac{M_{1\text{-}2}}{M_{12}} = \frac{1}{\rho^{*2}} \left[\frac{\dfrac{6\rho^* - 4\rho^{*3}}{1-\rho^{*2}} - 3\ln\left(\dfrac{1+\rho^*}{1-\rho^*}\right)}{\dfrac{2\rho^*}{1-\rho^{*2}} + \ln\left(\dfrac{1+\rho^*}{1-\rho^*}\right)} \right].$$

Hence, by having explicit expressions in the form of definite integrals of known power functions for the unknown coefficients X_1 and A_1, the complete solution to the problem corresponding to a homogeneous circular inclusion embedded within an infinite elastic matrix having a circumferentially inhomogeneous imperfect interface characterized by the spring - layer interface condition $m(\theta) = n(\theta)$ and the parameters $s = 2, \beta = 1$ and $\lambda = -2$ is now known. As a result, the stress potentials Φ_I, Φ_M, Ψ_I and Ψ_M given by (4.17 - 4.18) and (2.10), respectively can now be evaluated and the complete elastic stress distribution is established.

4.3.1. Average Stress

In contrast to case corresponding to $s = 1$ where the complete solution is required for the calculation of the average stress (i.e. to calculate the coefficient A_1 requires the evaluation of $\Phi_M(z)$), the case corresponding to $s = 2$ does not require the evaluation of the stress potentials, Φ_I and/or Φ_M, because the exact expressions for X_1 and A_1 have been derived. Therefore, in view of (4.30 - 4.31), the exact average mean, deviatoric and shear stresses can be calculated through conditions (2.20) and the effects of the circumferential inhomogeneity of an imperfect interface on the average stress field within the inclusion can be examined.

To demonstrate this, as before, we compare the inhomogeneous spring - layer interface described by

$$\frac{1}{n(\theta)} = \frac{R\left(\frac{\kappa_M}{\mu_M} + \frac{1}{\mu_I}\right)}{2\delta_o}\left[1 + b_2 \cos 2\theta\right], \qquad -1 < b_2 < 1,$$

$$\delta_o = 2\left(\frac{1-\rho^{*2}}{1+\rho^{*2}}\right), \tag{4.33}$$

with the following corresponding homogeneous spring - layer interface under otherwise identical conditions

$$\frac{1}{n} = \frac{R\left(\frac{\kappa_M}{\mu_M} + \frac{1}{\mu_I}\right)}{2\delta_o}, \qquad \delta_o = 2\left(\frac{1-\rho^{*2}}{1+\rho^{*2}}\right). \tag{4.34}$$

In addition, for convenience, we assume that $\mathrm{Im}[B] = 0$ (a biaxial stress state)

and that all the eigenstrains vanish. Then the average mean, deviatoric and shear stresses associated with the homogeneous interface (4.34), for a uniaxial stress state in the x-direction (i.e. $2A + B = 0$), is given by

$$(\sigma_x + \sigma_y)^H_{Avg} = 4A\left[\frac{(1+\eta)+\rho^{*2}(1-\eta)}{(2+\eta)+\rho^{*2}(2-\eta)}\right]$$
$$\left(\frac{\sigma_y - \sigma_x}{2} + i\sigma_{xy}\right)^H_{Avg} = -\frac{4A}{3}\left[\frac{(1+\eta)+\rho^{*2}(1-\eta)}{1+\rho^{*2}}\right] \qquad (4.35)$$

where the superscript H denotes stresses associated with the homogeneous interface. Note that the derivations for the homogeneous coefficients corresponding to X_1 and A_1 is given in Appendix D.

The corresponding average mean, deviatoric and shear stress, associated with the inhomogeneous interface (4.33) is obtained from (4.30 - 4.31) and given by

$$(\sigma_x + \sigma_y)_{Avg} = 4A\frac{\rho^*\left[2\left(1+\frac{M_{1\ 2}}{M_{12}}\right)-\left(\frac{M_{14}}{M_{12}}+\frac{M_{10}}{M_{12}}\right)\right]+(1+\rho^{*2})\left(1-2\frac{M_{10}}{M_{12}}\right)+2\eta(1-\rho^{*2})\left(1+2\frac{M_{10}}{M_{12}}\right)}{\rho^*\left[\frac{I_{10}}{I_{12}}-\frac{I_{14}}{I_{12}}-2\frac{M_{10}}{M_{12}}\right]+(1+2\eta)+\rho^{*2}(1-2\eta)} \qquad (4.36)$$

and

$$\left(\frac{\sigma_y-\sigma_x}{2}+i\sigma_{xy}\right)_{Avg}=-A\left\{\frac{1}{\rho^*}(1+\rho^*)(3\rho^*-1)-\left[\frac{M_{14}+M_{10}-2M_{1\text{-}2}}{M_{12}}\right]-2\left(\frac{M_{10}}{M_{12}}\right)\left[\frac{(1-2\eta)+\rho^{*2}(1+2\eta)}{\rho^*}\right]+2\left(\frac{M_{10}}{M_{12}}\right)\left[\frac{\rho^*\left[2\left(1+\frac{M_{1\text{-}2}}{M_{12}}\right)-\left(\frac{M_{14}}{M_{12}}+\frac{M_{10}}{M_{12}}\right)\right]+(1+\rho^{*2})\left(1-2\frac{M_{10}}{M_{12}}\right)+2\eta(1-\rho^{*2})\left(1+2\frac{M_{10}}{M_{12}}\right)}{\rho^*\left[\frac{I_{10}}{I_{12}}-\frac{I_{14}}{I_{12}}-2\frac{M_{10}}{M_{12}}\right]+(1+2\eta)+\rho^{*2}(1-2\eta)}\right]\right\},\tag{4.37}$$

respectively. It follows that the ratio $g(n,\rho^*)$ and $R(\eta,\rho^*)$ of the average stresses (i.e. the ratio of each the expressions in (4.37) and (4.36) to the corresponding expression in (4.35)) is given by

$$(\sigma_x + \sigma_y)_{Avg} = g(\eta, \rho^*)\,(\sigma_x + \sigma_y)^H_{Avg},$$

$$g(\eta,\rho^*) = \left[\begin{array}{c} \rho^*\left[2\left(1+\dfrac{M_{1\text{-}2}}{M_{12}}\right) - \left(\dfrac{M_{14}}{M_{12}} + \dfrac{M_{10}}{M_{12}}\right)\right] + (1+\rho^{*2})\left(1 - 2\dfrac{M_{10}}{M_{12}}\right) + \\ 2\eta\,(1-\rho^{*2})\left(1+2\dfrac{M_{10}}{M_{12}}\right) \\ \hline \rho^*\left[\dfrac{I_{10}}{I_{12}} - \dfrac{I_{14}}{I_{12}} - 2\dfrac{M_{10}}{M_{12}}\right] + (1+2\eta) + \rho^{*2}\,(1-2\eta) \end{array}\right] \times$$

$$\left[\frac{(2+\eta) + \rho^{*2}\,(2-\eta)}{(1+\eta) + \rho^{*2}\,(1-\eta)}\right], \tag{4.38}$$

and

$$\left(\frac{\sigma_y - \sigma_x}{2} + i\sigma_{xy}\right)_{Avg} = R(\eta,\rho^*)\left(\frac{\sigma_y - \sigma_x}{2} + i\sigma_{xy}\right)^H_{Avg},$$

$$R(\eta,\rho^*) = \left\{\frac{1}{\rho^*}(1+\rho^*)(3\rho^* - 1) - \left[\frac{M_{14} + M_{10} - 2M_{1\text{-}2}}{M_{12}}\right] - 2\left(\frac{M_{10}}{M_{12}}\right)\left[\frac{(1-2\eta) + \rho^{*2}\,(1+2\eta)}{\rho^*}\right] + 2\left(\frac{M_{10}}{M_{12}}\right)\left[\begin{array}{c} \rho^*\left[2\left(1+\dfrac{M_{1\text{-}2}}{M_{12}}\right) - \left(\dfrac{M_{14}}{M_{12}} + \dfrac{M_{10}}{M_{12}}\right)\right] + (1+\rho^{*2})\left(1 - 2\dfrac{M_{10}}{M_{12}}\right) + \\ 2\eta\,(1-\rho^{*2})\left(1+2\dfrac{M_{10}}{M_{12}}\right) \\ \hline \rho^*\left[\dfrac{I_{10}}{I_{12}} - \dfrac{I_{14}}{I_{12}} - 2\dfrac{M_{10}}{M_{12}}\right] + (1+2\eta) + \rho^{*2}\,(1-2\eta) \end{array}\right]\right\} \times$$

$$\frac{3}{4}\left[\frac{1+\rho^{*2}}{(1+\eta) + \rho^{*2}\,(1-\eta)}\right] \tag{4.39}$$

where $M_{10}, M_{12}, M_{14}, M_{1-2}, I_{10}, I_{12}$ and I_{14} are given by (4.32).

In addition, let us consider the case when the stress state is equal biaxial (i.e. $B = 0$). In this case the average mean stress associated with homogeneous interface (4.34) is given by

$$(\sigma_x + \sigma_y)^H_{Avg} = 4A\left[\frac{1+\eta+\rho^{*2}(1-\eta)}{2+\eta+\rho^{*2}(2-\eta)}\right], \tag{4.40}$$

and the corresponding average mean stress, associated with the inhomogeneous interface (4.33) is given by

$$(\sigma_x + \sigma_y)_{Avg} = 4A\left[\frac{1+2\eta+\rho^{*2}(1-2\eta)-\rho^*\left(\dfrac{M_{14}+M_{10}}{M_{12}}\right)}{\rho^*\left(\dfrac{I_{10}-I_{14}}{I_{12}}-2\dfrac{M_{10}}{M_{12}}\right)+1+2\eta+\rho^{*2}(1-2\eta)}\right]. \tag{4.41}$$

It follows that the ratio $h(\eta, \rho^*)$ of the average mean stresses (i.e. the ratio of the expression in (4.41) to the corresponding expression in (4.40)) is given by:

$$(\sigma_x + \sigma_y)_{Avg} = h(\eta,\ \rho^*)\,(\sigma_x + \sigma_y)^H_{Avg},$$

$$h(\eta,\ \rho^*) = \frac{\left[1+2\eta+\rho^{*2}(1-2\eta)-\rho^*\left(\dfrac{M_{14}+M_{10}}{M_{12}}\right)\right][2+\eta+\rho^{*2}(2-\eta)]}{\left[\rho^*\left(\dfrac{I_{10}-I_{14}}{I_{12}}-2\dfrac{M_{10}}{M_{12}}\right)+1+2\eta+\rho^{*2}(1-2\eta)\right][1+\eta+\rho^{*2}(1-\eta)]}. \tag{4.42}$$

The effects of the circumferential inhomogeneity of the interface, as represented by the functions $g(\eta,\rho^*), R(\eta,\rho^*)$ and $h(\eta,\rho^*)$ for the respective loading conditions, are illustrated in Figures 4-5, 4-6 and 4-7, respectively for several different

values of the parameter η. These results reinforce those established in section 4.2.1: that replacing the inhomogeneous spring - layer interface by its homogeneous counterpart has a significant effect on the estimation of even the average stresses induced within the inclusion. For example, for the case corresponding to the uniaxial stress state in the x-direction, replacing the inhomogeneous interface (4.33) by its homogeneous counterpart (4.34) leads to a relative error approaching 66% in the average deviatoric and shear stresses (Figure 4-6). Similarly, for the equal biaxial stress state, the relative error in the average mean stress approaches 95% (Figure 4-7). By comparison, in [80], Ru found that the circumferentially inhomogeneous imperfect interface in the case of the sliding interface has an negligible effect on the average stresses induced within the inclusion. Hence, once again, the results demonstrate convincingly the significant effect that a varying pointwise inhomogeneous imperfect interface has on even the average stress field induced within a circular inclusion.

4.4. Summary

A rigorous systematic study for two specific variations of the inhomogeneous spring - layer interface has been given. The results, from both these examples, clearly illustrate how the circumferential variation of the interface parameter has a signif-

icant and pronounced effect on even the calculation of the average stresses induced within the inclusion. Hence, replacing the inhomogeneous spring - layer interface by its homogeneous counterpart will significantly affect the stress field distributions. In addition, the results suggest that the influence of the inhomogeneity of interface imperfections, on the average stress, decreases with increasing circumferential number.

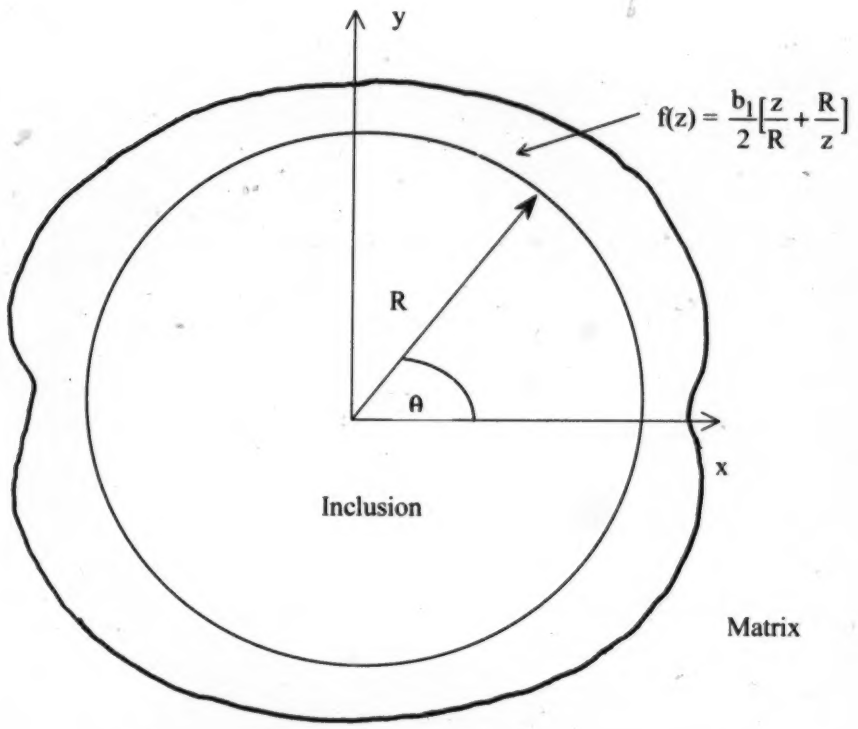

Figure 4 - 1. Schematic Representation of the Inhomogeneous Spring – Layer Interface having Circumferential Number s = 1

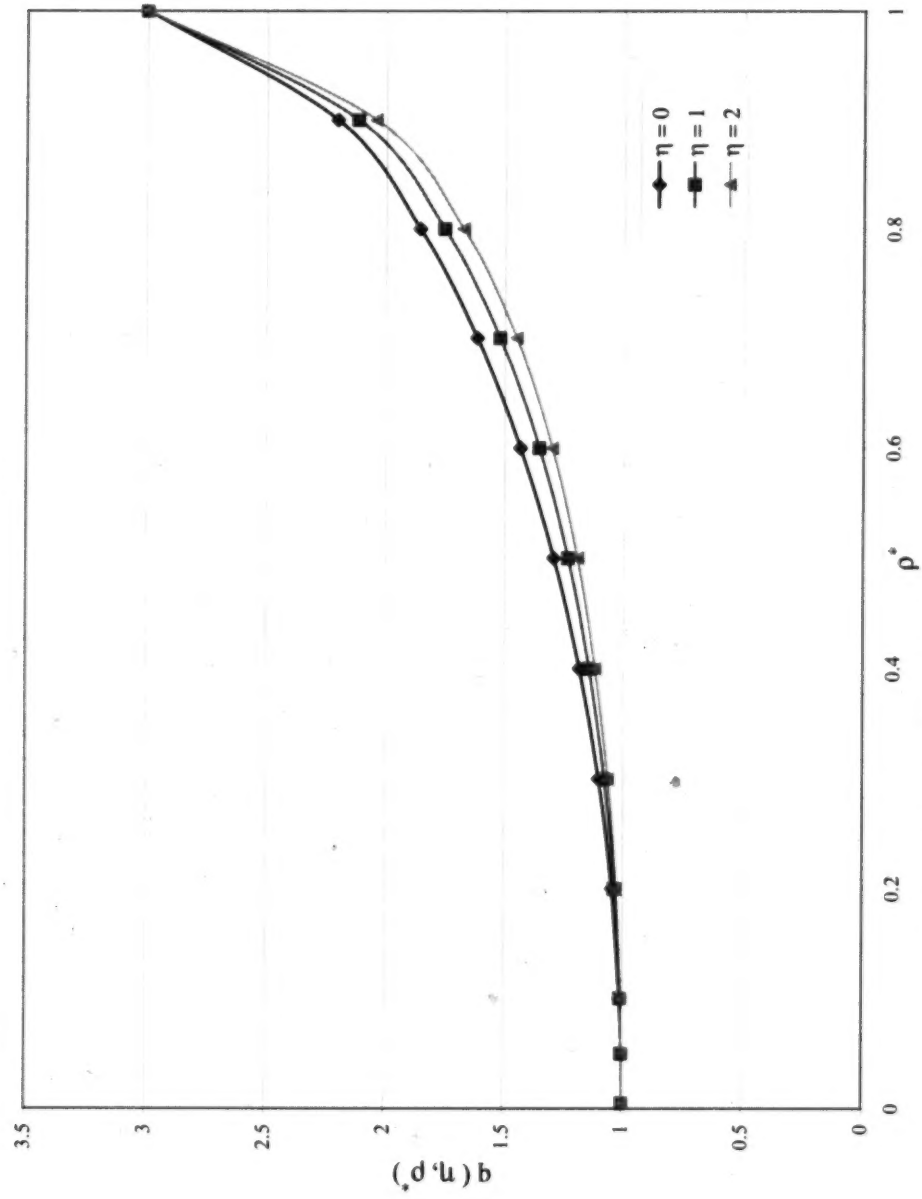

Figure 4-2. The Effect of the Circumferential Inhomogeneity on the Average Mean Stress inside the Circular Inclusion having Circumferential Number s = 1

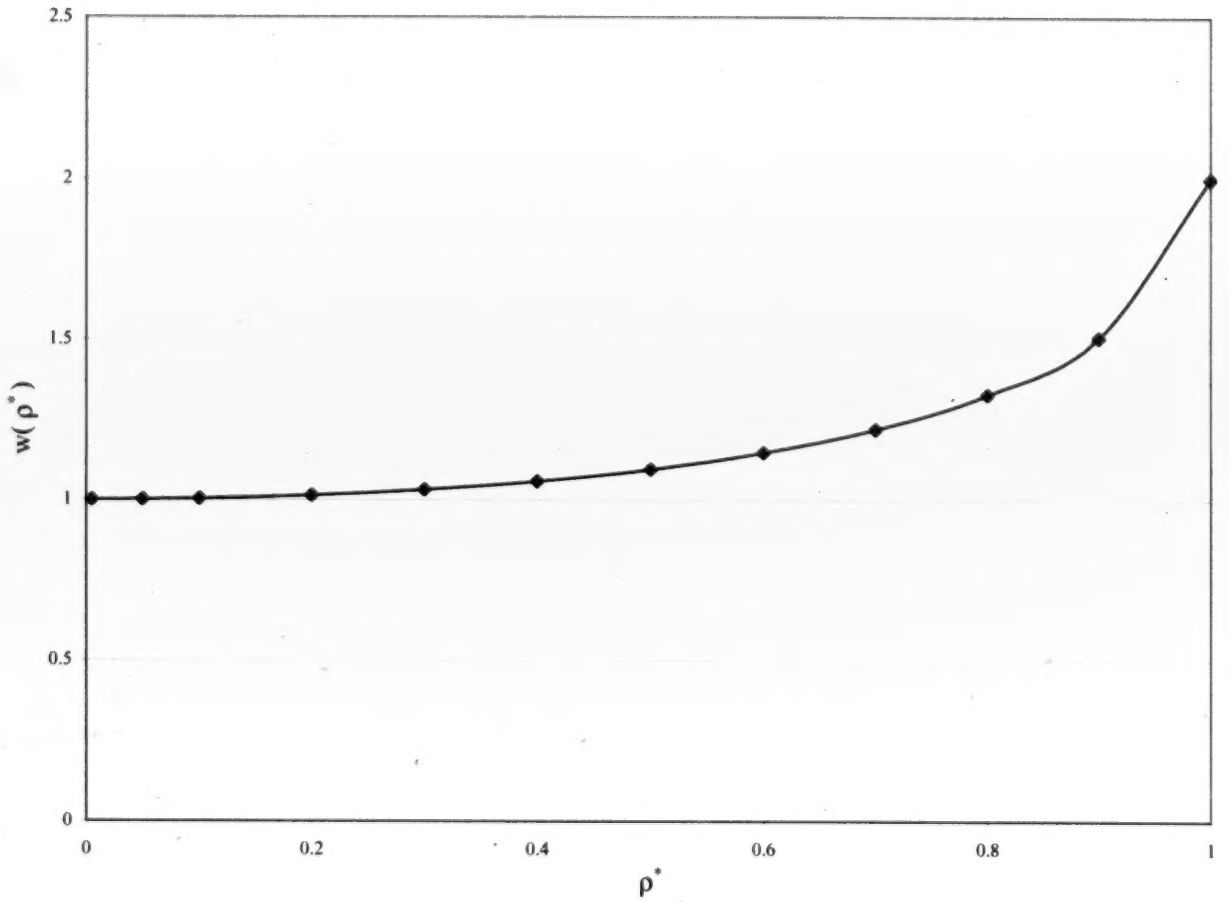

Figure 4-3. The Effect of the Circumferential Inhomogeneity
on the Average Deviatoric and Shear Stresses inside the Circular Inclusion having Circumferential Number s = 1

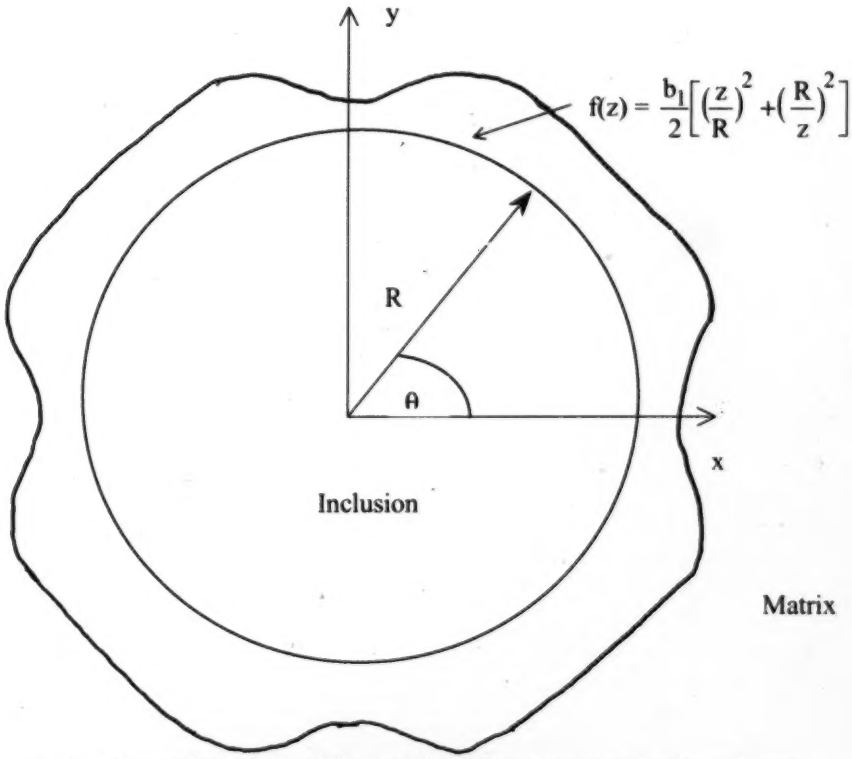

Figure 4 - 4. Schematic Representation of the Inhomogeneous Spring – Layer Interface having Circumferential Number $s \triangleq 2$

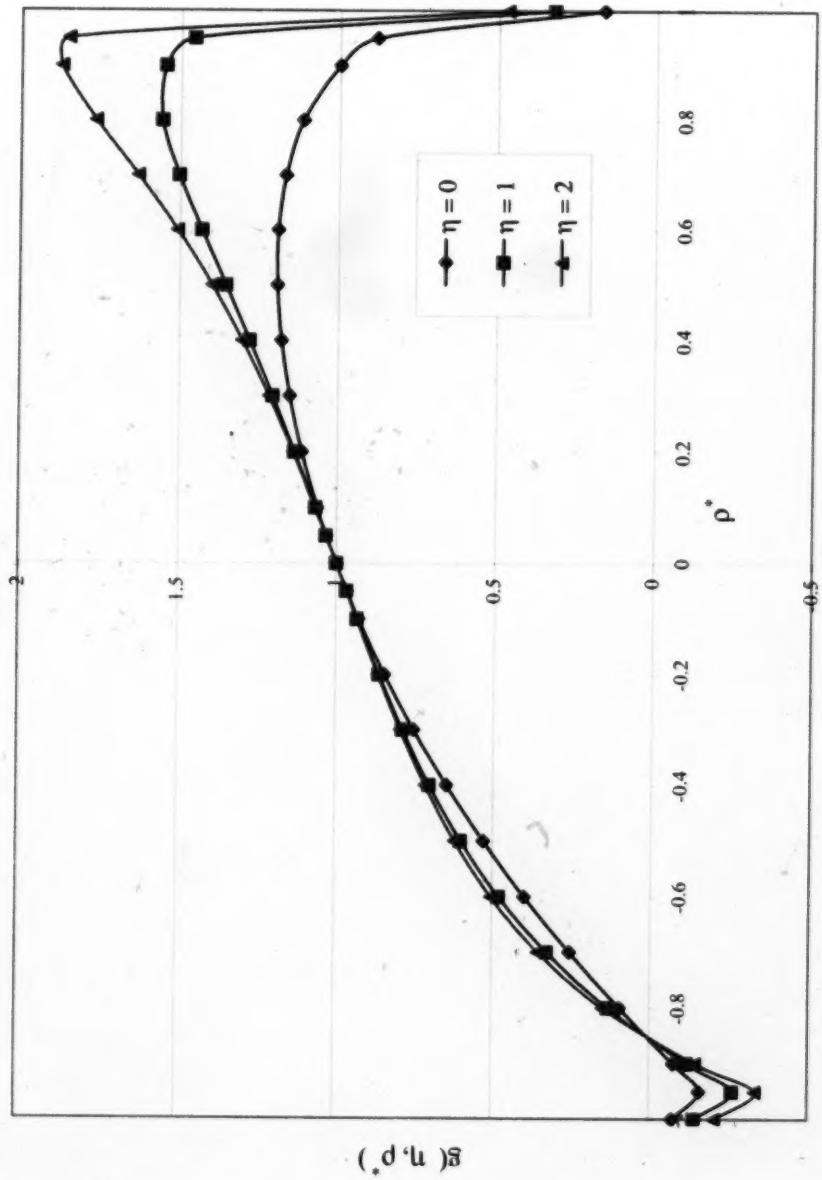

Figure 4-5. The Effect of the Circumferential Inhomogeneity on the Average Mean Stress Inside the Circular Inclusion having Circumferential Number s = 2 and Loading in x-direction

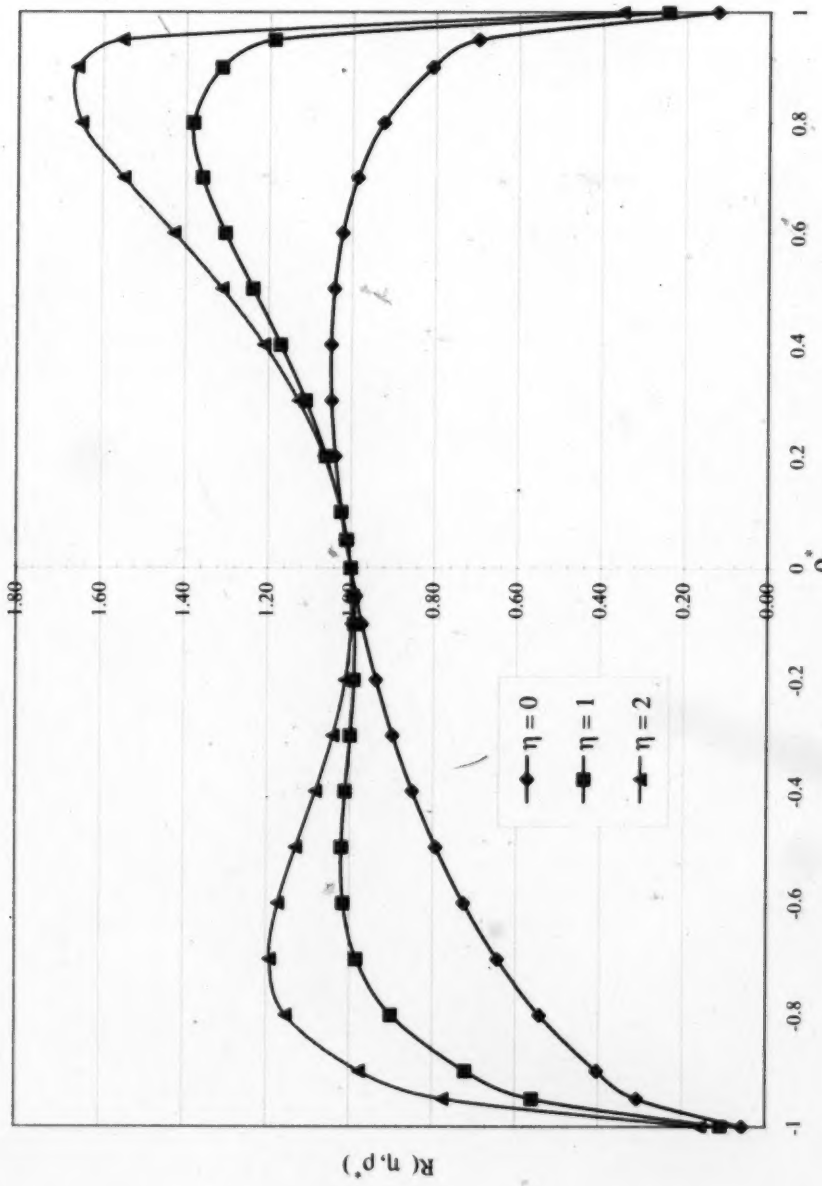

Figure 4-6. The Effect of the Circumferential Inhomogeneity on the Average Deviatoric and Shear Stress inside the Circular Inclusion having Circumferential Number s = 2 and Loading in x-direction

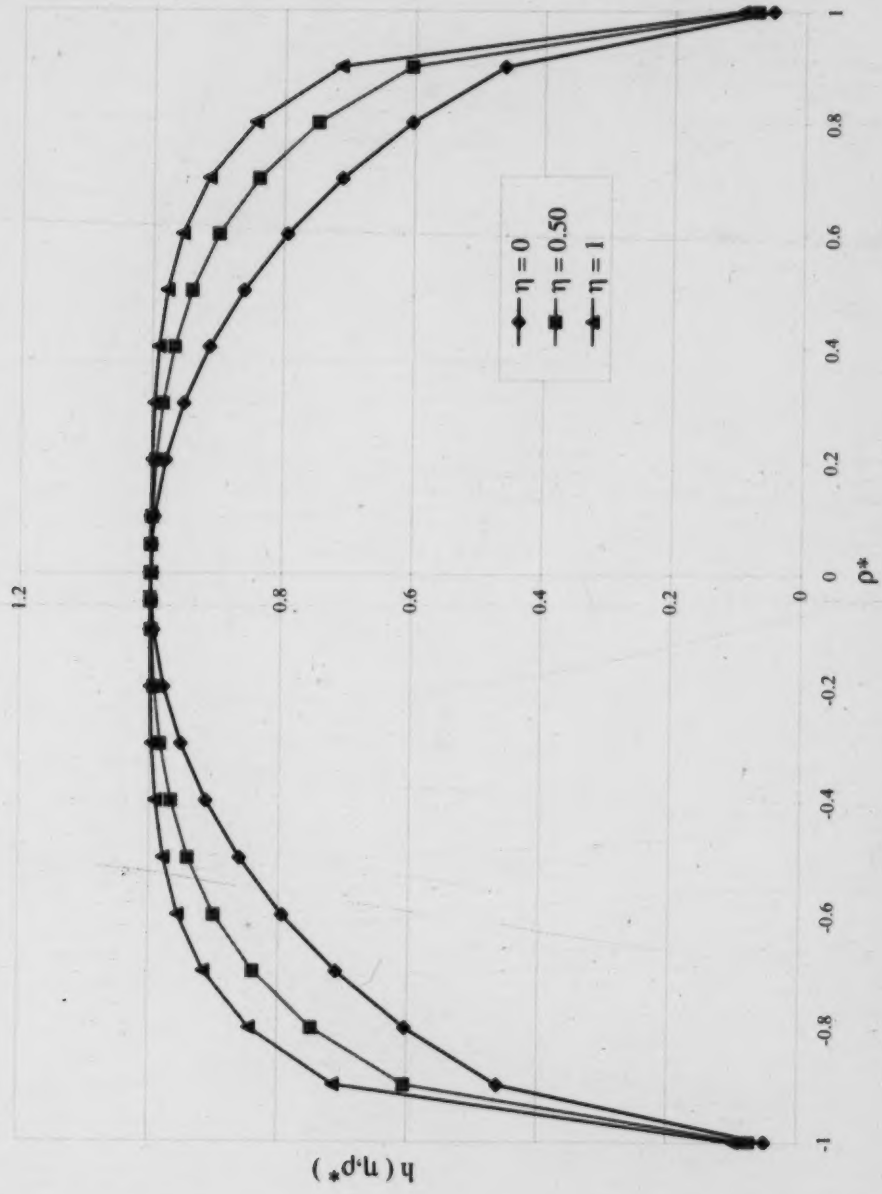

Figure 4-7. The Effect of the Circumferential Inhomogeneity on the Average Mean Stress inside the Circular Inclusion having Circumferential Number s = 2 and Equal Biaxial Loading

CHAPTER 5

Circumferential Inhomogeneous Non-slipping Interface

5.1. Introduction

This chapter will extend the single circular inclusion problem to deal with applications arising in biomechanics, specifically, prosthetic (implant) - bone interaction. The justification for using the single circular inclusion problem lies in the fact that since circular holes can be easily and readily made in host bone, the use of implants with circular cross-sections is common.

One of the major contributions to implant failure is the loosening of the implant from the host bone. The reason for this, as detailed in Chapter 1, is the non-uniformity of bone density along the implant - bone interface, formation of scar tissue and the presence of stress concentrations due to high interfacial stresses. Consequently, the effect of a non-slip interface condition, in particular, the inhomogeneity of normal imperfections on the stress field surrounding an implant is of great practical interest (see [84]). Hence, this chapter will focus on the rigorous solution method for the problem associated with an isotropic circular inclusion (implant) embedded within an infinite homogeneous matrix (bone) in plane elasticity.

The bonding at the implant - bone interface is circumferentially inhomogeneous as characterized by the non-slip condition $m(\theta)$ finite and $n(\theta) = \infty$. Physically, this type of imperfect interface corresponds to a very rough interphase layer. The presence of asperities and interdigitations allows for no relative shear displacements along the entire interface, but a certain relative normal displacement, which is proportional to the normal traction through an inhomogeneous interface parameter, is permitted across the interface (i.e. a mechanical interlock is formed - see Figure 5-1).

5.2. Non-Slipping Interface

As outlined above, we consider a circular inclusion for which the inhomogeneous imperfect interface is characterized by the non-slip condition $m(\theta)$ finite and $n(\theta) = \infty$. In this case, the interface conditions described by the inhomogeneous imperfect bonding model (2.2 - 2.3) take the form

$$\frac{\sigma_r}{m(\theta)} = \|u_r\| - u_r^o, \qquad \|u_\theta\| - u_\theta^o = 0, \quad z \in \Gamma. \tag{5.1}$$

Knowing that the displacements, in the tangential direction, are continuous, then in view of (2.16), $(5.1)_2$ can be given in terms of $\Phi_I(z)$ and $\Phi_M(z)$ as follows

$$\frac{1}{4}\left[\frac{\kappa_M}{\mu_M}+\frac{1}{\mu_I}\right]\frac{R}{z}\Phi_M(z)+\frac{1}{4}\left[\frac{\kappa_I}{\mu_I}+\frac{1}{\mu_M}\right]\frac{z}{R}\overline{\Phi_I}\left(\frac{R^2}{z}\right)+\frac{1}{4\mu_I}\left[\overline{B}\frac{R^2}{z^2}+\frac{\overline{C_2}}{z}\right]R-$$
$$\frac{1}{4\mu_M}\left[\overline{B}\frac{R^2}{z^2}+\frac{\overline{C_1}}{z}\right]R-\frac{1}{2z^2}\left(\varepsilon_2+i\varepsilon_3\right)R^3=\frac{1}{4}\left[\frac{\kappa_M}{\mu_M}+\frac{1}{\mu_I}\right]\frac{z}{R}\overline{\Phi_M}\left(\frac{R^2}{z}\right)+$$
$$\frac{1}{4}\left[\frac{\kappa_I}{\mu_I}+\frac{1}{\mu_M}\right]\frac{R}{z}\Phi_I(z)+\frac{1}{4R\mu_I}\left[Bz^2+AR^2+B_1-\overline{X_1}R^2+C_2z\right]- \qquad (5.2)$$
$$\frac{1}{4R\mu_M}\left[Bz^2+AR^2+B_1-\overline{X_1}R^2+C_1z\right]-\frac{R}{4\mu_I}\left[A+\frac{B_1}{R^2}-X_1\right]+$$
$$\frac{R}{4\mu_M}\left[A+\frac{B_1}{R^2}-X_1\right]-\frac{1}{2R}\left(\varepsilon_2-i\varepsilon_3\right)z^2, \qquad z\in\Gamma.$$

In view of (2.5), the right hand side of (5.2) is analytic in D_I and the left hand side is analytic in D_M except at infinity where the left hand side has the singular behavior

$$\frac{1}{4}\left[\frac{\kappa_M}{\mu_M}+\frac{1}{\mu_I}\right]AR+\frac{1}{4}\left[\frac{\kappa_I}{\mu_I}+\frac{1}{\mu_M}\right]\overline{X_1}R \qquad |z|\to\infty.$$

Then, using the principle of analytic continuation, the function, $\Xi(z)$, defined by

$$\Xi(z)=\begin{cases}\dfrac{1}{4}\left[\dfrac{\kappa_M}{\mu_M}+\dfrac{1}{\mu_I}\right]\dfrac{R}{z}\Phi_M(z)+\dfrac{1}{4}\left[\dfrac{\kappa_I}{\mu_I}+\dfrac{1}{\mu_M}\right]\dfrac{z}{R}\overline{\Phi_I}\left(\dfrac{R^2}{z}\right)+\\ \dfrac{1}{4\mu_I}\left[\overline{B}\dfrac{R^2}{z^2}+\dfrac{\overline{C_2}}{z}\right]R-\dfrac{1}{4\mu_M}\left[\overline{B}\dfrac{R^2}{z^2}+\dfrac{\overline{C_1}}{z}\right]R-\dfrac{1}{2z^2}\left(\varepsilon_2+i\varepsilon_3\right)R^3\\ -\dfrac{1}{4}\left[\dfrac{\kappa_M}{\mu_M}+\dfrac{1}{\mu_I}\right]AR-\dfrac{1}{4}\left[\dfrac{\kappa_I}{\mu_I}+\dfrac{1}{\mu_M}\right]\overline{X_1}R, \qquad z\in D_M,\\ \dfrac{1}{4}\left[\dfrac{\kappa_M}{\mu_M}+\dfrac{1}{\mu_I}\right]\dfrac{z}{R}\overline{\Phi_M}\left(\dfrac{R^2}{z}\right)+\dfrac{1}{4}\left[\dfrac{\kappa_I}{\mu_I}+\dfrac{1}{\mu_M}\right]\dfrac{R}{z}\Phi_I(z)+\\ \dfrac{1}{4R\mu_I}\left[Bz^2+AR^2+B_1-\overline{X_1}R^2+C_2z\right]-\dfrac{R}{4\mu_I}\left[A+\dfrac{B_1}{R^2}-X_1\right]-\\ \dfrac{1}{4R\mu_M}\left[Bz^2+AR^2+B_1-\overline{X_1}R^2+C_1z\right]+\dfrac{R}{4\mu_M}\left[A+\dfrac{B_1}{R^2}-X_1\right]-\\ \dfrac{1}{2R}\left(\varepsilon_2-i\varepsilon_3\right)z^2-\dfrac{1}{4}\left[\dfrac{\kappa_M}{\mu_M}+\dfrac{1}{\mu_I}\right]AR-\dfrac{1}{4}\left[\dfrac{\kappa_I}{\mu_I}+\dfrac{1}{\mu_M}\right]\overline{X_1}R, \qquad z\in D_I,\end{cases} \tag{5.3}$$

is analytic and single-valued in the whole complex plane including the point at infinity. Therefore, by Liouville's Theorem, $\Xi(z)$ must be a constant. In fact, since $\Xi(z)$ approaches zero at infinity it must be that the constant is identically equal to zero. Thus, with this condition, the two relations between $\Phi_I(z)$ and $\Phi_M(z)$ are then

$$\begin{aligned}&\frac{1}{4}\left[\frac{\kappa_M}{\mu_M}+\frac{1}{\mu_I}\right]\frac{R}{z}\Phi_M(z)+\frac{1}{4}\left[\frac{\kappa_I}{\mu_I}+\frac{1}{\mu_M}\right]\frac{z}{R}\overline{\Phi_I}\left(\frac{R^2}{z}\right)+\frac{1}{4\mu_I}\left[\overline{B}\frac{R^2}{z^2}+\frac{\overline{C_2}}{z}\right]R-\\ &\qquad\frac{1}{4\mu_M}\left[\overline{B}\frac{R^2}{z^2}+\frac{\overline{C_1}}{z}\right]R-\frac{1}{2z^2}\left(\varepsilon_2+i\varepsilon_3\right)R^3-\\ &\qquad\frac{1}{4}\left[\frac{\kappa_M}{\mu_M}+\frac{1}{\mu_I}\right]AR-\frac{1}{4}\left[\frac{\kappa_I}{\mu_I}+\frac{1}{\mu_M}\right]\overline{X_1}R=0, \qquad z\in D_M,\end{aligned} \tag{5.4}$$

and

$$\begin{aligned}
&\frac{1}{4}\left[\frac{\kappa_M}{\mu_M}+\frac{1}{\mu_I}\right]\frac{z}{R}\overline{\Phi_M}\left(\frac{R^2}{z}\right)+\frac{1}{4}\left[\frac{\kappa_I}{\mu_I}+\frac{1}{\mu_M}\right]\frac{R}{z}\Phi_I(z)+\\
&\frac{1}{4R\mu_I}\left[Bz^2+AR^2+B_1-\overline{X_1}R^2+C_2z\right]-\frac{R}{4\mu_I}\left[A+\frac{B_1}{R^2}-X_1\right] \qquad (5.5)\\
&-\frac{1}{4R\mu_M}\left[Bz^2+AR^2+B_1-\overline{X_1}R^2+C_1z\right]+\frac{R}{4\mu_M}\left[A+\frac{B_1}{R^2}-X_1\right]\\
&-\frac{1}{2R}\left(\varepsilon_2-i\varepsilon_3\right)z^2-\frac{1}{4}\left[\frac{\kappa_M}{\mu_M}+\frac{1}{\mu_I}\right]AR-\frac{1}{4}\left[\frac{\kappa_I}{\mu_I}+\frac{1}{\mu_M}\right]\overline{X_1}R=0, \qquad z\in D_I.
\end{aligned}$$

The functions Φ_I and/or Φ_M appearing in (5.4) must be compatible with those in (5.5). In fact, the compatibility between (5.4) and (5.5) gives the first compatibility condition

$$X_1=\overline{X_1}. \qquad (5.6)$$

In general, the imperfect bonding model, (2.3), can be written in the form

$$\frac{\sigma_r}{m(\theta)}-i\frac{\sigma_{r\theta}}{n(\theta)}=\left(\|u_r\|-u_r^o\right)-i\left(\|u_\theta\|-u_\theta^o\right), \quad z\in\Gamma,$$

but since we assume a continuity of tangential displacements (i.e. $n(\theta)=\infty$), then the normal interface condition $(5.1)_1$ can be rewritten as

$$\begin{aligned}
\frac{\sigma_r}{m(\theta)}&=\left(\|u_r\|-u_r^o\right)-i\left(\|u_\theta\|-u_\theta^o\right), \quad z\in\Gamma,\\
&=u_r^M-u_r^I-iu_\theta^M+iu_\theta^I-\left(u_r^o-iu_\theta^o\right), \quad z\in\Gamma,\\
&=\left(u_r^M-iu_\theta^M\right)-\left(u_r^I-iu_\theta^I\right)-\left(u_r^o-iu_\theta^o\right), \quad z\in\Gamma,
\end{aligned}$$

or, more precisely, as

$$\frac{\sigma_r}{m(\theta)} = \|u_r - iu_\theta\| - (u_r^o - iu_\theta^o), \quad z \in \Gamma. \tag{5.7}$$

As indicated in Chapter 2, it is convenient to express the stress free displacement components u_r^o and u_θ^o, appearing in (5.7), in terms of the eigenstrains themselves. Therefore, using condition (2.14), the stress free displacement components, on the inclusion-matrix boundary, can be expressed as

$$\begin{aligned}(u_r^o - iu_\theta^o) &= R\varepsilon_1 + R\varepsilon_2\cos 2\theta + R\varepsilon_3\sin 2\theta - iR\varepsilon_3\cos 2\theta + iR\varepsilon_2\sin 2\theta, \quad z \in \Gamma, \\ &= R\varepsilon_1 + R(\varepsilon_2 - i\varepsilon_3)[\cos 2\theta + i\sin 2\theta], \quad z \in \Gamma,\end{aligned}$$

and since $z = \mathrm{R}e^{i\theta}$ on the inclusion - matrix boundary, the above is simplified to the following

$$(u_r^o - iu_\theta^o) = R\varepsilon_1 + \frac{z^2}{R}(\varepsilon_2 - i\varepsilon_3), \quad z \in \Gamma. \tag{5.8}$$

Hence, using conditions (2.1), (2.10) and (5.5 - 5.8) we can eliminate $\Phi_M(z)$, the normal displacement interface condition $(5.1)_1$ can be given in terms of $\Phi_I(z)$ as follows (see Appendix E for details)

$$\left(\frac{1+\beta}{2}\right)\overline{\Phi_I}'\left(\frac{R^2}{z}\right)-\beta\frac{z}{R^2}\overline{\Phi}\left(\frac{R^2}{z}\right)-\frac{\overline{B}R^2}{2z^2}(1+\eta)-\frac{z^2(\varepsilon_2-i\varepsilon_3)}{R^2\left(\frac{\kappa_M}{\mu_M}+\frac{1}{\mu_I}\right)}+$$

$$\frac{1}{2}\left(A+\beta\overline{X_1}\right)+\frac{1}{2}\left(A+\beta X_1\right)+\left(\frac{1+\beta}{2}\right)\Phi_I'(z)-\frac{\beta}{z}\Phi_I(z)-\frac{Bz^2}{2R^2}(1+\eta)-$$

$$\frac{R^2(\varepsilon_2+i\varepsilon_3)}{z^2\left(\frac{\kappa_M}{\mu_M}+\frac{1}{\mu_I}\right)}+\frac{1}{2}\left(A+\frac{B_1}{R^2}-\overline{X_1}\right)+\frac{1}{2}\left(A+\frac{B_1}{R^2}-X_1\right)=$$

$$\frac{m(\theta)R}{2}\left(\frac{\kappa_M}{\mu_M}+\frac{1}{\mu_I}\right)\left\{-\frac{\beta}{z}\Phi_I(z)-\beta\frac{z}{R^2}\overline{\Phi_I}\left(\frac{R^2}{z}\right)+\frac{1}{2}\left(A+\beta\overline{X_1}\right)+\right. \tag{5.9}$$

$$\left.\frac{1}{2}\left(A+\beta X_1\right)-\frac{\eta}{2}\left(A+\frac{B_1}{R^2}-X_1\right)-\frac{\eta}{2}\left(A+\frac{B_1}{R^2}-\overline{X_1}\right)-\frac{2\varepsilon_1}{\left(\frac{\kappa_M}{\mu_M}+\frac{1}{\mu_I}\right)}\right\},\quad z\in\Gamma$$

where we have set

$$\beta\equiv\frac{\left(\frac{\kappa_I}{\mu_I}+\frac{1}{\mu_M}\right)}{\left(\frac{\kappa_M}{\mu_M}+\frac{1}{\mu_I}\right)}>0,\qquad \eta\equiv\frac{\frac{1}{\mu_M}-\frac{1}{\mu_I}}{\left(\frac{\kappa_M}{\mu_M}+\frac{1}{\mu_I}\right)}. \tag{5.10}$$

For convenience, as in Chapter 3, let the parameter $\delta(\theta)$ be introduced in place of $m(\theta)$ and defined by

$$\delta(\theta)\equiv\frac{m(\theta)R}{2}\left(\frac{\kappa_M}{\mu_M}+\frac{1}{\mu_I}\right) \tag{5.11}$$

Furthermore, let

$$1+f(\theta)=\frac{\delta_o}{\delta(\theta)},\qquad \delta_o>0,\qquad f(\theta)>-1, \tag{5.12}$$

where δ_o is a positive real number and $f(\theta)$ is a real periodic function prescribed on the inclusion - matrix boundary. Clearly, $\dfrac{1}{\delta(\theta)}$ must be a non-negative periodic function defined on Γ. Note that the functional form of $f(\theta)$ describes the circumferential variation in damage along the material interface. In addition, as $f(\theta) \to -1$ this is equivalent to $m(\theta) \to \infty$ which corresponds to a perfectly bonded interface.

Since $f(\theta)$ is a periodic function of θ in the space $C_p[0, 2\pi]$, then as in Chapter 3, let us represent $f(\theta)$ by the following finite Fourier series

$$f(\theta) = \sum_{k=1}^{s} a_k \sin k\theta + b_k \cos k\theta \tag{5.13}$$

$$a_s^2 + b_s^2 \neq 0 \text{ unless } f(\theta) \equiv 0 \text{ on } \Gamma,$$

where s is a natural number that defines the maximum order of the polynomial and a_k, b_k are some given real coefficients.

It has been shown [see Chapter 3, condition (3.7)] that $f(\theta)$ can be written in terms of the complex variable z on the inclusion - matrix boundary. Therefore, using conditions (3.7) (5.11) and (5.12) the interface condition, (5.9), can be written in the following form

$$[1+f(z)]\left[\left(\frac{1+\beta}{2}\right)\Phi_I'(z)+\frac{1}{2}\left(A+\frac{B_1}{R^2}-X_1\right)-B\frac{z^2}{2R^2}(1+\eta)-\right.$$

$$\left.\frac{z^2(\varepsilon_2-i\varepsilon_3)}{R^2\left(\dfrac{\kappa_M}{\mu_M}+\dfrac{1}{\mu_I}\right)}\right]+[\delta_o-1-f(z)]\left[\frac{\beta}{z}\Phi_I(z)-\frac{1}{2}(A+\beta X_1)\right]+\frac{\varepsilon_1\delta_o}{\dfrac{\kappa_M}{\mu_M}+\dfrac{1}{\mu_I}}+$$

$$\frac{\delta_o\eta}{2}\left(A+\frac{B_1}{R^2}-X_1\right)=-\left\{[1+f(z)]\left[\left(\frac{1+\beta}{2}\right)\overline{\Phi_I'}\left(\frac{R^2}{z}\right)+\frac{1}{2}\left(A+\frac{B_1}{R^2}-\overline{X_1}\right)-\right.\right.$$

$$\left.\overline{B}\frac{R^2}{2z^2}(1+\eta)-\frac{R^2(\varepsilon_2+i\varepsilon_3)}{z^2\left(\dfrac{\kappa_M}{\mu_M}+\dfrac{1}{\mu_I}\right)}\right]+[\delta_o-1-f(z)]\left[\beta\frac{z}{R^2}\overline{\Phi_I}\left(\frac{R^2}{z}\right)-\frac{1}{2}(A+\beta\overline{X_1})\right]$$

$$\left.+\frac{\varepsilon_1\delta_o}{\dfrac{\kappa_M}{\mu_M}+\dfrac{1}{\mu_I}}+\frac{\delta_o\eta}{2}\left(A+\frac{B_1}{R^2}-\overline{X_1}\right)\right\},\quad z\in\Gamma. \tag{5.14}$$

Hence, it remains to determine a single analytic function $\Phi_I(z)$ in D_I with the interface condition given by (5.14). It turns out that the solution for $\Phi_I(z)$ will depend on the circumferential variation of the imperfections in the interface. As a result of this dependency, the conventional power series method will lead to a coupled infinite system of algebraic equations for the unknown coefficients X_k $(k=1,2,...)$ and one cannot determine exact expressions for even the first few coefficients. To overcome this difficulty, analytic continuation is used to reduce (5.14) to a first order differential equation for $\Phi_I(z)$. In this way, a closed-form solution can be obtained for the general case of the circumferentially inhomogeneous

non-slip interface as described by the model given by (5.12) and (5.13).

5.2.1. The Differential Equation for $\Phi_I(z)$

To derive the differential equation for $\Phi_I(z)$ note that, in view of (2.5), the right hand side of (5.14) is analytic in D_M except at infinity where it approaches $-[L_o + L_1(z)]$. Here, $L_1(z)$ is defined by

$$L_1(z) \equiv \frac{1}{2}\sum_{k=1}^{s}(b_k - ia_k)\left(\frac{z}{R}\right)^k \sum_{j=0}^{k}\left[\left(\frac{1+\beta}{2}\right)j - \beta\right]\overline{X_j}\left(\frac{R^2}{z}\right)^{j-1} + \frac{1}{4}\left(2A + \frac{B_1}{R^2} - (1-\beta)\overline{X_1}\right)\sum_{k=1}^{s}(b_k - ia_k)\left(\frac{z}{R}\right)^k - \frac{1}{2}\left[\frac{\overline{B}}{2}(1+\eta) + \frac{\varepsilon_2 + i\varepsilon_3}{\frac{\kappa_M}{\mu_M} + \frac{1}{\mu_I}}\right]\sum_{k=3}^{s}(b_k - ia_k)\left(\frac{z}{R}\right)^{k-2} \tag{5.15}$$

and the constant term L_o is defined by

$$L_o \equiv \frac{1}{2}\sum_{k=1}^{s}(b_k - ia_k)R^k\left[\left(\frac{1+\beta}{2}\right)(k+1) - \beta\right]\overline{X_{k+1}} - \frac{1}{2}(b_2 - ia_2)\left[\frac{\overline{B}}{2}(1+\eta) + \frac{\varepsilon_2 + i\varepsilon_3}{\frac{\kappa_M}{\mu_M} + \frac{1}{\mu_I}}\right] + \left[\frac{1}{2}(1+\beta) + (\delta_o - 1)\beta\right]\overline{X_1} - \frac{1}{2}(\delta_o - 1)\left(A + \beta\overline{X_1}\right) + \frac{\varepsilon_1\delta_o}{\frac{\kappa_M}{\mu_M} + \frac{1}{\mu_I}} + \frac{1}{2}\left(A + \frac{B_1}{R^2} - \overline{X_1}\right) + \frac{\delta_o\eta}{2}\left(A + \frac{B_1}{R^2} - \overline{X_1}\right). \tag{5.16}$$

Furthermore, since the left hand side of (5.12) is the complex conjugate of the right hand side, it must be that the left hand side is analytic in D_I except at the origin where it has the following singular behavior

$$\overline{L_1}\left(\frac{R^2}{z}\right). \tag{5.17}$$

Denoting the sum of the above two expressions by $L(z)$, namely

$$L(z) \equiv \overline{L_1}\left(\frac{R^2}{z}\right) - [L_1(z) + L_o] \tag{5.18}$$

then, as outlined before, using the principle of analytic continuation and Liouville's Theorem we obtain the following expressions

$$[1+f(z)]\left[\left(\frac{1+\beta}{2}\right)\Phi_I'(z) + \frac{1}{2}\left(A + \frac{B_1}{R^2} - X_1\right) - B\frac{z^2}{2R^2}(1+\eta) - \frac{z^2(\varepsilon_2 - i\varepsilon_3)}{R^2\left(\frac{\kappa_M}{\mu_M} + \frac{1}{\mu_I}\right)}\right]$$
$$+ [\delta_o - 1 - f(z)]\left[\frac{\beta}{z}\Phi_I(z) - \frac{1}{2}(A + \beta X_1)\right] + \frac{\varepsilon_1\delta_o}{\frac{\kappa_M}{\mu_M} + \frac{1}{\mu_I}} +$$
$$\frac{\delta_o\eta}{2}\left(A + \frac{B_1}{R^2} - X_1\right) = L(z), \qquad z \in D_I \tag{5.19}$$

and

$$-\left\{[1+f(z)]\left[\left(\frac{1+\beta}{2}\right)\overline{\Phi_I'}\left(\frac{R^2}{z}\right)+\frac{1}{2}\left(A+\frac{B_1}{R^2}-\overline{X_1}\right)-\overline{B}\frac{R^2}{2z^2}(1+\eta)-\right.\right.$$

$$\left.\left.\frac{R^2(\varepsilon_2+i\varepsilon_3)}{z^2\left(\frac{\kappa_M}{\mu_M}+\frac{1}{\mu_I}\right)}\right]+[\delta_o-1-f(z)]\left[\beta\frac{z}{R^2}\overline{\Phi_I}\left(\frac{R^2}{z}\right)-\frac{1}{2}\left(A+\beta\overline{X_1}\right)\right]+\right.$$

$$\left.\frac{\varepsilon_1\delta_o}{\frac{\kappa_M}{\mu_M}+\frac{1}{\mu_I}}+\frac{\delta_o\eta}{2}\left(A+\frac{B_1}{R^2}-\overline{X_1}\right)\right\}=L(z),\qquad z\in D_M. \tag{5.20}$$

The function $\Phi_I(z)$ determined from (5.19) must be compatible with that obtained from (5.20). Therefore, in view of (2.5) and (5.15 - 5.18) and letting $z\to 0$ inside the inclusion, (5.19) reduces to the following

$$\left(\frac{1+\beta}{2}\right)X_1+\frac{1}{2}\left(A+\frac{B_1}{R^2}-X_1\right)-\frac{\delta_o}{2}(A+\beta X_1)+\frac{1}{2}(A+\beta X_1)+\delta_o\beta X_1-\beta X_1+$$

$$\frac{\varepsilon_1\delta_o}{\frac{\kappa_M}{\mu_M}+\frac{1}{\mu_I}}+\frac{\delta_o\eta}{2}\left(A+\frac{B_1}{R^2}-X_1\right)-\frac{B}{4}(1+\eta)(b_2+ia_2)-\frac{(\varepsilon_2-i\varepsilon_3)}{2\left(\frac{\kappa_M}{\mu_M}+\frac{1}{\mu_I}\right)}(b_2+ia_2)$$

$$+\left(\frac{1+\beta}{4}\right)\sum_{k=1}^{s}(k+1)(b_k+ia_k)X_{k+1}R^k-\frac{\beta}{2}\sum_{k=1}^{s}(b_k+ia_k)X_{k+1}R^k=-L_o.$$

Simplifying the above into a convenient form yields

$$\frac{1}{2}\sum_{k=1}^{s}(b_k+i\hat{a}_k)R^k\left[\left(\frac{1+\beta}{2}\right)(k+1)-\beta\right]X_{k+1}-\frac{1}{2}\left[\frac{B}{2}(1+\eta)+\frac{(\varepsilon_2-i\varepsilon_3)}{\frac{\kappa_M}{\mu_M}+\frac{1}{\mu_I}}\right]+$$

$$\left[\frac{1}{2}(1+\beta)+(\delta_o-1)\beta\right]X_1-\frac{1}{2}(\delta_o-1)(A+\beta X_1)+\frac{\varepsilon_1\delta_o}{\frac{\kappa_M}{\mu_M}+\frac{1}{\mu_I}}+\frac{1}{2}\left(A+\frac{B_1}{R^2}-X_1\right)$$

$$+\frac{\delta_o\eta}{2}\left(A+\frac{B_1}{R^2}-X_1\right)=-L_o.$$

Therefore, in view of condition (5.16), the following is a necessary and sufficient condition for the required compatibility of $\Phi_I(z)$

$$\overline{L_o}=-L_o. \tag{5.21}$$

Hence, within the circular inclusion D_I, the governing differential equation is give as

$$\Phi_I'(z)+\left(\frac{2\beta}{1+\beta}\right)\left[\frac{\delta_o-1-f(z)}{1+f(z)}\right]\frac{\Phi_I(z)}{z}=P(z),\qquad z\in D_I \tag{5.22}$$

where $P(z)$ is given by

$$[1+f(z)]\left(\frac{1+\beta}{2}\right)P(z)=L(z)+\frac{1}{2}[\delta_o-1-f(z)](A+\beta X_1)-[1+f(z)]\times$$

$$\left[\frac{1}{2}\left(A+\frac{B_1}{R^2}-X_1\right)-B\frac{z^2}{2R^2}(1+\eta)-\frac{z^2(\varepsilon_2-i\varepsilon_3)}{R^2\left(\frac{\kappa_M}{\mu_M}+\frac{1}{\mu_I}\right)}\right]-\frac{\varepsilon_1\delta_o}{\frac{\kappa_M}{\mu_M}+\frac{1}{\mu_I}}- \tag{5.23}$$

$$\frac{\delta_o\eta}{2}\left(A+\frac{B_1}{R^2}-X_1\right).$$

Equation (5.22) is a first order linear differential equation with variable coefficients for the unknown $\Phi_I(z)$. The general solution of (5.22) is given by

$$\Phi_I(z) = I(z)e^{T(z)}, \qquad T(z) = \frac{2\beta}{1+\beta}\int \frac{1+f(z)-\delta_o}{z\,[1+f(z)]}dz,$$

$$I(z) = \int_{z_I}^{z} P(t)e^{-T(t)}dt + C_o, \qquad z \in D_I \tag{5.24}$$

where z_I is some arbitrary point in D_I and C_o is some arbitrary constant of integration.

Clearly, the right hand side of (5.22) (i.e. the non-homogeneous term $P(z)$) includes the $(s+1)$ undetermined constants X_k $(k = 1, 2, ..., s+1)$, in view of (2.5), any admissable solution Φ_I of (5.22) must satisfy the consistency condition

$$X_k = \frac{\Phi_I^k(0)}{k!}, \qquad k = 1, 2, ..., s+1. \tag{5.25}$$

To verify (5.25), assume that (5.22) has an analytic solution $\Phi_I(z)$ in D_I which admits a Taylor expansion (say $\Phi_I(z) = \sum_{r=0}^{\infty} Q_r z^r$). Substituting this expansion into (5.22) gives

$$[1+f(z)]\left(\frac{1+\beta}{2}\right)\sum_{r=0}^{\infty} rQ_r z^{r-1} + \beta\left(\frac{\delta_o - 1 - f(z)}{z}\right)\sum_{r=0}^{\infty} Q_r z^r = L(z) +$$

$$\frac{1}{2}[\delta_o - 1 - f(z)](A + \beta X_1) - [1+f(z)]\left[\frac{1}{2}\left(A + \frac{B_1}{R^2} - X_1\right) - B\frac{z^2}{2R^2}(1+\eta) -\right.$$

$$\left.\frac{z^2(\varepsilon_2 - i\varepsilon_3)}{R^2\left(\dfrac{\kappa_M}{\mu_M} + \dfrac{1}{\mu_I}\right)}\right] - \frac{\varepsilon_1\delta_o}{\dfrac{\kappa_M}{\mu_M} + \dfrac{1}{\mu_I}} - \frac{\delta_o\eta}{2}\left(A + \frac{B_1}{R^2} - X_1\right).$$

In view of (3.7) and (5.18), comparing all the non-positive powers of z (i.e. $z^{-s}, ..., z^0$) in the above expression gives $(s+1)$ conditions that satisfy

$$\frac{1}{2}\sum_{k=1}^{s}(b_k+ia_k)\,R^k\left[\left(\frac{1+\beta}{2}\right)(k+1)-\beta\right]Q_{k+1}+\frac{1}{2}\sum_{k=1}^{s}(b_k+ia_k)\left(\frac{R}{z}\right)^k\times$$
$$\sum_{j=0}^{k}\left[\left(\frac{1+\beta}{2}\right)j-\beta\right]Q_j z^{j-1}=\frac{1}{2}\sum_{k=1}^{s}(b_k+ia_k)\,R^k\left[\left(\frac{1+\beta}{2}\right)(k+1)-\beta\right]X_{k+1}+$$
$$\frac{1}{2}\sum_{k=1}^{s}(b_k+ia_k)\left(\frac{R}{z}\right)^k\sum_{j=0}^{k}\left[\left(\frac{1+\beta}{2}\right)j-\beta\right]X_j z^{j-1}$$

which proves that any analytic solution $\Phi_I(z)$ of (5.22) automatically satisfies the consistency condition given by (5.25) provided that $\beta \neq 1$. If, on the other hand, $\beta = 1$ then one of the aforementioned $(s+1)$ conditions, obtained by equating the coefficient of z^{-s}, becomes an identity. Therefore, when $\beta = 1$, the first one of the $(s+1)$ conditions given by (5.25) cannot be automatically satisfied by the analytic solution of (5.22); as a result, the admissable analytic solution of (5.22) must be required to satisfy the additional condition

$$X_1 = \Phi_I'(0), \qquad \text{only if } \beta = 1. \tag{5.26}$$

The presence of singular points, such as poles or branch points of the multi-valued functions appearing in (5.22 - 5.23), means that the solution of Φ_I given by (5.24), is in general, defined only in a simply connected domain obtained by cutting D_I along some appropriately chosen lines. However, Φ_I given by (5.24)

is not, in general, analytic in its uncut domain. For example, Φ_I can become discontinuous across branch cuts and/or may become unbounded at some or all isolated singular points. Therefore, to ensure the analyticity of Φ_I in its uncut domain we must verify the following:

- Φ_I given by (5.24) must be bounded at all singular points, and
- Φ_I given by (5.24) must be continuous across all branch cuts.

In summary, the solution for Φ_I is given by (5.24), which includes a total of $(s+1)$ undetermined constants X_k $(k = 1, 2, ..., s+1)$. These constants are determined via the analyticity requirements of Φ_I, the consistency condition given by (5.26) and the compatibility conditions given by (5.6) and (5.21). Once $\Phi_I(z)$ is determined, the remaining three other stress potentials $\Phi_M(z)$, $\Psi_M(z)$ and $\Psi_I(z)$ can be found from (5.4) and (2.10), respectively. In the following section, a particular class of inhomogeneous non-slip interface will be examined in order to illustrate the method.

5.3. A Class of Inhomogeneous Non-slip Interface

For the purposes of illustrating the method, consider a class of inhomogeneous non-slip interface defined by (see Figure 5-2)

$$f(\theta) = b_s \cos[s\theta] = \frac{b_s}{2}\left(\frac{z^s}{R^s} + \frac{R^s}{z^s}\right), \qquad -1 < b_s < 1 \tag{5.27}$$

As described previously, the solution for $\Phi_I(z)$ depends on the circumferential variation of the interface imperfections. However, by considering the roots of the polynomial $[1 + f(z)]$ this variation is eliminated and a solution can be obtained. Therefore, as in Chapter 3, the polynomial equation of degree $2s$

$$\left(\frac{z}{R}\right)^{2s} + \frac{2}{b_s}\left(\frac{z}{R}\right)^{s} + 1 = 0 \tag{5.28}$$

has s roots located within the circular inclusion. Let these s roots be denoted as

$$\rho_1, \rho_2, \ldots, \rho_s$$

then they can be determined by

$$\left(\frac{z}{R}\right)^{s} = \rho^s = \rho^* \tag{5.29}$$

where ρ^* is a real number, contained in the open interval $-1 < \rho^* < 1$, and given by

$$\rho^* = \begin{cases} -\sqrt{\dfrac{1}{b_s^2} - 1} - \dfrac{1}{b_s} > 0, & \text{if } b_s < 0, \\ \sqrt{\dfrac{1}{b_s^2} - 1} - \dfrac{1}{b_s} < 0, & \text{if } b_s > 0, \end{cases} \tag{5.30}$$

Note that

$$\frac{1+f(z)-\delta_o}{z[1+f(z)]}=\frac{R[1+f(z)-\delta_o]}{z[1+f(z)]}=\frac{1}{\left(\frac{z}{R}\right)}-\frac{\delta_o}{\left(\frac{z}{R}\right)[1+f(z)]}$$

but, in view of (3.24) the above is rewritten as

$$\frac{1+f(z)-\delta_o}{z[1+f(z)]}=\frac{R[1+f(z)-\delta_o]}{z[1+f(z)]}=\frac{1}{\left(\frac{z}{R}\right)}+\lambda\frac{\left(\frac{z}{R}\right)^{s-1}}{\left[\left(\frac{z}{R}\right)^{s}-\rho^{*}\right]}-\lambda\frac{\left(\frac{z}{R}\right)^{s-1}}{\left[\left(\frac{z}{R}\right)^{s}-\frac{1}{\rho^{*}}\right]},$$

$$\lambda\equiv-\delta_o\left(\frac{1+\rho^{*2}}{1-\rho^{*2}}\right)<0 \tag{5.31}$$

then, following a similar procedure outlined in Appendix B, the general solution of (5.24) takes the following form

$$\Phi_I(z)=\left(\frac{z}{R}\right)^{\frac{2\beta}{1+\beta}}\left[\left(\frac{z}{R}\right)^{s}-\rho^{*}\right]^{\frac{2\beta\lambda}{s(1+\beta)}}\left[\left(\frac{z}{R}\right)^{s}-\frac{1}{\rho^{*}}\right]^{-\frac{2\beta\lambda}{s(1+\beta)}}\times$$

$$\int_{z_I}^{z}P(t)\left(\frac{t}{R}\right)^{-\frac{2\beta}{1+\beta}}\left[\left(\frac{t}{R}\right)^{s}-\rho^{*}\right]^{-\frac{2\beta\lambda}{s(1+\beta)}}\left[\left(\frac{t}{R}\right)^{s}-\frac{1}{\rho^{*}}\right]^{\frac{2\beta\lambda}{s(1+\beta)}}dt,\qquad z\in D_I. \tag{5.32}$$

The solution Φ_I, given by (5.32), is well defined in D_I.

The domain, D_I, is cut along some non-intersecting straight lines originating from each of the singular points (i.e. $z=R\rho_k, k=1,2,...,s$). In other words, branch cuts are made from each of the s branch points of the multi-valued function appearing in (5.32) with each branch cut running parallel to the real axis in such a way that there is no overlap. Since $\lambda<0$ and $\beta>0$ the integral in (5.32) converges at each of the s branch points (i.e. the integral in (5.32) is a weakly

singular kernel). In addition, to guarantee that Φ_I is bounded at $z = R\rho_1$ it must be that $C_o = 0$, and the other remaining $(s-1)$ branch points give

$$\int_{R\rho_1}^{R\rho_k} P(t)\left(\frac{t}{R}\right)^{-\frac{2\beta}{1+\beta}}\left[\left(\frac{t}{R}\right)^{s}-\rho^{*}\right]^{-\frac{2\beta\lambda}{s(1+\beta)}}\left[\left(\frac{t}{R}\right)^{s}-\frac{1}{\rho^{*}}\right]^{\frac{2\beta\lambda}{s(1+\beta)}} dt = 0, \qquad k = 2,3,...,s, \tag{5.33}$$

respectively.

It remains to prove that Φ_I, given by (5.32), is continuous across each of the s branch cuts. Since the integral is convergent at each of the s branch points, then the integration path can be taken along the edges of any one of the s branch cuts made from $z = R\rho_k (k = 1,2,...,s)$ and pass through any one of the s integrable branch points. In this way, the multi-valued functions appearing outside and under the integral sign compensate each other; consequently, Φ_I, given by (5.32), is continuous across each of the s branch cuts (see Chapter 3 for discussion).

Hence, to the determine the $(s+1)$ undetermined, in general, complex coefficients X_k, we use the two real compatibility conditions, (5.6) and (5.21), along with the $(s-1)$ boundedness conditions given by (5.33). However, we must note that the two real compatibility conditions gives only one complex condition, this means one additional complex condition is required. Following the work of [80], this additional complex condition will be provided by the analyticity of Φ_I, given

by (5.32), at the remaining singular point $z = 0$. Since its form depends on the value of the parameter β, three separate cases must be discussed.

5.3.1. Case I $\beta < 1$

In this case, rewrite condition (5.32) as follows

$$\frac{\Phi_I(z)}{\left(\frac{z}{R}\right)} = \left(\frac{z}{R}\right)^{\frac{\beta-1}{1+\beta}} \left[\left(\frac{z}{R}\right)^s - \rho^*\right]^{\frac{2\beta\lambda}{s(1+\beta)}} \left[\left(\frac{z}{R}\right)^s - \frac{1}{\rho^*}\right]^{-\frac{2\beta\lambda}{s(1+\beta)}} \times$$
$$\int_{z_I}^{z} P(t) \left(\frac{t}{R}\right)^{-\frac{2\beta}{1+\beta}} \left[\left(\frac{t}{R}\right)^s - \rho^*\right]^{-\frac{2\beta\lambda}{s(1+\beta)}} \left[\left(\frac{t}{R}\right)^s - \frac{1}{\rho^*}\right]^{\frac{2\beta\lambda}{s(1+\beta)}} dt \qquad (5.34)$$

then, in view of conditions (2.5 - 2.6), it must be that at the point $z = 0$ the left hand side of (5.34) is analytic and thus bounded within D_I. Furthermore, owing to the fact that $\beta <$ 1and non-negative it follows that

$$\int_{R\rho_1}^{0} P(t) \left(\frac{t}{R}\right)^{-\frac{2\beta}{1+\beta}} \left[\left(\frac{t}{R}\right)^s - \rho^*\right]^{-\frac{2\beta\lambda}{s(1+\beta)}} \left[\left(\frac{t}{R}\right)^s - \frac{1}{\rho^*}\right]^{\frac{2\beta\lambda}{s(1+\beta)}} dt = 0, \qquad (5.35)$$

and since $\lambda < 0$ the integrand in (5.35) is weakly singular and as such, the integration path can pass through the branch point corresponding to $z = 0$. Thus, $\Phi_I(z)$ given by (42) is analytic and continuous in D_I including the singular point $z = 0$. Hence, the $(s + 1)$ undetermined coefficients X_k are determined by (5.6), (5.21), (5.33) and (5.35).

5.3.2. Case II $\beta > 1$

In this case $\Phi_I(z)$, given by (5.32), is zero when $z = 0$. However, we must guarantee that Φ_I is analytic in D_I by verifying that (5.32) is continuous across the straight branch cut made from the branch point $z = 0$. To show this, let us rewrite (5.32) as follows

$$\Phi_I(z) = \int_{R\rho_1}^{z} P(t) \left(\frac{z}{t}\right)^{\frac{2\beta}{1+\beta}} \left[\frac{\left[\left(\frac{z}{R}\right)^s - \rho^*\right]}{\left[\left(\frac{t}{R}\right)^s - \rho^*\right]}\right]^{\frac{2\beta\lambda}{s(1+\beta)}} \left[\frac{\left[\left(\frac{t}{R}\right)^s - \frac{1}{\rho^*}\right]}{\left[\left(\frac{z}{R}\right)^s - \frac{1}{\rho^*}\right]}\right]^{\frac{2\beta\lambda}{s(1+\beta)}} dt. \tag{5.36}$$

Therefore, we require that two limit values of the varying limit integral, given by (5.36), are equal when the upper limit approaches any point on the branch cut (made form the branch point corresponding to $z = 0$) from both sides respectively. Here, the integrand has an unintegrable singularity at the point $z = 0$; consequently, the integration path cannot pass through the point $z = 0$. Hence, to guarantee that Φ_I is analytic across the straight branch cut we consider, as shown in Chapter 3, the difference $\Phi_I(z^+) - \Phi_I(z^-)$ where $\Phi_I(z^\pm)$ denotes the values of $\Phi_I(z)$ as z approaches the straight branch cut from above and below, respectively. This condition must hold for all points provided that it holds for any particular point on the branch cut. So then, let $\tilde{z}$ be any particular point on the straight

branch cut. Hence, for Φ_I to be continuous across the branch cut at the point $z = \widetilde{z}$ we must have that $\Phi_I(\widetilde{z}) = [\Phi_I(z^+) - \Phi_I(z^-)] = 0$ from which it follows that

$$\int_{\Upsilon} P(t) \left(\frac{\widetilde{z}}{t}\right)^{\frac{2\beta}{1+\beta}} \left[\frac{\left[\left(\frac{\widetilde{z}}{R}\right)^s - \rho^*\right]}{\left[\left(\frac{t}{R}\right)^s - \rho^*\right]}\right]^{\frac{2\beta\lambda}{s(1+\beta)}} \left[\frac{\left[\left(\frac{t}{R}\right)^s - \frac{1}{\rho^*}\right]}{\left[\left(\frac{\widetilde{z}}{R}\right)^s - \frac{1}{\rho^*}\right]}\right]^{\frac{2\beta\lambda}{s(1+\beta)}} dt = 0 \qquad (5.37)$$

where Υ is some arbitrary closed curve within D_I enclosing the singular point $z = 0$ and passing through the points $z = \widetilde{z}$ and $z = R\rho_1$. Note that the value of $\widetilde{z}$ in (5.37) jumps from one edge of the branch cut to the opposite edge when the variable of integration, t, passes through the point $z = R\rho_1$ along Υ. Thus, the $(s+1)$ undetermined constants X_k are determined by (5.6), (5.21), (5.33) and (5.37).

5.3.3. Case III $\beta = 1$

Finally, consider the case corresponding to $\beta = 1$. At the branch point $z = 0$, $P(0) = 0$, thus the expression $\dfrac{P(t)}{t}$ is non-singular at the point $z = 0$ (i.e. there is no unintegrable singularity at the point $z = 0$).

The proof of this result is as follows. From (5.23) with $\beta = 1$, we have

$$[1+f(z)]\,P(z) = L(z) + \frac{1}{2}\,[\delta_o - 1 - f(z)]\,(A+\beta X_1) - [1+f(z)]\times$$

$$\left[\frac{1}{2}\left(A+\frac{B_1}{R^2}-X_1\right) - B\frac{z^2}{2R^2}(1+\eta) - \frac{z^2(\varepsilon_2 - i\varepsilon_3)}{R^2\left(\frac{\kappa_M}{\mu_M}+\frac{1}{\mu_I}\right)}\right] - \frac{\varepsilon_1\delta_o}{\frac{\kappa_M}{\mu_M}+\frac{1}{\mu_I}} -$$

$$\frac{\delta_o\eta}{2}\left(A+\frac{B_1}{R^2}-X_1\right).$$

Now, as $z \to 0$ the above reduces to the following

$$P(0) + \frac{P(0)}{2}\sum_{k=1}^{s}(b_k+ia_k)\left(\frac{R}{z}\right)^k = \frac{1}{2}\sum_{k=1}^{s}(b_k+ia_k)\left(\frac{R}{z}\right)^k \sum_{j=0}^{k}(j-1)X_j z^{j-1} +$$

$$\frac{1}{2}\sum_{k=1}^{s} k\,(b_k+ia_k)\,R^k X_{k+1} + \delta_o X_1,$$

$\Longleftrightarrow$

$$\frac{P(0)}{\frac{1}{2}\sum_{k=1}^{s}(b_k+ia_k)\left(\frac{R}{z}\right)^k} + P(0) = \sum_{j=0}^{k}(j-1)X_j z^{j-1} + \frac{\frac{1}{2}\sum_{k=1}^{s} k\,(b_k+ia_k)\,R^k X_{k+1}}{\frac{1}{2}\sum_{k=1}^{s}(b_k+ia_k)\left(\frac{R}{z}\right)^k} +$$

$$\frac{\delta_o X_1}{\frac{1}{2}\sum_{k=1}^{s}(b_k+ia_k)\left(\frac{R}{z}\right)^k},$$

which clearly shows that $P(0) \equiv 0$ when $z = 0$.

Hence, Φ_I, given by (5.32), is identically equal to zero at the branch point $z = 0$. However, the consistency condition (5.26), which applies only when $\beta = 1$,

gives the following

$$RX_1 = (-\rho^*)^{\frac{\lambda}{s}} \left(\frac{-1}{\rho^*}\right)^{-\frac{\lambda}{s}} \int_{R\rho_1}^{0} \frac{P(t)}{\left(\frac{t}{R}\right)} \left[\left(\frac{t}{R}\right)^s - \rho^*\right]^{-\frac{\lambda}{s}} \left[\left(\frac{t}{R}\right)^s - \frac{1}{\rho^*}\right]^{\frac{\lambda}{s}} dt. \quad (5.38)$$

Thus, when $\beta = 1$ the $(s+1)$ undetermined coefficients X_k are determined by (5.6), (5.21), (5.33) and (5.38).

5.4. Summary

This chapter has extended the single inclusion problem to deal with problems relevant to biomechanics. The rigorous solution of a model of a single circular inclusion with circumferentially inhomogeneous non-slip interface characterized by the condition $m(\theta)$ finite and $n(\theta) = \infty$ has been presented. Our method has been developed as a consequence of the fact that the circumferential variation of the interface parameter leads to the failure of the conventional power series method. Instead analytic continuation is used to obtain an exact closed form solution for $\Phi_I(z)$, which is given by (5.32). The $(s+1)$ undetermined constants X_k are determined by a system of $(s+1)$ linear algebraic equations that can be given in terms of definite integrals of known power functions. This method will be illustrated for two specific variations of the interface parameter in Chapter 6.

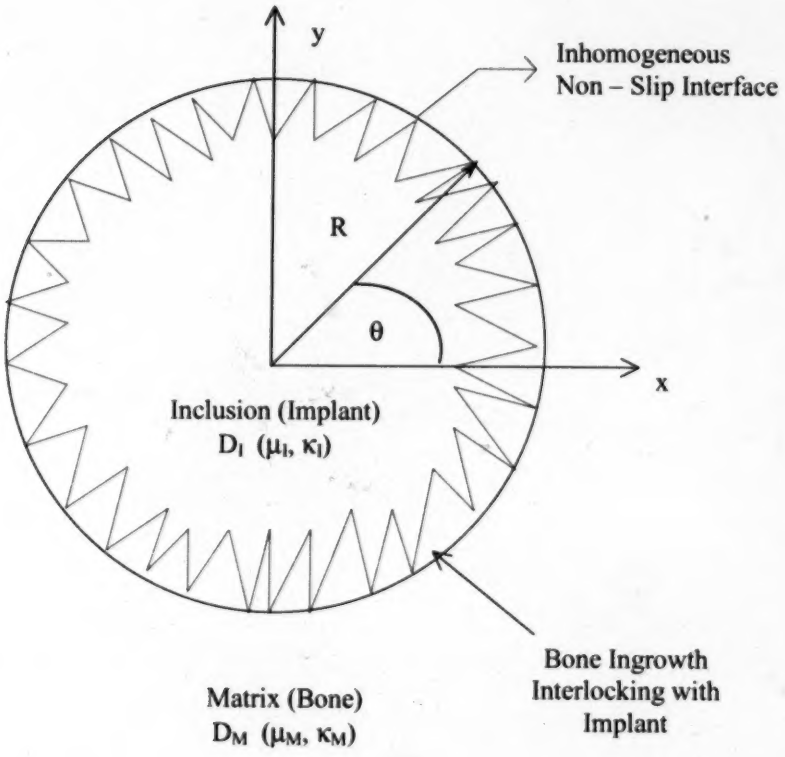

Figure 5-1. A Homogeneous Circular Inclusion with Circumferentially Inhomogeneous Non – Slip Interface

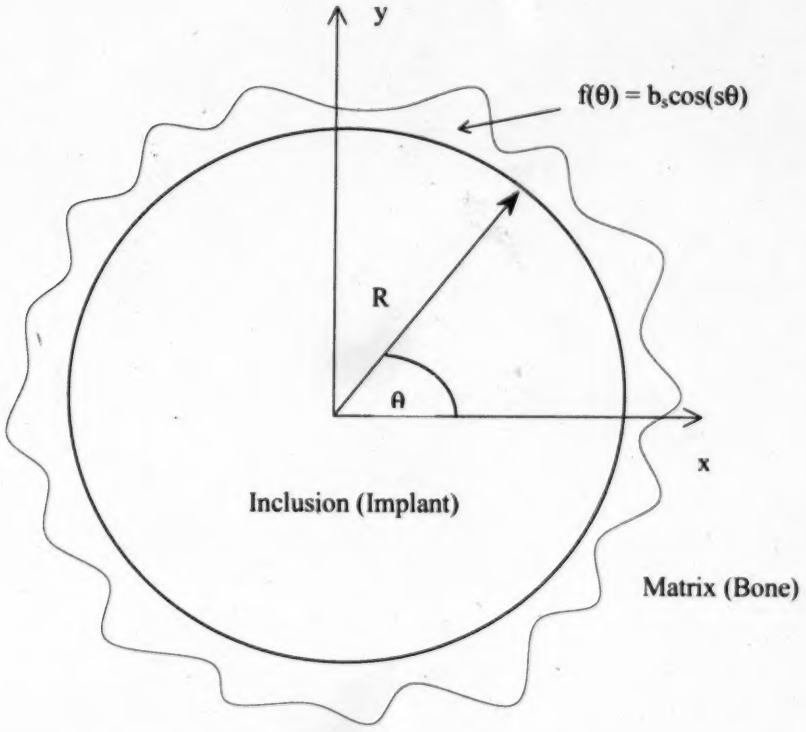

Figure 5-2. Schematic Representation of the Inhomogeneous Non – Slipping Interface

CHAPTER 6

Examples of the Inhomogeneous Non-Slipping Interface

6.1. Introduction

This chapter presents examples illustrating the methodology of the solution process derived in Chapter 5. In particular, two specific examples corresponding to the functional form of the inhomogeneous non-slipping interface will be illustrated. In the first case, the functional form of the inhomogeneous non-slipping interface is given by the circumferential number $s = 1$. In this instance only two coefficients need to be determined. In the second case, the inhomogeneity of the non-slipping interface is given by the circumferential number $s = 2$. In contrast to the first example, this second case is slightly more complicated in that three coefficients need to be determined. Note that the variation or distribution in interface imperfections depends on the specific value of the parameter s. Therefore, if the maximum order of the polynomial that describes the inhomogeneous non-slipping interface takes on the value $s = 2$, the variation in imperfections along the material interface corresponding to this case is greater than that corresponding to a variation

of imperfection given by say $s = 1$. Hence, the larger the order of the polynomial (i.e. circumferential number) describing the inhomogeneous non-slipping interface the greater the variation of interface imperfection.

In addition, the effects of the inhomogeneous non-slipping interface parameter on the average stresses induced within the inclusion will be examined for both cases, respectively. As well, the interfacial shear stress will be computed for the case corresponding to the circumferential number $s = 1$.

For definiteness, we confine ourselves to the case $\beta = 1$. In this instance, the stress potential $\Phi_I(z)$ is given as follows

$$\Phi_I(z) = \left(\frac{z}{R}\right)\left[\left(\frac{z}{R}\right)^s - \rho^*\right]^{\frac{\lambda}{s}}\left[\left(\frac{z}{R}\right)^s - \frac{1}{\rho^*}\right]^{-\frac{\lambda}{s}} \times$$
$$\int_{R\rho_1}^{z} P(t)\left(\frac{t}{R}\right)^{-1}\left[\left(\frac{t}{R}\right)^s - \rho^*\right]^{-\frac{\lambda}{s}}\left[\left(\frac{t}{R}\right)^s - \frac{1}{\rho^*}\right]^{\frac{\lambda}{s}} dt, \qquad z \in D_I \tag{6.1}$$

where $P(t)$ is given by condition (5.23) which includes the $(s+1)$ undetermined coefficients X_k, $k = 1, 2, ..., (s+1)$.

6.2. Inhomogeneous Non-Slipping Interface with Circumferential Number $s = 1$

In this situation, the functional form of the inhomogeneous non-slipping imperfect interface is given by the following (see Figure 6-1)

$$f(z) = \frac{b_1}{2}\left(\frac{z}{R} + \frac{R}{z}\right), \quad -1 < b_1 < 1. \tag{6.2}$$

In this particular instance, the only two undetermined coefficients are X_1 and X_2. These constants can be obtained from conditions (5.6), (5.21) and (5.38). Using these results, the solutions for X_1 and X_2 are given by

$$X_1\left[\delta_o(1+\eta)+2\right] = A\delta_o(1+\eta) - \frac{2\delta_o\varepsilon_1}{\dfrac{\kappa_M}{\mu_M}+\dfrac{1}{\mu_I}} - \frac{b_1 R}{2}\left(X_2 + \overline{X_2}\right) \tag{6.3}$$

and

$$X_2 R^2 \frac{\rho^*}{\lambda\left(1-\rho^{*2}\right)} = 2X_1 I_1 - \left[\frac{B}{2}(1+\eta) + \frac{(\varepsilon_2 - i\varepsilon_3)}{\dfrac{\kappa_M}{\mu_M}+\dfrac{1}{\mu_I}}\right] I_2, \tag{6.4}$$

where

$$I_1 \equiv (-\rho^*)^\lambda \left(-\frac{1}{\rho^*}\right)^{-\lambda} \int_{R\rho^*}^{0} \left(\frac{t}{R}\right)\left[\frac{t}{R}-\rho^*\right]^{-(\lambda+1)}\left[\frac{t}{R}-\frac{1}{\rho^*}\right]^{\lambda-1} dt,$$

$$I_2 \equiv (-\rho^*)^\lambda \left(-\frac{1}{\rho^*}\right)^{-\lambda} \int_{R\rho^*}^{0} \left(\frac{t}{R}\right)\left[\frac{t}{R}-\rho^*\right]^{-\lambda}\left[\frac{t}{R}-\frac{1}{\rho^*}\right]^{\lambda} dt. \tag{6.5}$$

If, for example, $\lambda = -1$, then integrating (6.5) and substituting into (6.4), the general expression for X_2 is found to be

$$RX_2\left(\frac{\rho^*}{1-\rho^{*2}}\right) = \left[\frac{B}{2}(1+\eta) + \frac{(\varepsilon_2 - i\varepsilon_3)}{\frac{\kappa_M}{\mu_M} + \frac{1}{\mu_I}}\right]\left[\frac{\rho^{*2}-2}{2\rho^{*2}} + \left(\frac{1-\rho^{*2}}{\rho^{*4}}\right)\ln\left(\frac{1}{1-\rho^{*2}}\right)\right] - \frac{2X_1}{\rho^{*2}}\left[\ln\left(\frac{1}{1-\rho^{*2}}\right) - \frac{\rho^{*2}}{1-\rho^{*2}}\right]. \tag{6.6}$$

Having found the coefficient X_2, the value for the coefficient X_1 is readily obtained from condition (6.3). Obviously, once X_1 and X_2 are known, the rigorous solution for $\Phi_I(z)$ is given by (6.1) in closed-form. Furthermore, with Φ_I computed, the remaining stress potentials $\Psi_M(z)$, $\Psi_I(z)$ and $\Phi_M(z)$,can be readily obtained from conditions (2.10) and (5.4), respectively. This will be shown in the upcoming section discussing interfacial stress.

6.2.1. Average Stress

The calculation of the average stress inside the inclusion gives important information regarding the overall understanding and behavior of composite material (see Chapter 1). In this case, the formulation for the average stress is identical to that given in Chapter 2. However, there is a slight modification in the derivation of the expression $(\sigma_x - i\sigma_{xy})_{Avg}$.

From (2.20) we have

$$(\sigma_x - i\sigma_{xy})_{Avg} = X_1 + \overline{X_1} - B - \frac{1}{R^2}\overline{A_1}.$$

Now, from condition (5.5), comparing coefficients of powers of z^2 yields an expression for $\overline{A}_1$, which gives

$$-\frac{\overline{A_1}}{R^2} = \beta R^2 X_3 - B\eta - 2\frac{(\varepsilon_2 - i\varepsilon_3)}{\left(\frac{\kappa_M}{\mu_M} + \frac{1}{\mu_I}\right)}.$$

Thus, the expressions for the average stresses induced within the inclusion are given by

$$(\sigma_x + \sigma_y)_{Avg} = 2\left(X_1 + \overline{X_1}\right),$$

$$(\sigma_x - i\sigma_{xy})_{Avg} = X_1 + \overline{X_1} - 2\left[B\left(\frac{1+\eta}{2}\right) + \frac{(\varepsilon_2 - i\varepsilon_3)}{\frac{\kappa_M}{\mu_M} + \frac{1}{\mu_I}} - \frac{\beta R^2}{2}X_3\right]. \qquad (6.7)$$

Note that the subscript *Avg* denotes the average value.

To demonstrate the effects of the circumferential inhomogeneous non-slip interface parameter on the average stress induced within the inclusion for the case $s = 1, \beta = 1$ and $\lambda = -1$, we compare the inhomogeneous nonslip interface defined by

$$\frac{1}{m(\theta)} = \frac{R\left(\frac{\kappa_M}{\mu_M} + \frac{1}{\mu_I}\right)}{2\delta_o}\left[1 + b_1\cos(\theta)\right], \qquad -1 < b_1 < 1$$

$$\delta_o = \left(\frac{1-\rho^{*2}}{1+\rho^{*2}}\right) \tag{6.8}$$

with the following corresponding homogeneous non-slip interface under otherwise identical conditions

$$\frac{1}{m} = \frac{R\left(\frac{\kappa_M}{\mu_M} + \frac{1}{\mu_I}\right)}{2\delta_o}, \qquad \delta_o = \left(\frac{1-\rho^{*2}}{1+\rho^{*2}}\right). \tag{6.9}$$

Note that when the interface parameter $\rho^* = 0$ (i.e. corresponding homogeneous non-slip interface condition) it is easily shown that (following procedures outlined in Appendix C and D) (6.3) and (6.4) reduce to the following

$$X_2 = 0$$

$$X_1\left(1 + \eta + \frac{2}{\delta_o}\right) = A(1+\eta) - \frac{2\varepsilon_1}{\frac{\kappa_M}{\mu_M} + \frac{1}{\mu_I}}. \tag{6.10}$$

Therefore, in view of (6.10) and assuming no eigenstrains, the average mean stress associated with a homogeneous interface (6.9), under otherwise identical conditions is, given by

$$(\sigma_x + \sigma_y)^H_{Avg} = \frac{4A(1+\eta)(1-\rho^{*2})}{3 + \eta + \rho^{*2}(1-\eta)}. \tag{6.11}$$

Here, as before, the superscript H denotes the stresses associated with the homogeneous interface.

For the average mean stress corresponding to the inhomogeneous interface, let us assume, as before, that all eigenstrains vanish as well as that $\mathrm{Im}[B] = 0$ (a state of biaxial stress). Hence, in view of (6.3) and (6.6) the average mean stress associated with the inhomogeneous interface (6.8) is given by

$$(\sigma_x + \sigma_y)_{Avg} = \frac{4(1+\eta)\left[A + B\left[\frac{\rho^{*2}-2}{2\rho^{*2}} + \left(\frac{1-\rho^{*2}}{\rho^{*4}}\right)\ln\left(\frac{1}{1-\rho^{*2}}\right)\right]\right]}{\frac{4}{\rho^{*2}}\ln\left(\frac{1}{1-\rho^{*2}}\right) + (\eta - 1)} \tag{6.12}$$

It follows that the ratio $G(\eta, \rho^*)$ of the average mean stress (i.e. the ratio of the expressions in (6.12) to the corresponding expression in (6.11)) is given by

$$(\sigma_x + \sigma_y)_{Avg} = G(\eta, \rho^*)\,(\sigma_x + \sigma_y)^H_{Avg}\ ,$$

$$G(\eta, \rho^*) = \frac{(3 + \eta + \rho^{*2}(1-\eta))\left[A + B\left[\frac{\rho^{*2}-2}{2\rho^{*2}} + \left(\frac{1-\rho^{*2}}{\rho^{*4}}\right)\ln\left(\frac{1}{1-\rho^{*2}}\right)\right]\right]}{A(1-\rho^{*2})\left(\frac{4}{\rho^{*2}}\ln\left(\frac{1}{1-\rho^{*2}}\right) + (\eta - 1)\right)}. \tag{6.13}$$

Note that the behavior of (6.13) at the limiting points of ρ^* will depend on the orientation of loading. For example, consider the case when we have a uniaxial stress state in the y-direction (i.e. $2A - B = 0$). In this case, (6.13) reduces to the following

$$(\sigma_x + \sigma_y)_{Avg} = G(\eta, \rho^*)\,(\sigma_x + \sigma_y)^H_{Avg}\ ,$$

$$G(\eta, \rho^*) = \frac{2\,(3 + \eta + \rho^{*2}(1-\eta))\left[\dfrac{1}{\rho^{*2}}\ln\left(\dfrac{1}{1-\rho^{*2}}\right) - 1\right]}{4\ln\left(\dfrac{1}{1-\rho^{*2}}\right) - \rho^{*2}\,(1-\eta)} \tag{6.14}$$

Clearly, there is no singular behavior in the ratio of the average mean stress at the limiting points of ρ^*.

If, on the other hand, we consider a uniaxial stress state in the x-direction (i.e. $2A + B = 0$) then (6.13) becomes

$$(\sigma_x + \sigma_y)_{Avg} = H(\eta, \rho^*)\,(\sigma_x + \sigma_y)^H_{Avg}\ ,$$

$$H(\eta, \rho^*) = \frac{2\,(3 + \eta + \rho^{*2}(1-\eta))\left[1 - \left(\dfrac{1-\rho^{*2}}{\rho^{*2}}\right)\ln\left(\dfrac{1}{1-\rho^{*2}}\right)\right]}{(1-\rho^{*2})\left(4\ln\left(\dfrac{1}{1-\rho^{*2}}\right) - \rho^{*2}\,(1-\eta)\right)} \tag{6.15}$$

In this loading configuration, it is clear that when $\rho^{*2} \to 1$, the ratio of the average stresses tends to infinity. The reason for this behavior is the presence of the polynomial term $(1 - \rho^{*2})$ appearing in the denominator which makes the ratio $H(\eta, \rho^*)$ unbounded as $\rho^{*2} \to 1$.

The effects of the circumferential inhomogeneity of the interface, as represented by the functions $G(\eta, \rho^*)$ and $H(\eta, \rho^*)$ for the two respective loading conditions, are given in Figures 6-2 and 6-3, respectively. In both loading configurations, the

results show that replacing the inhomogeneous non - slip interface by its homogeneous counterpart has a significant effect on the estimation of the average mean stress induced within the circular inclusion. For example, under uniaxial loading in the y-direction, the relative error in the average mean stress caused by neglecting the inhomogeneity of interface imperfections approaches 90% (Figure 6-2). Hence, the current results reinforce those established in Chapter 4: in that replacing an inhomogeneous interface by its homogeneous counterpart leads to significant errors in even the calculation of the average stresses induced within the inclusion.

6.2.2. Interfacial Shear Stress

As outlined in Chapter 1, the issue of having high interfacial stress peaks, provoked by shear stresses, is of primary concern regarding the stability of the implant. High interfacial stress peaks indicate that the load transfer is poorly distributed and interface failure is possible. Thus, achieving uniform interfacial stresses by controlling where load transfer is concentrated is essential in maintaining a stable implant.

In order to determine the interfacial stress distribution around the circular implant, requires the evaluation of only three stress potentials Φ_I, Φ_M, and Ψ_I, respectively (see [109]). Therefore, in view of conditions (6.1) and the parameters

corresponding to $s = 1, \beta = 1$ and $\lambda = -1$, $\Phi_I(z)$ is given by the following expression

$$\Phi_I(z) = X_1 z \left\{ \frac{3-\rho^{*2}}{1-\rho^{*2}} - 2\frac{\left[\frac{z}{R} - \frac{1}{\rho^*}\right]}{\left[\frac{z}{R} - \rho^*\right]} \log\left[\frac{1-\rho^*\frac{z}{R}}{1-\rho^{*2}}\right] \right\} - X_2 R\left(\frac{\rho^*}{1-\rho^{*2}}\right) z +$$
$$\left[\frac{B}{2}(1+\eta) + \frac{(\varepsilon_2 - i\varepsilon_3)}{\left(\frac{\kappa_M}{\mu_M} + \frac{1}{\mu_I}\right)}\right] \left\{ z\left[\frac{z}{R} - \frac{1}{\rho^*}\right]\left[\frac{z}{2R} + \frac{1}{\rho^*} - \frac{\rho^*}{2}\right] + \right.$$
$$\left. z\left(\frac{1-\rho^{*2}}{\rho^{*2}}\right) \frac{\left[\frac{z}{R} - \frac{1}{\rho^*}\right]}{\left[\frac{z}{R} - \rho^*\right]} \log\left[\frac{1-\rho^*\frac{z}{R}}{1-\rho^{*2}}\right] \right\}, \quad z \in D_I. \tag{6.16}$$

The solution for $\Phi_M(z)$ is obtained by solving (5.4). To this end, the expression for $\Phi_M(z)$ is given by

$$\Phi_M(z) = Az + 2\overline{X_1}z\left\{\frac{\left[\frac{R}{z}-\frac{1}{\rho^*}\right]}{\left[\frac{R}{z}-\rho^*\right]}\log\left[\frac{1-\rho^*\frac{R}{z}}{1-\rho^{*2}}\right]-\frac{1}{1-\rho^{*2}}\right\}+\overline{X_2}R\left(\frac{\rho^*}{1-\rho^{*2}}\right)z$$

$$-\left[\frac{\overline{B}}{2}(1+\eta)+\frac{(\varepsilon_2+i\varepsilon_3)}{\left(\frac{\kappa_M}{\mu_M}+\frac{1}{\mu_I}\right)}\right]\left\{z\left[\frac{R}{z}-\frac{1}{\rho^*}\right]\left[\frac{R}{2z}+\frac{1}{\rho^*}-\frac{\rho^*}{2}\right]+\right.$$

$$\left.z\left(\frac{1-\rho^{*2}}{\rho^{*2}}\right)\frac{\left[\frac{R}{z}-\frac{1}{\rho^*}\right]}{\left[\frac{R}{z}-\rho^*\right]}\log\left[\frac{1-\rho^*\frac{R}{z}}{1-\rho^{*2}}\right]\right\}+\left[\overline{B}\eta+2\frac{(\varepsilon_2+i\varepsilon_3)}{\left(\frac{\kappa_M}{\mu_M}+\frac{1}{\mu_I}\right)}\right]\frac{R^2}{z}$$

$$+\frac{\frac{\overline{C_1}}{\mu_M}-\frac{\overline{C_2}}{\mu_I}}{\left(\frac{\kappa_M}{\mu_M}+\frac{1}{\mu_I}\right)}, \quad z\in D_M. \tag{6.17}$$

Having obtained the expressions for $\Phi_I(z)$ and $\Phi_M(z)$, the remaining stress potential $\Psi_I(z)$ can be obtained form condition $(2.10)_2$. To this end, the expression for $\Psi_I(z)$ is given as follows

$$\Psi_I(z) = X_1 \frac{R^2}{z} \left\{ \frac{2}{\left[\frac{z}{R} - \rho^*\right]^2} \log\left[\frac{1-\rho^*\frac{z}{R}}{1-\rho^{*2}}\right] \left[2\left(\frac{z}{R}\right)^2 - \left(\frac{1+3\rho^{*2}}{\rho^*}\right)\frac{z}{R} + 2\right] + \right.$$

$$\left. \frac{4\rho^* - 2\left(\frac{z}{R}\right)(1+\rho^{*2})}{(1-\rho^{*2})\left[\frac{z}{R} - \rho^*\right]} \right\} + \left[B(1+\eta) + 2\frac{(\varepsilon_2 - i\varepsilon_3)}{\left(\frac{\kappa_M}{\mu_M} + \frac{1}{\mu_I}\right)} \right] z -$$

$$\left[\frac{B}{2}(1+\eta) + \frac{(\varepsilon_2 - i\varepsilon_3)}{\left(\frac{\kappa_M}{\mu_M} + \frac{1}{\mu_I}\right)} \right] \left(\frac{R^2}{z}\right) \left\{ 2\left(\frac{z}{R}\right)^2 + \frac{3}{2}\left(\frac{1}{\rho^*} - \rho^*\right)\frac{z}{R} + 1 - \frac{2}{\rho^{*2}} + \right.$$

$$\left. \left(\frac{1-\rho^{*2}}{\rho^{*2}}\right) \frac{\frac{z}{R}}{\left[\frac{z}{R} - \rho^*\right]} + \left(\frac{1-\rho^{*2}}{\rho^{*2}}\right) \frac{\log\left[\frac{1-\rho^*\frac{z}{R}}{1-\rho^{*2}}\right]}{\left[\frac{z}{R} - \rho^*\right]^2} \left[2\left(\frac{z}{R}\right)^2 - \left(\frac{1+3\rho^{*2}}{\rho^*}\right)\frac{z}{R} + 2\right] \right\}$$

$$+ \frac{\frac{C_2\kappa_M + C_1}{\mu_M}}{\left(\frac{\kappa_M}{\mu_M} + \frac{1}{\mu_I}\right)}, \quad z \in D_I. \tag{6.18}$$

Note that the constants C_1 and C_2 need not be determined explicitly. They merely reflect a rigid body translation and have no influence on the corresponding stress fields.

As detailed in Chapter 1, cementless implants have a rough porous coating applied to them. Thus, in this case, one can assume that the bone, at the interface, is subjected to a biaxial load while contacting the implant. This biaxial

load consists of a normal compressive stress in the direction perpendicular to the direction of bone ingrowth as well as a normal compressive stress in the direction of bone ingrowth (i.e. in this case $\mathrm{Im}[B] = 0$). Then, depending on the ratio

$$\varpi = \frac{\sigma_x^\infty}{\sigma_y^\infty} = \frac{2A - B}{2A + B}, \tag{6.19}$$

where σ_x^∞ and σ_y^∞ are the applied loadings, the interface stresses are obtained via Muskhelishvili's results, (2.1). In particular, the interfacial stresses can be obtained through

$$\sigma_r - i\sigma_{r\theta} = \Phi_I'(z) + \overline{\Phi_I'(z)} - e^{2i\theta}\left[\bar{z}\Phi_I''(z) + \Psi_I'(z)\right] \tag{6.20}$$

and since the tractions are continuous across the inclusion - matrix boundary, the interface stresses can be approached from the inclusion side by noting that $z = \mathrm{R}e^{i\theta}$ at the boundary. Hence, using conditions (6.3), (6.6), (6.16 - 6.19) and separating real and imaginary parts from (6.20), the interfacial shear stress is determined and given by

$$\sigma_{r\theta} = A\frac{(1-\varpi)(1+\eta)}{(1+\varpi)}\left\{\sin\theta\left[6\cos\theta+\left(\frac{1-\rho^{*2}}{\rho^{*}}\right)\right]+2\left(\frac{1-\rho^{*2}}{\rho^{*2}}\right)\times\right.$$
$$\left[\begin{array}{c}\left(\frac{1-\rho^{*2}}{\rho^{*}}\right)\sin\theta\ln\left[\frac{(1-2\rho^{*}\cos\theta+\rho^{*2})^{1/2}}{1-\rho^{*2}}\right]+\\ \frac{\left(\frac{1+\rho^{*2}}{\rho^{*}}\right)\cos\theta\tan^{-1}\left(\frac{\rho^{*}\sin\theta}{1-\rho^{*}\cos\theta}\right)-2\tan^{-1}\left(\frac{\rho^{*}\sin\theta}{1-\rho^{*}\cos\theta}\right)}{1-2\rho^{*}\cos\theta+\rho^{*2}}\end{array}\right]\Bigg\}-$$
$$4X_1\left[\begin{array}{c}\left(\frac{1-\rho^{*2}}{\rho^{*}}\right)\sin\theta\ln\left[\frac{(1-2\rho^{*}\cos\theta+\rho^{*2})^{1/2}}{1-\rho^{*2}}\right]+\\ \frac{\left(\frac{1+\rho^{*2}}{\rho^{*}}\right)\cos\theta\tan^{-1}\left(\frac{\rho^{*}\sin\theta}{1-\rho^{*}\cos\theta}\right)-2\tan^{-1}\left(\frac{\rho^{*}\sin\theta}{1-\rho^{*}\cos\theta}\right)}{1-2\rho^{*}\cos\theta+\rho^{*2}}\end{array}\right] \tag{6.21}$$

where the coefficient X_1 is given as

$$X_1 = A\frac{(1+\eta)\rho^{*2}(1-\rho^{*2})}{(1+\varpi)}\left[\frac{(1+\varpi)+2(1-\varpi)\left[\begin{array}{c}\frac{\rho^{*2}-2}{2\rho^{*2}}+\\ \left(\frac{1-\rho^{*2}}{\rho^{*4}}\right)\ln\left(\frac{1}{1-\rho^{*2}}\right)\end{array}\right]}{\begin{array}{c}\rho^{*2}(3+\eta)+\rho^{*4}(1-\eta)+4(1-\rho^{*2})\times\\ \left[\ln\left(\frac{1}{1-\rho^{*2}}\right)-\frac{\rho^{*2}}{1-\rho^{*2}}\right]\end{array}}\right] \tag{6.22}$$

Hence, to study the effects of the interfacial shear stress, let us non-dimensionalize the above by dividing through by $\left(\sigma_x^\infty + \sigma_y^\infty\right) = 4A$. Figures 6-4 - 6-8 illustrate, for various interface imperfections and loading configurations, the non-monotonic behavior of the interfacial shear stress as a function of position. These curves indicate that the high interfacial stress peaks (or stress concentrations) occur at the apexes along the curved portions of the circular implant. For example, Figure 6-4 shows that for a uniaxial load in the y-direction and having positive interface imperfections, the maximum interfacial stress occurs at approximately 48 and 312 degrees, respectively. Alternatively, considering the same loading but having negative interface imperfections, the maximum interfacial shear stress occurs at approximately 130 and 230 degrees, respectively (Figure 6-5). This suggests that load transfer is poorly distributed along the interface. In addition, the effect of the interface imperfections, for example when. $\rho^* > 0$, on the interfacial shear stress occurring at the maximum positions (i.e. $\theta = 48$ and 312 degrees, respectively) and under a uniaxial load, is presented in Figures 6-8. This result shows that as the degree of imperfection increases the interfacial shear stress decreases monotonically. This suggests that by increasing the level of imperfections along the interface one can reduce the interfacial stress thereby minimizing the potential of interface failure. Of course, interface failure is determined not only by the

driving force (such as interface stresses), but also by the critical stress, strain or strain energy density of the interphase (i.e. failure criterion for the interphase). Therefore, alternative measures, such as optimizing the stem shape, tailoring the elastic properties of the implant or a combination of both, may be used to reduce the high interfacial stress peaks in order to reach a stable implant design (see [104] and [113] for details).

6.3. Inhomogeneous Non-Slipping Interface with Circumferential Number $s = 2$

In this situation, the functional form of the inhomogeneous non-slipping imperfect interface is given by the following (see Figure 6-9)

$$f(z) = \frac{b_2}{2}\left[\left(\frac{z}{R}\right)^2 + \left(\frac{R}{z}\right)^2\right], \quad -1 < b_2 < 1. \tag{6.23}$$

In contrast to case corresponding to the circumferential number $s = 1$, this case is slightly more complicated, in that we have three undetermined coefficients: X_1, X_2 and X_3 which are determined via conditions (5.6), (5.21), (5.33) and (5.38). In addition, note that (see Chapter 4)

$$\rho_2 = -\rho_1, \qquad \rho_2^2 = \rho_1^2 = \rho^*.$$

Using these conditions, we arrive at the following expressions for the unknown coefficients

$$X_1\left[\delta_o(1+\eta)+2\right] = A\delta_o(1+\eta) - \frac{2\varepsilon_1\delta_o}{\frac{\kappa_M}{\mu_M}+\frac{1}{\mu_I}} + \frac{b_2}{2}\left[\left(\frac{1+\eta}{2}\right)(B+\overline{B}) + \frac{2\varepsilon_2}{\frac{\kappa_M}{\mu_M}+\frac{1}{\mu_I}}\right]$$
$$-b_2R^2\left(X_3+\overline{X_3}\right),$$
$$X_2 = 0, \tag{6.24}$$

and

$$2R^2X_3\frac{\rho^*}{\lambda(1-\rho^{*2})} = \frac{2X_1}{R}I_3 + \left[B\left(\frac{1+\eta}{2}\right) + \frac{(\varepsilon_2-i\varepsilon_3)}{\frac{\kappa_M}{\mu_M}+\frac{1}{\mu_I}}\right]\cdot\left(\frac{\rho^*}{\lambda(1-\rho^{*2})} - \frac{I_4}{R}\right) \tag{6.25}$$

where

$$I_3 \equiv (-\rho^*)^{\frac{\lambda}{2}}\left(-\frac{1}{\rho^*}\right)^{-\frac{\lambda}{2}}\int_{R\rho_1}^{0}\left(\frac{t}{R}\right)^3\left[\left(\frac{t}{R}\right)^2-\rho^*\right]^{-(\frac{\lambda}{2}+1)}\left[\left(\frac{t}{R}\right)^2-\frac{1}{\rho^*}\right]^{\frac{\lambda}{2}-1}dt$$
$$I_4 \equiv (-\rho^*)^{\frac{\lambda}{2}}\left(-\frac{1}{\rho^*}\right)^{-\frac{\lambda}{2}}\int_{R\rho_1}^{0}\left(\frac{t}{R}\right)\left[\left(\frac{t}{R}\right)^2-\rho^*\right]^{-\frac{\lambda}{2}}\left[\left(\frac{t}{R}\right)^2-\frac{1}{\rho^*}\right]^{\frac{\lambda}{2}}dt. \tag{6.26}$$

If, for example, we take $\lambda = -2$, then integrating (6.26) and substituting into (6.25), the general expression for X_3 is given as

$$2X_3R^2 = \left[B\left(\frac{1+\eta}{2}\right) + \frac{(\varepsilon_2 - i\varepsilon_3)}{\frac{\kappa_M}{\mu_M} + \frac{1}{\mu_I}}\right]\left[\frac{2\rho^{*2} - \delta_o(1+\rho^{*2})}{2\rho^{*2}} + \frac{\delta_o(1-\rho^{*4})}{2\rho^{*4}}\ln\left(\frac{1}{1-\rho^{*2}}\right)\right]$$
$$-X_1\frac{\delta_o(1+\rho^{*2})}{\rho^{*3}}\left[\ln\left(\frac{1}{1-\rho^{*2}}\right) - \frac{\rho^{*2}}{1-\rho^{*2}}\right] \qquad (6.27)$$

Having found coefficient X_3, the solution for X_1 follows immediately from $(6.24)_1$. As before, once X_1 and X_3 are known, the complete solution for $\Phi_I(z)$ is given by (6.1) in a closed-form. Furthermore, with Φ_I computed, the remaining stress potentials $\Psi_M(z)$, $\Psi_I(z)$ and $\Phi_M(z)$,can be readily obtained from conditions (2.10) and (5.4), respectively.

It is also verified, that when $\rho^* = 0$ (corresponding homogeneous non-slip interface), $(6.24)_1$ and (6.27) reduce to the following

$$X_1\left(1+\eta+\frac{2}{\delta_o}\right) = A(1+\eta) - \frac{2\varepsilon_1}{\frac{\kappa_M}{\mu_M} + \frac{1}{\mu_I}},$$
$$4X_3R^2 = \left[B\left(\frac{1+\eta}{2}\right) + \frac{(\varepsilon_2 - i\varepsilon_3)}{\frac{\kappa_M}{\mu_M} + \frac{1}{\mu_I}}\right]\left(2 - \frac{\delta_o}{2}\right). \qquad (6.28)$$

6.3.1. Average Stress

Let us now consider the average stresses corresponding to the case $s = 2, \lambda = -2, \beta = 1$. Thus, in view of (6.28) and assuming zero eigenstrains, the average mean, deviatoric and shear stresses associated with a homogeneous interface (6.9), under otherwise identical conditions, are given by

$$(\sigma_x + \sigma_y)^H_{Avg} = \frac{4A(1+\eta)(1-\rho^{*2})}{2+\eta(1-\rho^{*2})},$$
$$\left(\frac{\sigma_y - \sigma_x}{2} + i\sigma_{xy}\right)^H_{Avg} = B\left(\frac{1+\eta}{8}\right)\left(\frac{7+5\rho^{*2}}{1+\rho^{*2}}\right). \tag{6.29}$$

Here, as before, the superscript H denotes the stresses associated with the homogeneous interface.

For the average mean, deviatoric and shear stresses corresponding to the inhomogeneous interface, let us assume, as before, that all eigenstrains vanish as well as that $\mathrm{Im}[B] = 0$ (a biaxial stress state). Then, in view of (6.24) and (6.27) the average stresses associated with the inhomogeneous interface (6.8) are given by

$$(\sigma_x+\sigma_y)_{Avg}=\frac{2(1+\eta)\left[2A+B\left[\left(\frac{1-\rho^{*2}}{\rho^{*3}}\right)\ln\left(\frac{1}{1-\rho^{*2}}\right)-\frac{1}{\rho^*}\right]\right]}{\frac{2}{\rho^{*2}}\ln\left(\frac{1}{1-\rho^{*2}}\right)+\eta}, \tag{6.30}$$

$$\left(\frac{\sigma_y-\sigma_x}{2}+i\sigma_{xy}\right)_{Avg}=\frac{B(1+\eta)\left\{\begin{array}{c}\ln\left(\frac{1}{1-\rho^{*2}}\right)\left(\frac{8-\eta\rho^{*2}}{4\rho^{*2}}\right)+\eta+\\ \left[\frac{\eta(2\rho^{*2}-1)-2}{4\rho^{*4}}\right]\left[\ln\left(\frac{1}{1-\rho^{*2}}\right)-\rho^{*2}\right]\end{array}\right\}}{\frac{2}{\rho^{*2}}\ln\left(\frac{1}{1-\rho^{*2}}\right)+\eta}$$

$$+\frac{A(1+\eta)\left[\left(\frac{1-\rho^{*2}}{\rho^{*3}}\right)\ln\left(\frac{1}{1-\rho^{*2}}\right)-\frac{1}{\rho^*}\right]}{\frac{2}{\rho^{*2}}\ln\left(\frac{1}{1-\rho^{*2}}\right)+\eta}, \tag{6.31}$$

respectively.

To judge the effects of the circumferential inhomogeneity on the average stresses induced inside the inclusion, consider, for example, a uniaxial stress state in the x-direction (i.e. $2A+B=0$). Then the ratios $T(\eta,\rho^*)$ and $Q(\eta,\rho^*)$ of the average stresses (i.e. the ratio of the expressions in (6.30) to the corresponding expressions in (6.29)) is given by

$$(\sigma_x+\sigma_y)_{Avg}=T(\eta,\rho^*)\,(\sigma_x+\sigma_y)^H_{Avg},$$

$$T(\eta,\rho^*)=\frac{[2+\eta(1-\rho^{*2})]\left[\frac{1}{\rho^*(1-\rho^*)}-\frac{1}{\rho^{*3}}\ln\left(\frac{1}{1-\rho^{*2}}\right)\right]}{\frac{2}{\rho^{*2}}\ln\left(\frac{1}{1-\rho^{*2}}\right)+\eta} \tag{6.32}$$

and

$$\left(\frac{\sigma_y-\sigma_x}{2}+i\sigma_{xy}\right)_{Avg}=Q(\eta,\rho^*)\left(\frac{\sigma_y-\sigma_x}{2}+i\sigma_{xy}\right)^H_{Avg}$$

$$Q(\eta,\rho^*)=\frac{4(1+\rho^{*2})\left\{\begin{array}{c}\left[\dfrac{2(\rho^*+2)^2-10-\eta\rho^{*3}}{2\rho^{*3}}\right]\ln\left(\dfrac{1}{1-\rho^{*2}}\right)+\dfrac{2\eta\rho^*+1}{\rho^*}+\\ \left[\dfrac{\eta\,(2\rho^{*2}-1)-2}{2\rho^{*4}}\right]\left[\ln\left(\dfrac{1}{1-\rho^{*2}}\right)-\rho^{*2}\right]\end{array}\right\}}{(7+5\rho^{*2})\left[\dfrac{2}{\rho^{*2}}\ln\left(\dfrac{1}{1-\rho^{*2}}\right)+\eta\right]} \tag{6.33}$$

Note that in condition (6.31), as $\rho^* \to 1$, the ratio of the average mean stress, $T(\eta,\rho^*)$, tends to infinity. The reason for this behavior is the monomial term $(1-\rho^*)$ appearing in the numerator which causes the numerator to increase at a faster rate than the denominator as $\rho^* \to 1$. Furthermore, the results for the uniaxial load in the y-direction can be obtained from the results of the uniaxial load in the x-direction by changing the sign of ρ^* (i.e. changing from $+\rho^*$ to $-\rho^*$). In other words, this is merely a rotation of the loading through 90 degrees.

Let us consider an additional result when we have an equal but opposite biaxial stress field (i.e. $A=0$). In this case, the average deviatoric and shear stresses are given by the following condition

$$\left(\frac{\sigma_y-\sigma_x}{2}+i\sigma_{xy}\right)_{Avg}=S(\eta,\rho^*)\left(\frac{\sigma_y-\sigma_x}{2}+i\sigma_{xy}\right)^{H}_{Avg},$$

$$S(\eta,\rho^*)=\frac{4\left(1+\rho^{*2}\right)\left\{\begin{array}{c}\left[\dfrac{8-\eta\rho^{*2}}{2\rho^{*2}}\right]\ln\left(\dfrac{1}{1-\rho^{*2}}\right)+\\ \left[\dfrac{\eta\left(2\rho^{*2}-1\right)-2}{2\rho^{*4}}\right]\left[\ln\left(\dfrac{1}{1-\rho^{*2}}\right)-\rho^{*2}\right]+2\eta\end{array}\right\}}{\left(7+5\rho^{*2}\right)\left[\dfrac{2}{\rho^{*2}}\ln\left(\dfrac{1}{1-\rho^{*2}}\right)+\eta\right]} \tag{6.34}$$

The effects of the circumferential inhomogeneity of the interface, as represented by the functions $T(\eta,\rho^*)$, $Q(\eta,\rho^*)$ and $S(\eta,\rho^*)$ for the respective loading conditions, are illustrated in Figures 6-10, 6-11 and 6-12, respectively. For example, under a uniaxial load in the x-direction, the relative error in the average mean stress caused by neglecting the inhomogeneity of interface imperfections is in excess of 40% (Figure 6-10). Hence, in all the loading configurations, the results demonstrate convincingly that replacing the inhomogeneous non - slip interface by its homogeneous counterpart has a significant effect on even the estimation of the average stresses induced within the circular inclusion.

6.4. Summary

A rigorous systematic study for two specific variations of the inhomogeneous non-slipping interface has been given. The results, from both these examples, clearly illustrate how the circumferential variation of the interface parameter has a significant and pronounced effect on the interface stresses and even the average stresses induced within the inclusion.

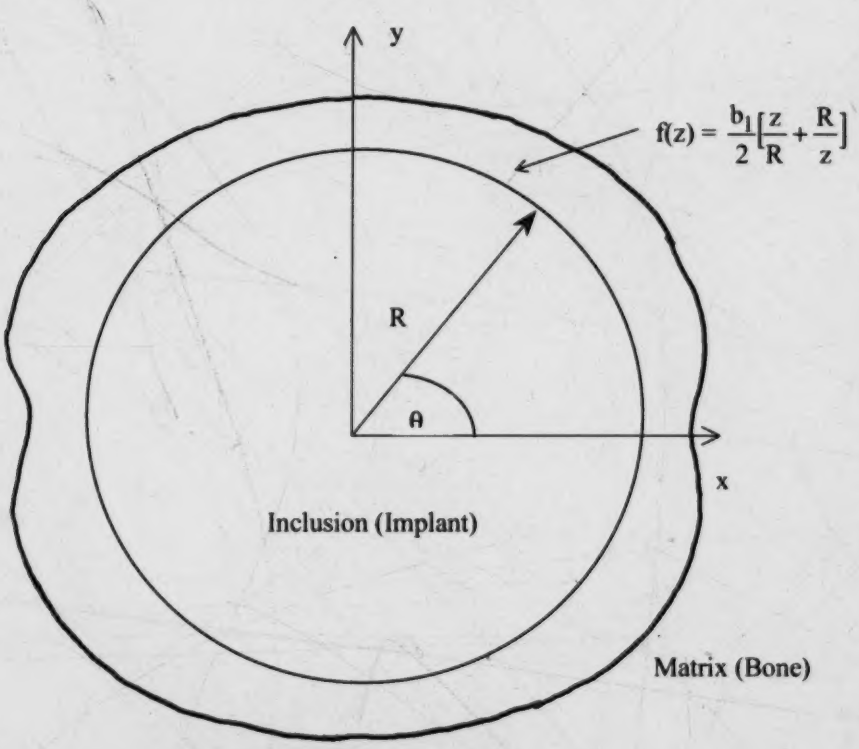

Figure 6 - 1. Schematic Representation of the Inhomogeneous Non-Slip Interface having Circumferential Number s = 1

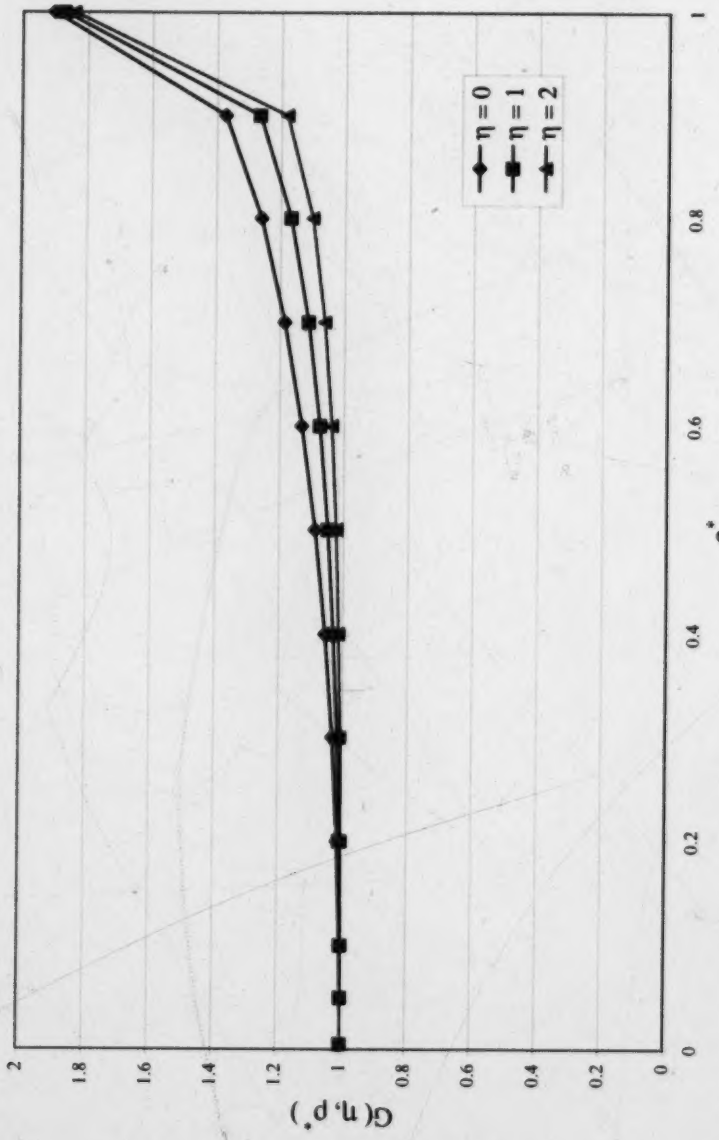

Figure 6-2. The Effect of the Circumferential Inhomogeneity on the Average Mean Stress inside the Circular Inclusion having Circumferential Number s = 1 and Loading in y-direction

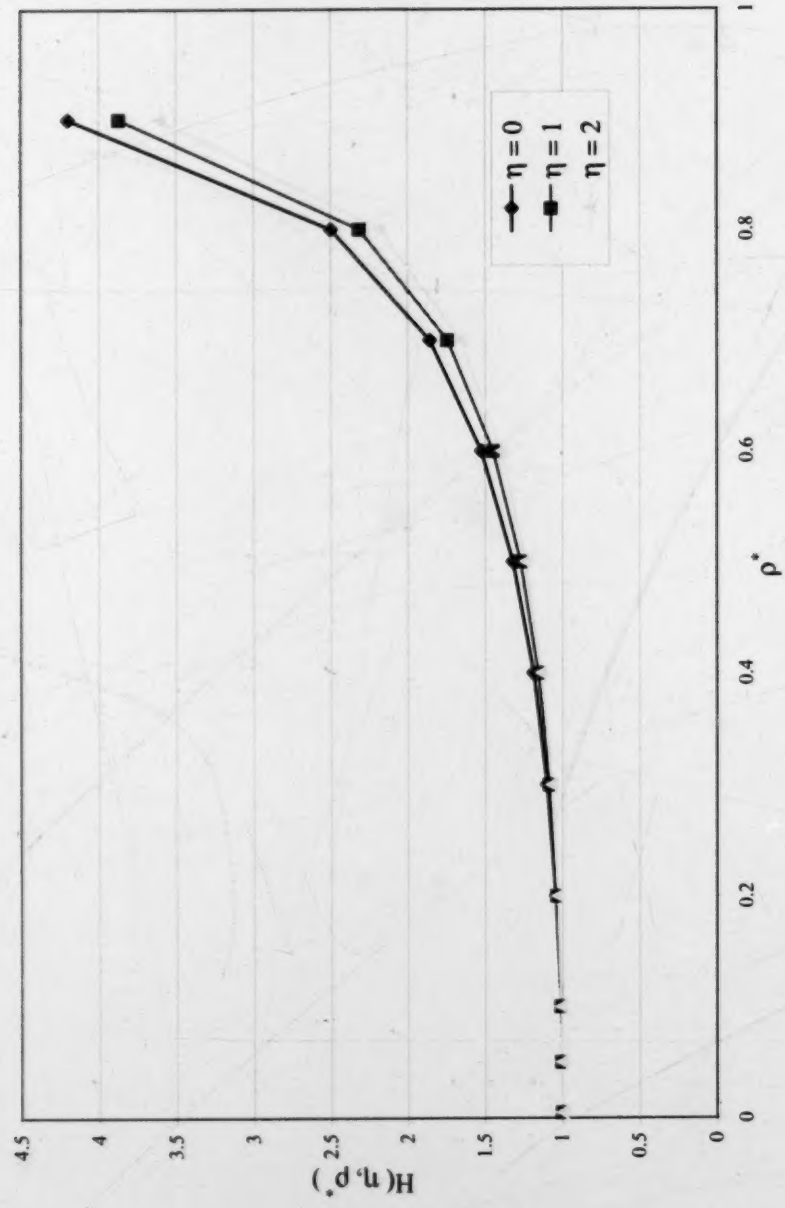

Figure 6-3. The Effect of the Circumferential Inhomogeneity on the Average Mean Stress inside the Circular Inclusion having Circumferential Number s = 1 and Loading in x-direction

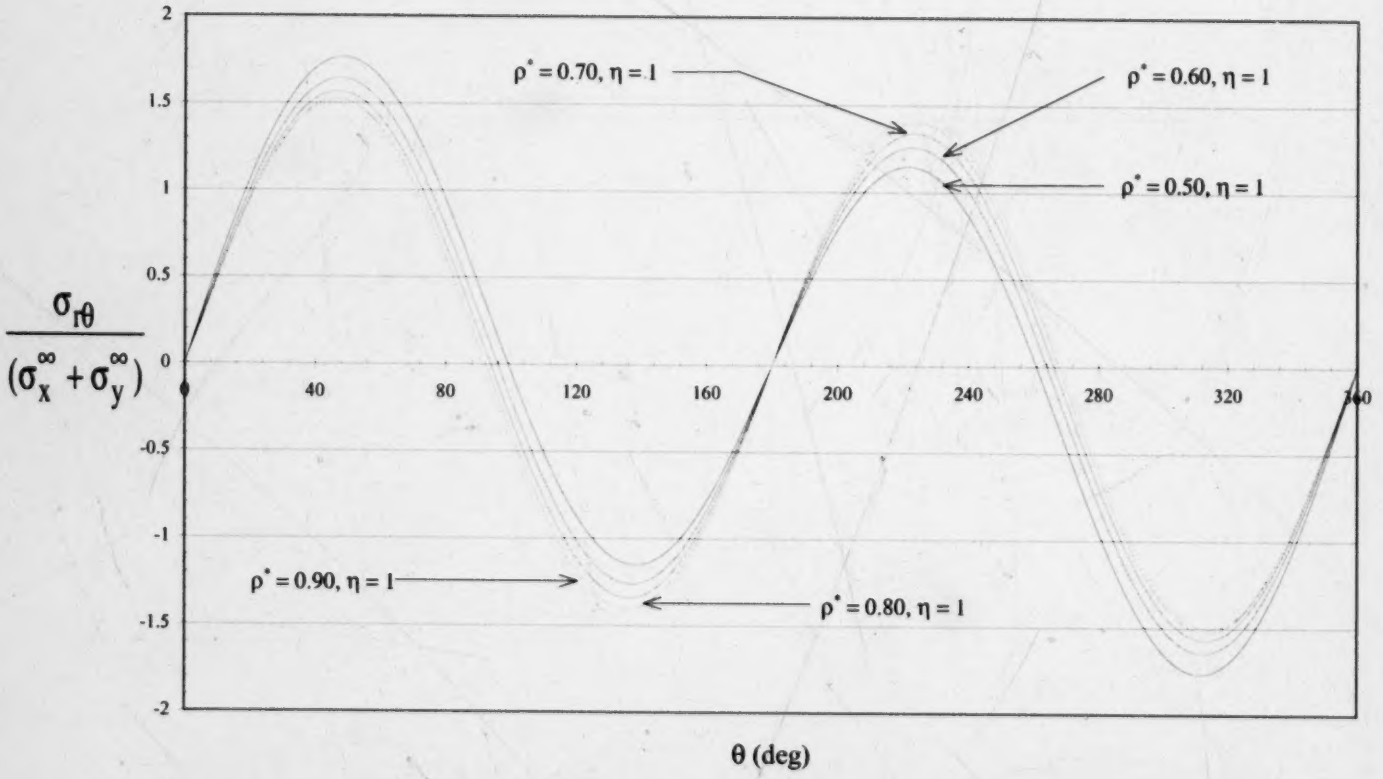

Figure 6-4. Non-Uniformity of the Interfacial Shear Stress for various positive Interface Imperfections as a function of Position and Loading in y-direction

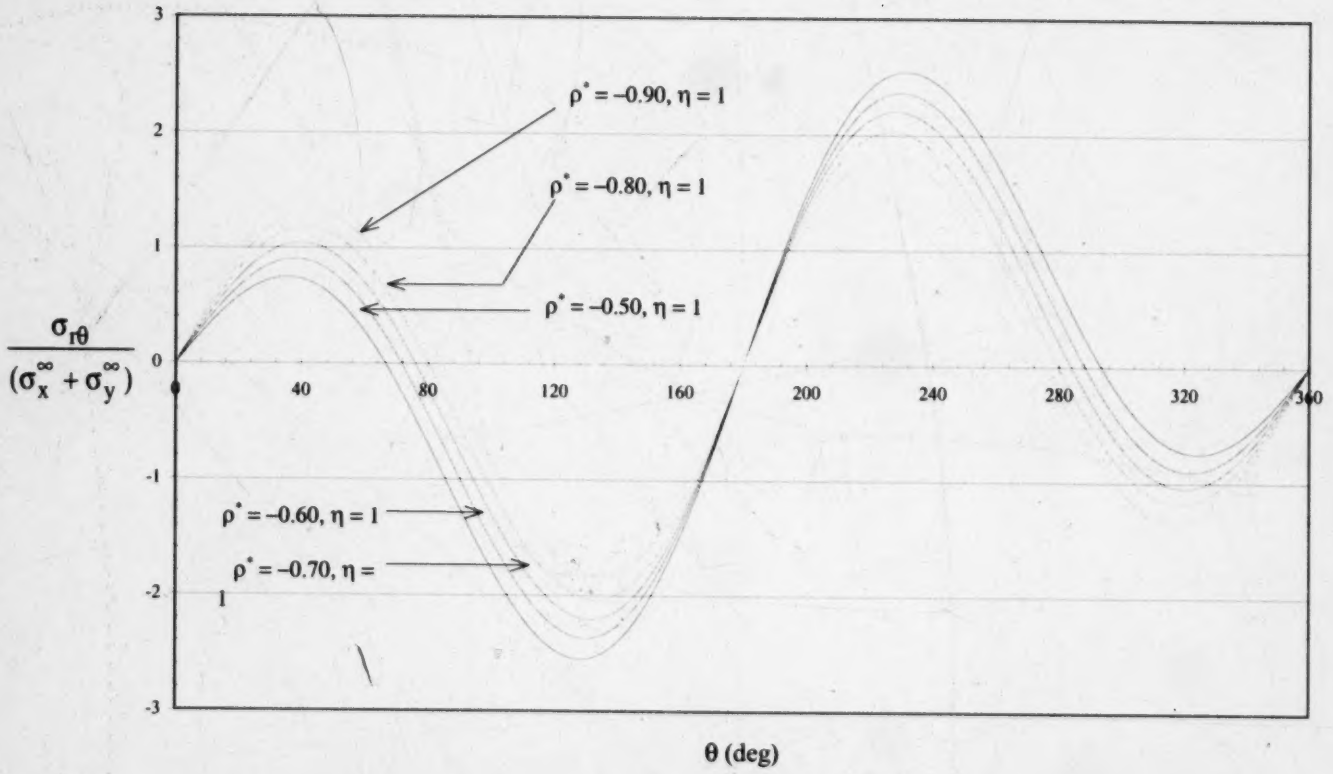

Figure 6-5. Non-Uniformity of the Interfacial Shear Stress for various negative Interface Imperfections as a function of Position and Loading in y-direction

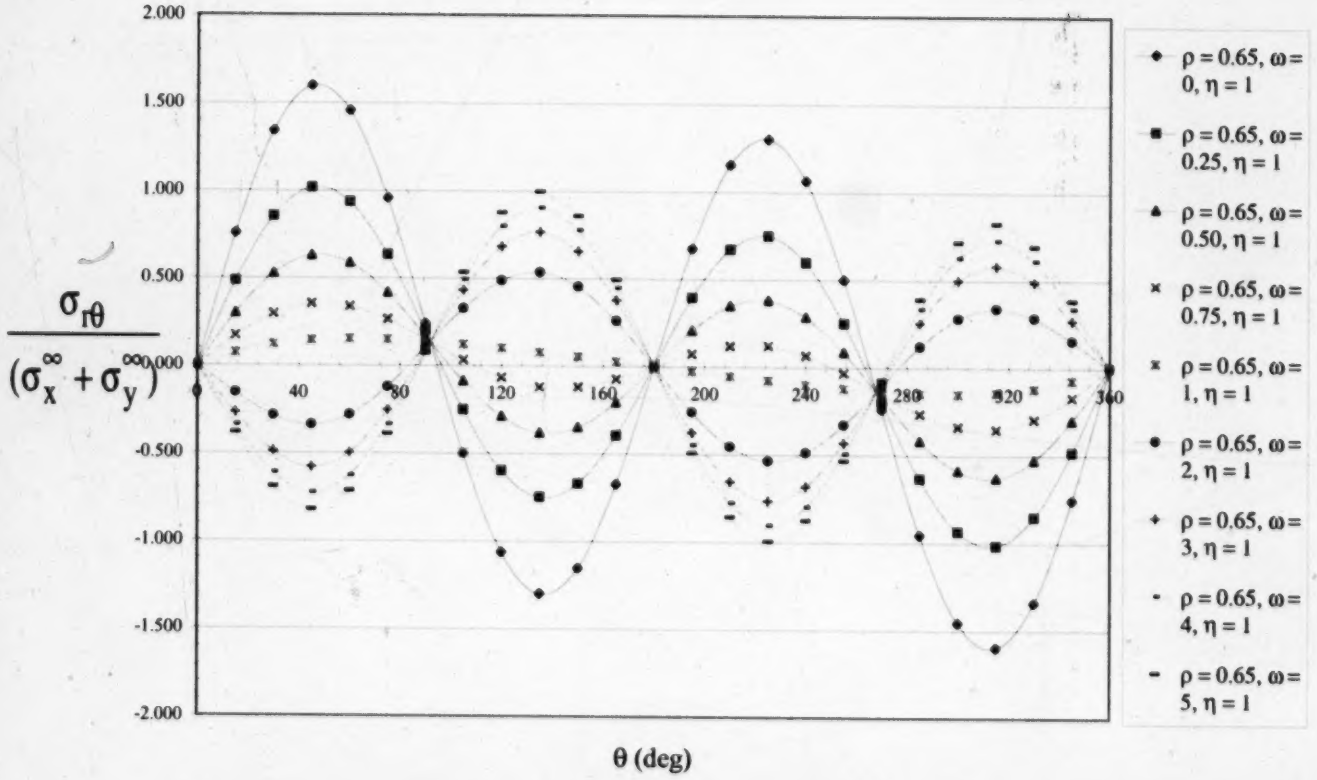

Figure 6-6. Non-Uniformity of the Interfacial Shear Stress for a particular positive Interface Imperfection as a function of Position and various Loading Configurations

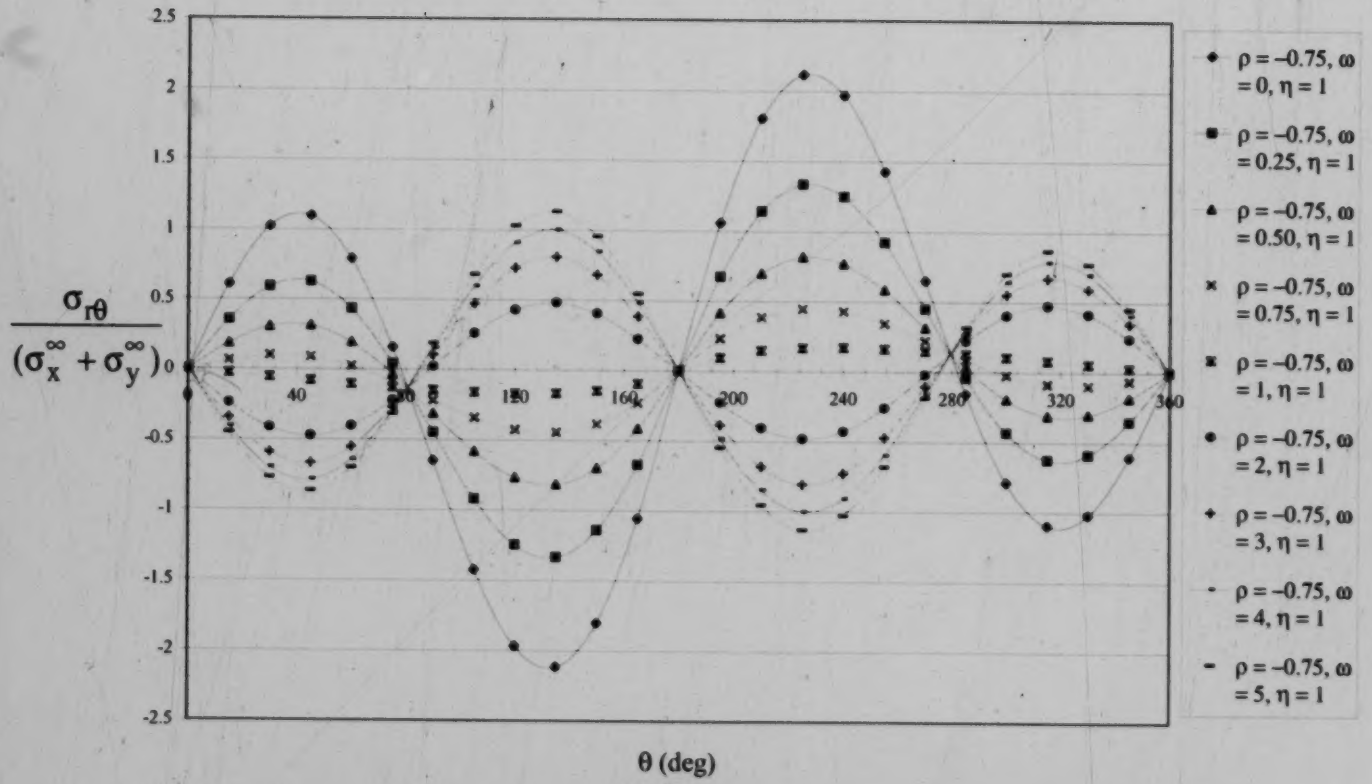

$$\frac{\sigma_{r\theta}}{(\sigma_x^{\infty} + \sigma_y^{\infty})_0}$$

Figure 6-7. Non-Uniformity of the Interfacial Shear Stress for a particular negative Interface Imperfection as a function of Position and various Loading Configurations

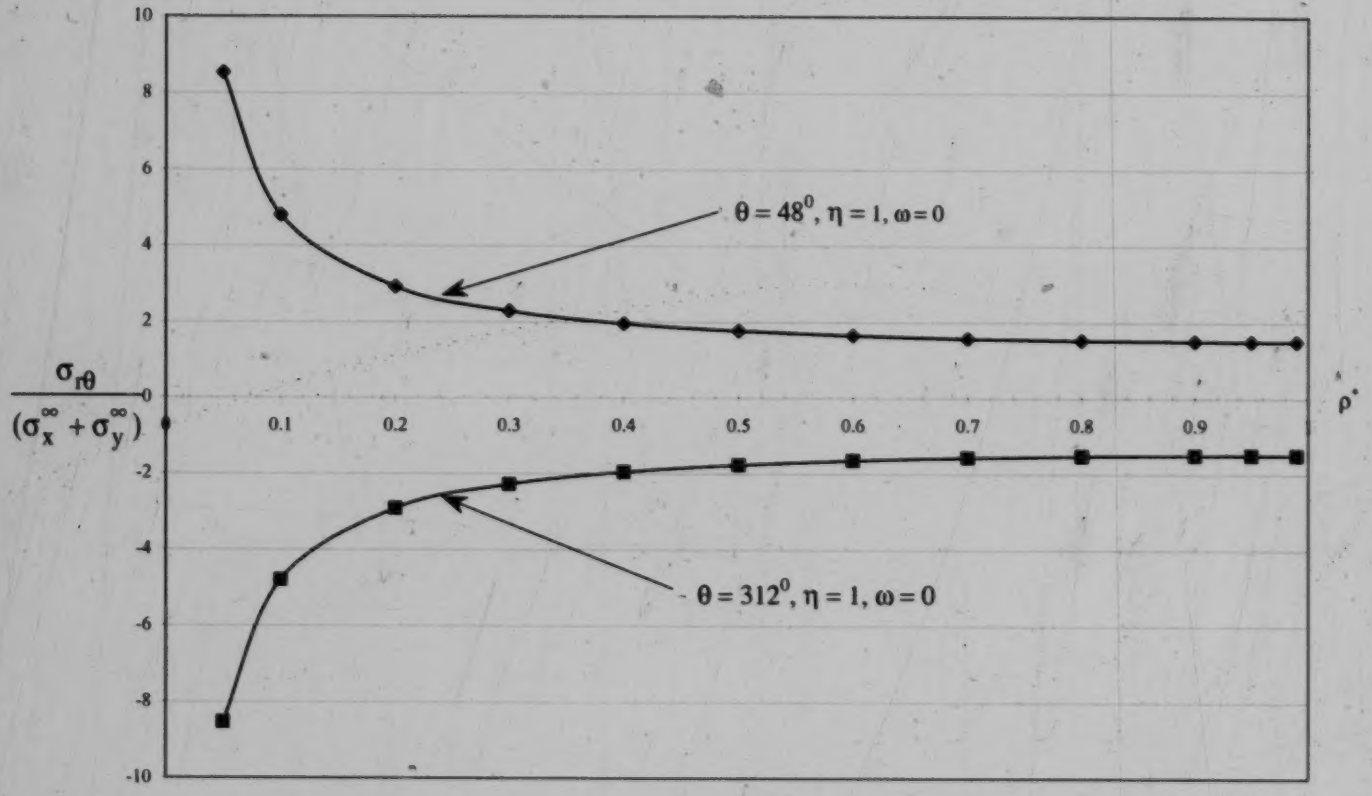

Figure 6-8. The Effect of the Interface Parameter on the Interfacial Shear Stress corresponding to the Maximum Position and Loading in y-direction

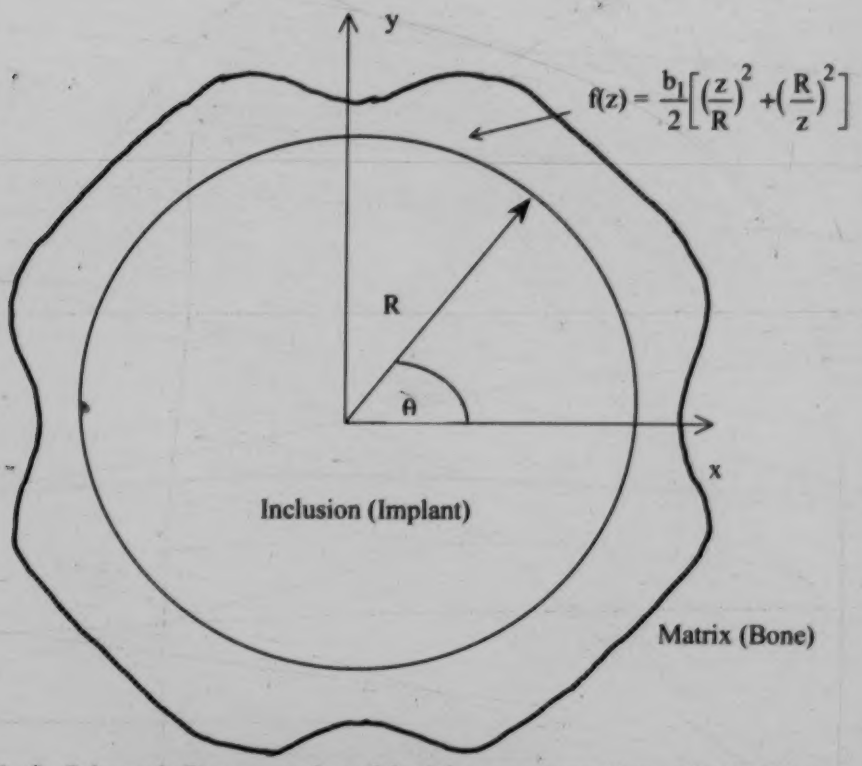

Figure 6 - 9. Schematic Representation of the Inhomogeneous Non - Slip Interface having Circumferential Number s = 2

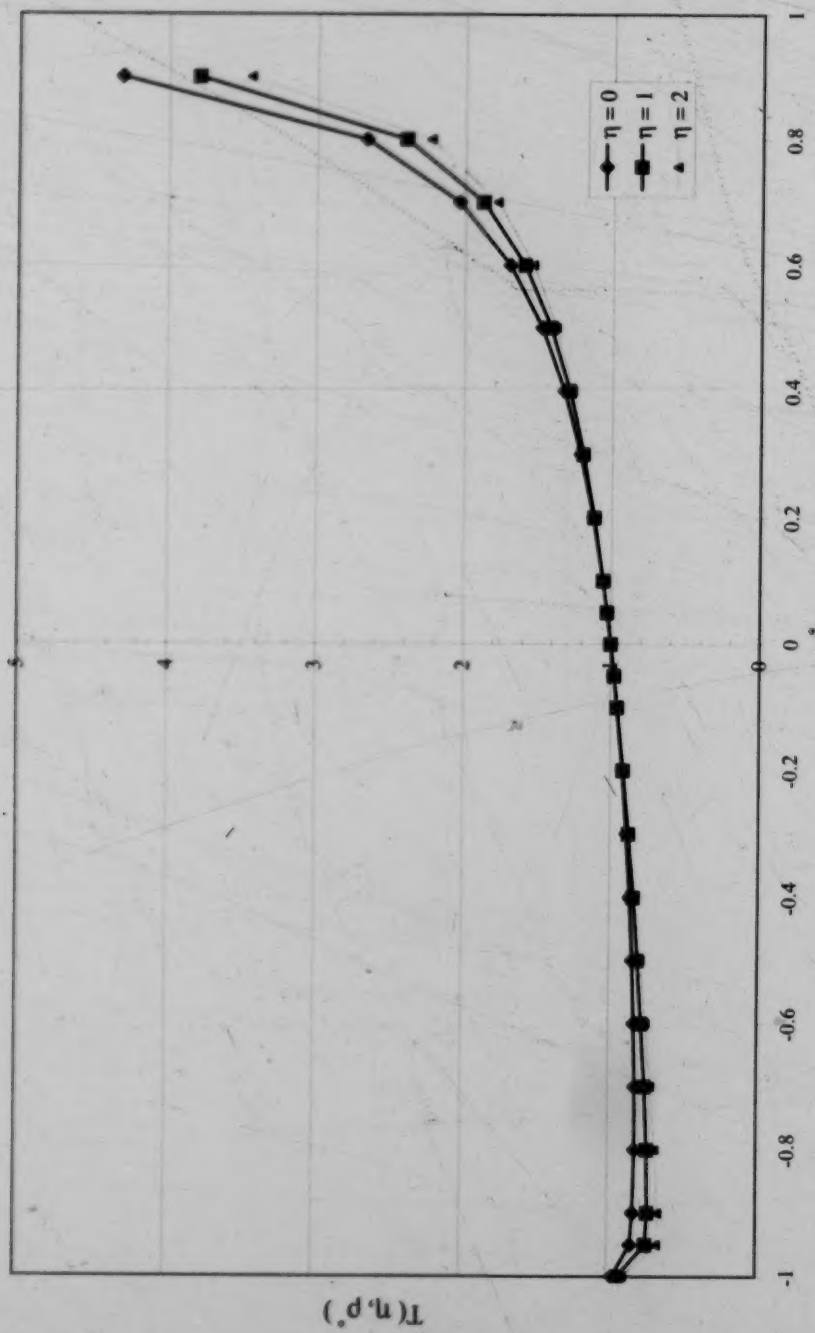

Figure 6-10. The Effect of the Circumferential Inhomogeneity on the Average Mean Stress inside the Circular Inclusion having Circumferential Number s = 2 and Loading in x-direction

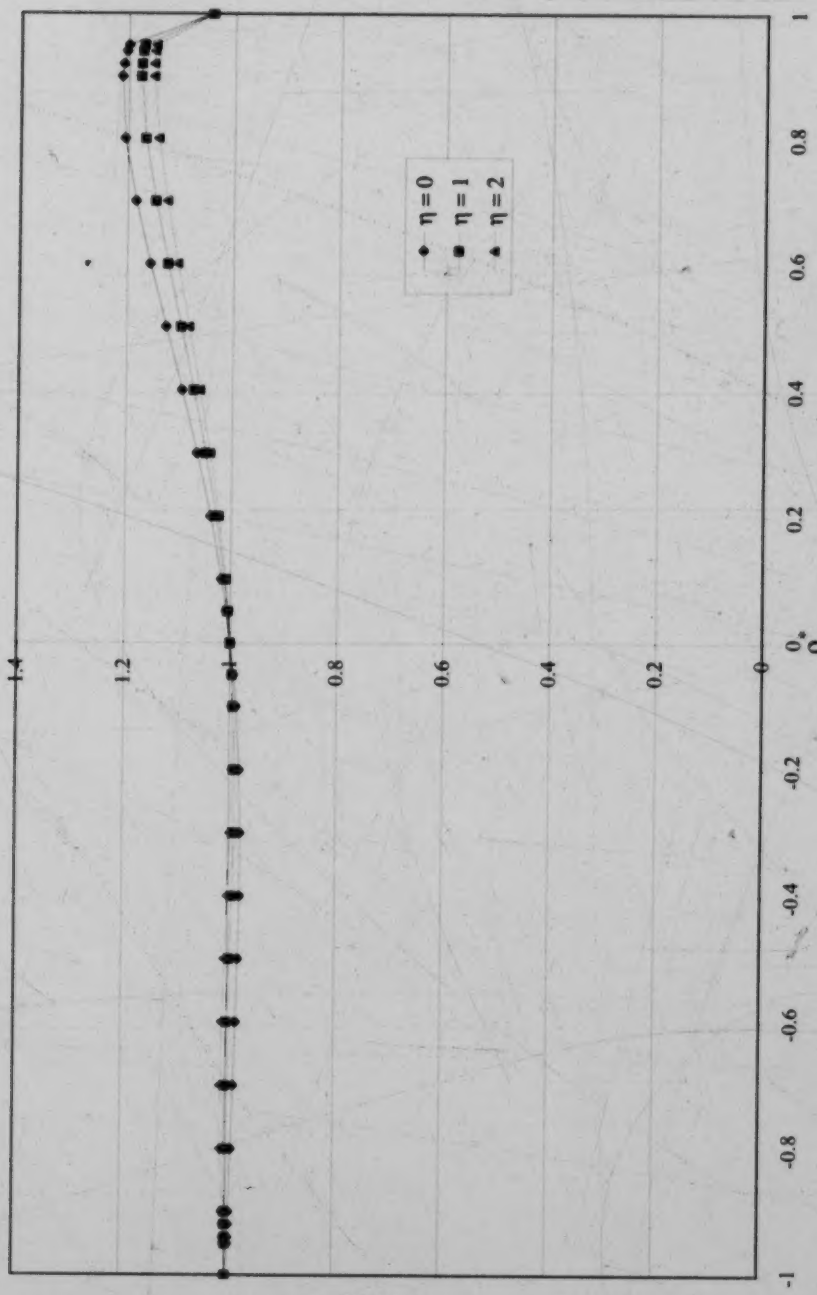

Figure 6-11. The Effect of the Circumferential Inhomogeneity on the Average Deviatoric and Shear Stress inside the Circular Inclusion having Circumferential Number s = 2 and Loading in x-direction

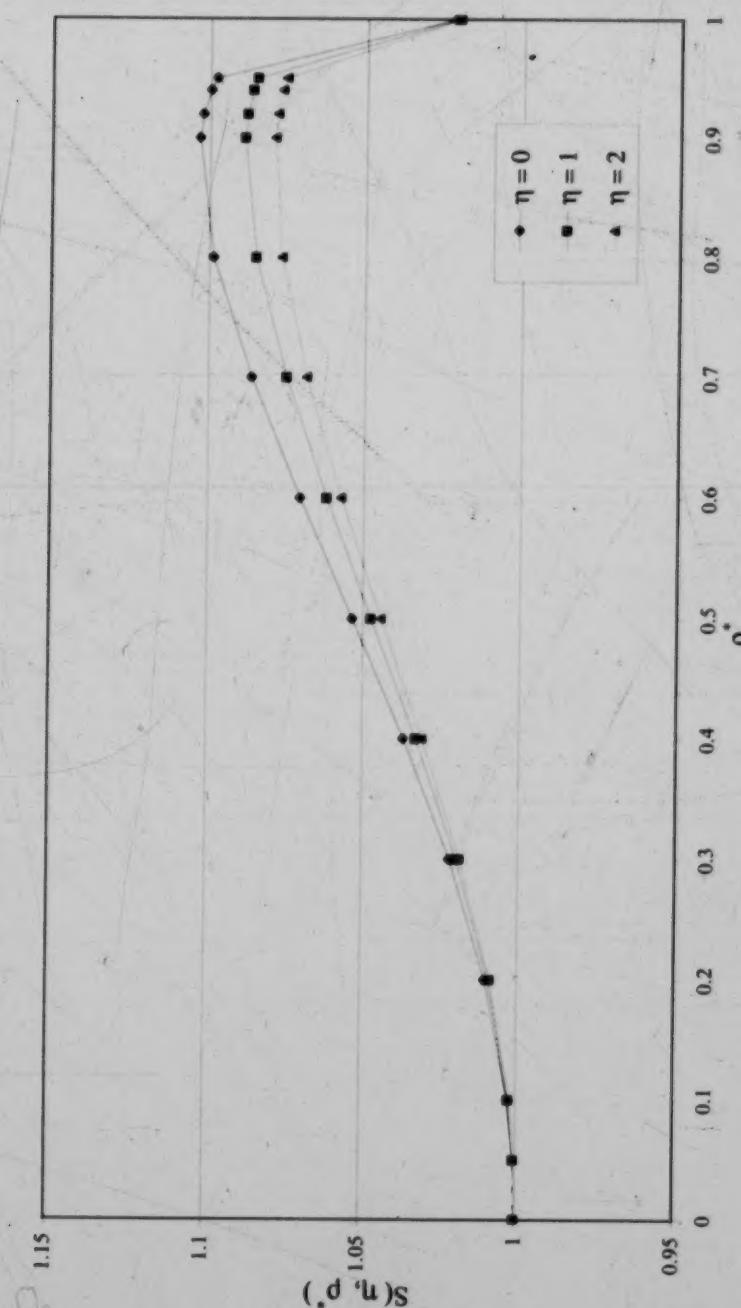

Figure 6.12. Effect of the Circumferential Inhomogeneity on the Average Deviatoric and Shear Stress inside the Circular Inclusion having Circumferential Number s = 2 and Equal-Opposite Biaxial Load

CHAPTER 7

Verification of the Solution Procedure

This chapter presents a verification of the general solutions obtained from the two circumferential inhomogeneous imperfect interfaces. In particular, the general solutions obtained from the inhomogeneous spring - layer interface and the inhomogeneous non - slip interface, respectively are shown to reduce to the known solutions corresponding to the homogeneous spring - layer and non - slip interface, respectively. This serves as a necessary condition for the correctness of the general solutions. To begin with, we consider the case corresponding to the inhomogeneous imperfect spring - layer interface characterized by the condition $m(\theta) = n(\theta)$.

7.1. Inhomogeneous Spring - Layer Interface

7.1.1. The Interface with Circumferential Number $s = 1$

To verify the correctness of the general solutions which are given in Chapters 3 and 4, for the case $s = 1, \lambda = -1$ and $\beta = 1$, select the interface parameter ρ^* to be zero. This reduces the general expressions given by (4.7 - 4.9) to the corresponding homogeneous spring - layer interface solutions. For example, it was shown in Appendix C that when the parameters $\lambda = -1, \beta = 1$, the coefficient X_1

reduces to the following

$$X_1 (3 + \delta_o \eta) = A\delta_o (1 + \eta) - \frac{2\delta_o \varepsilon_1}{\frac{\kappa_M}{\mu_M} + \frac{1}{\mu_I}}. \tag{7.1}$$

By using conditions (3.4 - 3.5) and noting that when $\rho^* = 0 \Longleftrightarrow f(\theta) = 0$ condition (7.1) is rewritten as

$$X_1 = \frac{A\left(\frac{\kappa_M + 1}{2\mu_M}\right) - \varepsilon_1}{\frac{3}{nR} + \frac{1}{2}\left(\frac{1}{\mu_M} - \frac{1}{\mu_I}\right)}.$$

Rewriting the denominator gives

$$X_1 = \frac{A\left(\frac{\kappa_M + 1}{2\mu_M}\right) - \varepsilon_1}{\frac{2}{nR} + \frac{1}{\mu_M} + \frac{\kappa_I - 1}{2\mu_I}} \tag{7.2}$$

which is exactly identical to that given by [80] for the corresponding homogeneous spring - layer interface. Furthermore, if $\rho^* = 0$, the expressions for $\Phi_I(z)$ and $\Phi_M(z)$ given by (4.8) and (4.9), respectively, reduce to the following

$$\begin{aligned} \Phi_I(z) &= X_1 z, \\ \Phi_M(z) &= Az + \frac{A_1}{z}, \end{aligned} \tag{7.3}$$

where the coefficient A_1 is given by

$$A_1 = \overline{B}\frac{R^2}{2}(\eta - 1) + R^2 \frac{(\varepsilon_2 + i\varepsilon_3)}{\frac{\kappa_M}{\mu_M} + \frac{1}{\mu_I}}. \tag{7.4}$$

Therefore, expressions (7.3 - 7.4) are identical to those given by [80] for the corresponding homogeneous spring - layer interface. Note that in the case corresponding to the homogeneous spring - layer interface (i.e. $m = n$) the stress field inside the inclusion is uniform.

Thus, for the special case corresponding to $\rho^* = 0$ and when the circumferential number $s = 1$, the general solutions obtained from the inhomogeneous spring - layer interface reduce to the known solutions.

7.1.2. The Interface with Circumferential Number $s = 2$

Let us follow the same procedure, as above, and show that in the more general coupled case the solutions, corresponding to the inhomogeneous spring - layer interface with the parameters $s = 2, \lambda = -2$ and $\beta = 1$, reduce to the known homogeneous case. In fact, one condition has already been verified: that being the coefficient X_2, given by (4.29), is identically equal to zero which agrees with the result established in [80] for the corresponding homogeneous spring - layer interface.

It has been shown in Appendix D that the coefficient X_1 reduces to

$$X_1 (4 + \delta_o \eta) = A (2 + \delta_o \eta) - \frac{2\delta_o \varepsilon_1}{\left(\frac{\kappa_M}{\mu_M} + \frac{1}{\mu_I}\right)}. \tag{7.5}$$

By using conditions (3.4 - 3.5) and noting that when $\rho^* = 0 \Longleftrightarrow f(\theta) = 0$ condition (7.5) is rewritten as

$$X_1\left[\frac{8+nR\left(\frac{1}{\mu_M}-\frac{1}{\mu_I}\right)}{2}\right] = A\left[\frac{4+nR\left(\frac{1}{\mu_M}-\frac{1}{\mu_I}\right)}{2}\right] - nR\varepsilon_1,$$

$$\Longleftrightarrow X_1 = \frac{A\left[\frac{2}{nR}+\frac{1}{2}\left(\frac{1}{\mu_M}-\frac{1}{\mu_I}\right)\right]-\varepsilon_1}{\frac{4}{nR}+\frac{1}{2}\left(\frac{1}{\mu_M}-\frac{1}{\mu_I}\right)}. \tag{7.6}$$

Also, since $\lambda = -2$ and $\rho^* = 0$, this implies that $\delta_o = 2$, therefore,

$$\frac{1}{nR} = \frac{1}{4}\left(\frac{\kappa_M}{\mu_M}+\frac{1}{\mu_I}\right)$$

consequently, (7.6) becomes

$$X_1 = \frac{A\left(\frac{\kappa_M+1}{2\mu_M}\right)-\varepsilon_1}{\frac{2}{nR}+\frac{1}{\mu_M}+\left(\frac{\kappa_I-1}{2\mu_I}\right)}. \tag{7.7}$$

Similarly, from Appendix D, we have

$$A_1 = -\frac{\overline{B}R^2}{3}(1-\delta_o\eta)+\frac{2\delta_o(\varepsilon_2+i\varepsilon_3)}{3\left(\frac{\kappa_M}{\mu_M}+\frac{1}{\mu_I}\right)}R^2, \tag{7.8}$$

and since $\lambda = -2$ and $\rho^* = 0$ this implies that $\delta_o = 2$, therefore, (7.7) becomes

$$A_1 = -\frac{\overline{B}R^2}{3}(1-2\eta)+\frac{4(\varepsilon_2+i\varepsilon_3)}{3\left(\frac{\kappa_M}{\mu_M}+\frac{1}{\mu_I}\right)}R^2. \tag{7.9}$$

Hence, conditions (7.7) and (7.9) are identical to those established by [80] when $\rho^* = 0$. Thus, the general solutions obtained from the inhomogeneous spring - layer interface, for the case $s = 2$ and $\rho^* = 0$, are shown to reduce to the known homogeneous solutions. Let us now consider a similar analysis for the inhomogeneous non-slipping interface characterized by the condition $m(\theta)$ finite and $n(\theta) = \infty$ as given in Chapters 5 and 6.

7.2. Inhomogeneous Non-Slipping Interface

7.2.1. The Interface with Circumferential Number $s = 1$

It has been shown (see Chapter 5) that when $s = 1, \lambda = -1, \beta = 1$ and $\rho^* = 0$, the general solutions corresponding to (6.3) and (6.4) reduce to the following

$$X_2 = 0,$$

$$X_1\left(1+\eta+\frac{2}{\delta_o}\right) = A(1+\eta) - \frac{2\varepsilon_1}{\dfrac{\kappa_M}{\mu_M}+\dfrac{1}{\mu_I}}. \tag{7.10}$$

Clearly, the coefficient X_2 automatically agrees with the result established in [80]. In the case of X_1, since $\lambda = -1, \rho^* = 0 \Longrightarrow \delta_o = 1$, we have

$$X_1(3+\eta) = A(1+\eta) - \frac{2\varepsilon_1}{\dfrac{\kappa_M}{\mu_M}+\dfrac{1}{\mu_I}},$$

$$\Longleftrightarrow X_1\left[3\frac{\kappa_M}{\mu_M}+\frac{2}{\mu_I}+\frac{1}{\mu_M}\right] = A\left[\frac{\kappa_M+1}{\mu_M}\right] - 2\varepsilon_1. \tag{7.11}$$

Noting that $\beta = 1$ and when $\rho^* = 0 \Longleftrightarrow f(\theta) = 0$ gives

$$\frac{2}{mR} = \frac{\kappa_I}{\mu_I} + \frac{1}{\mu_M}$$

from which it follows that

$$3\frac{\kappa_M}{\mu_M} + \frac{2}{\mu_I} + \frac{1}{\mu_M} \equiv \frac{\kappa_I - 1}{\mu_I} + \frac{4}{mR} + \frac{2}{\mu_M}.$$

Substituting the above into (7.11) gives

$$X_1 = \frac{A\left[\dfrac{\kappa_M + 1}{2\mu_M}\right] - \varepsilon_1}{\dfrac{2}{mR} + \dfrac{1}{\mu_M} + \dfrac{\kappa_I - 1}{2\mu_I}}, \tag{7.12}$$

which is identical to that established in [80] for the corresponding homogeneous non - slip interface.

In addition, the stress potentials Φ_I, Φ_M and Ψ_I, derived in Chapter 6, also serve as a verification to the correctness of the solution. For example, when $\rho^* = 0$ the stress potential Φ_I can be written as

$$\Phi_I(z) = X_1 z + \frac{1}{3}\left[\frac{B}{2}(1+\eta) + \frac{\varepsilon_2 - i\varepsilon_3}{\dfrac{\kappa_M}{\mu_M} + \dfrac{1}{\mu_I}}\right]\frac{z^3}{R^2}. \tag{7.13}$$

Also, when $\rho^* = 0$, the derivative of $\Psi_I(z)$ is given as

$$\Psi_I'(z) = \frac{2}{3}\left[\frac{B}{2}(1+\eta) + \frac{\varepsilon_2 - i\varepsilon_3}{\dfrac{\kappa_M}{\mu_M} + \dfrac{1}{\mu_I}}\right]. \tag{7.14}$$

These two results, (7.13 - 7.14), are identical to those established in [80]. Consequently, the solutions obtained for the inhomogeneous non-slip interface, corresponding to the circumferential number $s = 1$, are shown to reduce to the known homogeneous solution when the interface parameter $\rho^* = 0$.

7.2.2. The Interface with Circumferential Number $s = 2$

Let us follow the same procedure, as above, and show that in the case $s = 2$ the general solutions obtained from the inhomogeneous non - slip interface reduce to the known homogeneous case established in [80] when the interface parameter $\rho^* = 0$.

It has been shown (see Chapter 5) that when $s = 2, \lambda = -2, \beta = 1$ and $\rho^* = 0$, the general solutions corresponding to (6.24) and (6.25) reduce to the following

$$X_1\left(1+\eta+\frac{2}{\delta_o}\right) = A(1+\eta) - \frac{2\varepsilon_1}{\frac{\kappa_M}{\mu_M}+\frac{1}{\mu_I}},$$

$$X_2 = 0 \tag{7.15}$$

$$4X_3R^2 = \left[B\left(\frac{1+\eta}{2}\right) + \frac{(\varepsilon_2 - i\varepsilon_3)}{\frac{\kappa_M}{\mu_M}+\frac{1}{\mu_I}}\right]\left(2-\frac{\delta_o}{2}\right).$$

Once again, the coefficient X_2 automatically satisfies the corresponding result in [80]. In the case of X_1, since $\lambda = -2, \rho^* = 0 \Longrightarrow \delta_o = 2$, we have

$$X_1(2+\eta) = A(1+\eta) - \frac{2\varepsilon_1}{\frac{\kappa_M}{\mu_M} + \frac{1}{\mu_I}},$$

$$\Longleftrightarrow X_1\left[2\frac{\kappa_M}{\mu_M} + \frac{1}{\mu_I} + \frac{1}{\mu_M}\right] = A\left(\frac{\kappa_M + 1}{\mu_M}\right) - \varepsilon_1 \tag{7.16}$$

Noting that $\beta = 1$ gives

$$\frac{4}{mR} = \frac{\kappa_I}{\mu_I} + \frac{1}{\mu_M}$$

from which it follows that

$$2\frac{\kappa_M}{\mu_M} + \frac{1}{\mu_I} + \frac{1}{\mu_M} \equiv \frac{\kappa_I - 1}{\mu_I} + \frac{4}{mR} + \frac{2}{\mu_M}.$$

Substituting the above into (7.16) yields

$$X_1 = \frac{A\left[\frac{\kappa_M + 1}{2\mu_M}\right] - \varepsilon_1}{\frac{2}{mR} + \frac{1}{\mu_M} + \frac{\kappa_I - 1}{2\mu_I}}. \tag{7.17}$$

Similarly, for the coefficient X_3, when $\rho^* = 0$ and $\lambda = -2 \Longrightarrow \delta_o = 2$, we have

$$4X_3R^2 = \left[B\left(\frac{1+\eta}{2}\right) + \frac{(\varepsilon_2 - i\varepsilon_3)}{\frac{\kappa_M}{\mu_M} + \frac{1}{\mu_I}}\right]. \tag{7.18}$$

Thus, conditions (7.17 - 7.18) are found to be identical to those established in [80].

7.3. Summary

The solutions obtained in Chapters 3 - 6, based on the inhomogeneous spring - layer interface and the inhomogeneous non - slip interface, respectively, are found to reduce to the known homogeneous solutions by considering the special case: that being when the interface parameter, ρ^*, is chosen to be zero. This verification serves as a necessary condition to ensure that the solutions derived in Chapters 3 - 6 are valid.

CHAPTER 8

Conclusions and Recommendations for Future Work

8.1. Conclusions

A commonly adopted premise in the theory of the mechanical behavior of composites is the assumption of continuity of tractions and displacements across the inclusion-matrix boundary, the so-called perfect bonding condition. Such perfect interface conditions are convenient idealizations of a much more complex situation. In fact, this classic condition effectively ignores the presence of interphase damage arising from imperfect adhesions, microcracks and voids.

It is well known that load transfer between fiber and matrix depends significantly on the properties of the interphase layer. Consequently, the incorporation of an interphase layer into any micromechancial analysis is essential in describing the physical and mechanical behavior of the composite material. The concept known as imperfect bonding has been developed in order to take into account various degrees of damage within the interphase layer.

One of the more widely used mechanical models in describing an imperfect bonding condition is based on the premise that the interphase layer has mechan-

ical properties different than those of either the inclusion or the matrix. The interphase effect can then be described by continuous tractions but discontinuous displacements across the interphase layer. In this context, one of the most useful assumptions is that the displacement jumps are proportional, in terms of spring-factor type interface parameters, to their respective traction components. This type of condition corresponds to modeling the imperfectly bonded interphase layer by a linear spring-layer of vanishing thickness (i.e. an imperfect interface). The usefulness of this particular model lies in the fact that it allows the representation of intermediate states of bonding between the inclusion and the matrix: from perfect bonding to complete debonding.

Unlike the homogeneous imperfect interface condition, where the spring factor interface parameters are assumed to be a constant along the entire material interface, the focus of this dissertation is to systematically study, for the first time, the physically more realistic scenario of inhomogeneous interface damage in which the extent of damage at the inclusion - matrix interface varies pointwise along the interface itself. In particular, a model of a single homogeneous circular elastic inclusion embedded within an infinite isotropic matrix having circumferentially inhomogeneous imperfect damage as characterized by the inhomogeneous spring - layer interface (i.e. $m(\theta) = n(\theta)$) and the inhomogeneous non - slip interface (i.e.

$m(\theta)$ finite, $n(\theta) = \infty$), respectively has been developed and solved rigorously in plane elastostatics.

Our method has been developed as a consequence of the fact that the circumferential variation of the interface parameter leads to the failure of the conventional power series method. Instead, complex variable techniques are used to obtain exact closed-form solutions in which any of the unknown constants are determined from analyticity requirements and certain other supplementary conditions.

The method of solution is illustrated by considering a particular class of circumferentially inhomogeneous interfaces with explicit results derived for several examples of the circumferential variation of the interface parameter. Thus, in the case of the inhomogeneous spring - layer interface it was found that:

1. On using analytic continuation, the basic boundary value problem for four analytic functions is reduced to two *coupled* first order linear differential equations for two analytic functions - $\Phi_M(z)$ and $\Phi_I(z)$. Despite the presence of variable coefficients, exact closed - form solutions are obtained for the unknown functions $\Phi_M(z)$ and $\Phi_I(z)$, respectively which include a total of $(2s-1)$ undetermined, in general, complex coefficients $X_k\,(k = 1, 2, ..., s)$ and $A_k\,(k = 1, 2, ..., s-1)$. These complex constants are determined via $2(s-1)$ boundedness conditions as well as another supplementary condi-

tion. The remaining analytic functions, $\Psi_M(z)$ and $\Psi_I(z)$, are also expressed in closed - form and their solution depends on the solutions of $\Phi_M(z)$ and $\Phi_I(z)$.

2. Depending on the circumferential variation of interface parameter along the material interface, the evaluation of the unknown coefficients X_k and A_k is different. For example, when the circumferential number equals one (i.e. $s = 1$) the only unknown coefficient is X_1 (decoupled case) which is determined from the single supplementary condition. On the other hand, when the circumferential number equals two (i.e. $s = 2$) the unknown coefficients are now X_1, X_2 and A_1 (coupled case) which are determined from two boundedness conditions as well as the single supplementary condition. In general, these coefficients are expressed in terms of definite integrals of known power functions.

3. As the circumferential number increases the influence of the inhomogeneity of interface imperfections on the average stress decreases. This is seen by considering the two specific variations of the interface parameter. For example, when the circumferential number equals one (i.e. $s = 1$) the relative error in the average mean stress caused by neglecting the inhomogeneity of

interface imperfections approaches 200%. In addition, the relative error in the average deviatoric and shear stresses approach 100%. Note that in this case the average stresses are independent of any loadings. However, in the case when the circumferential number equals two (i.e. $s = 2$), the relative errors in the average stress show a decrease, for example, the relative error in the average deviatoric and shear stresses for a uniaxial load in the x-direction approaches 66%. Similarly, for an equal biaxial stress field, the relative error in the average deviatoric and shear stresses approaches 95%.

4. The effects of the circumferential inhomogeneity of the interface has a significant and pronounced effect on even the estimation of the average stresses induced within the inclusion. Consequently, replacing an inhomogeneous spring - layer interface by its homogeneous counterpart will lead to significant errors not only in the calculation of the average stresses but also on the stress fields in the inclusion and matrix, respectively.

Alternatively, in the case of the inhomogeneous non - slip interface it was found that:

1. On using the principle of analytic continuation, the basic boundary value problem for four analytic functions is reduced to a linear first order un-

coupled differential equation for a single analytic function, $\Phi_I(z)$, defined inside the inclusion. Despite the presence of variable coefficients, the exact closed - form solution for the unknown function, $\Phi_I(z)$, is obtained which includes a total of $(s+1)$ undetermined, in general, complex coefficients $X_k\,(k = 1, 2, ..., s+1)$. These complex constants are determined via two real compatibility conditions, $(s-1)$ boundedness conditions as well as an additional complex condition that is provided by the analyticity of $\Phi_I(z)$ at the remaining singular point corresponding to $z = 0$ whose form depends on the value of the material parameter β. The remaining analytic functions, $\Psi_M(z)$, $\Psi_I(z)$ and $\Phi_M(z)$ are also expressed in closed - form and their solutions depend on the solution of $\Phi_I(z)$.

2. The evaluation of the unknown coefficients X_k are determined by a system of $(s+1)$ linear algebraic equations that can be given in terms of definite integrals of known power functions. For instance, when the circumferential number equals one (i.e. $s = 1$) the only undetermined coefficients are X_1 and X_2. These constants are determined via the two real compatibility conditions as well as the single complex condition corresponding to the singular point $z = 0$. In particular, selecting $\beta = 1$, this complex condition takes the form $X_1 = \Phi_I'(0)$. On the other hand, if the circumferential

number equals two (i.e. $s = 2$) then 3 undetermined coefficients need to determined - X_1, X_2 and X_3. These coefficients are determined via the two real compatibility conditions, one boundedness condition and the single complex condition corresponding to the singular point $z = 0$.

3. The interfacial shear stress decreases with increasing interface imperfection. This result suggests that by increasing the level of interface imperfections high interfacial stress peaks can be reduced, thereby achieving a more uniform distribution of interface stresses and minimizing the possibility of interface failure. Of course, interface failure is determined not only by the driving force (such as interface stresses), but also by the critical stress, strain or strain energy density of the interface (i.e. failure criterion of the interphase).

4. The effect of the circumferential inhomogeneity has a significant and pronounced effect on even the average stresses induced within the inclusion For example when the circumferential number equals one (i.e. $s = 1$), the relative error in the average mean stress caused by neglecting the inhomogeneity of interface imperfections, for a uniaxial load in the y-direction, approaches 90%. In the case when the circumferential number equals two (i.e. $s = 2$), the relative error in the average mean stress, for a uniaxial load in the x-direction,

exceeds 40%. These results demonstrate conclusively that replacing an inhomogeneous non-slip interface by its homogeneous counterpart will lead to significant errors in not only the calculation of the average stresses, but also on the stress fields in the inclusion, interface and matrix, respectively.

8.2. Future Work

In this dissertation, the problem of a single isotropic circular inclusion embedded within an infinite homogeneous matrix was used to systematically study the effects of an inhomogeneous imperfect interface on the corresponding stress fields, specifically, the average stresses induced within the inclusion. Hence, this work serves as a foundation for the development of future work dealing with the effects of inhomogeneous interface imperfections. In particular, the future of this research work could include:

1. The systematic study of the effects of an inhomogeneous imperfect interface on the effective properties of the composite. The justification for studying this problem comes from the results already established in this dissertation; the inhomogeneity of interface imperfections has a significant and pronounced effect on the average stresses (strains) within the inclusion which could, undoubtedly, affect the effective properties of composites. To our knowledge,

this topic has yet to be investigated.

2. The systematic evaluation of the effects of an inhomogeneous imperfect interface on the stress fields in the matrix. The justification for studying this problem comes from the fact that the variation of interphase parameters causes pronounced changes in the stress distribution within the inclusion and matrix; consequently, failure of the composite in the matrix could be affected by the inhomogeneous interface. For instance, in an effort to control matrix cracking, it has been suggested by Achenbach and Zhu [51] that the circumferential interfacial stress depends strongly on the variation of interphase stiffness and position.

3. Use of the exact closed - form solutions developed in this thesis as a measure of the accuracy of the approximate power series method. In other words, by comparing the exact closed - form solutions developed in this thesis with those obtained via the approximate power series method will give an evaluation of the effectiveness, in terms of convergence rates, of the power series method.

4. The optimization of the inhomogeneous imperfect interface, in particular, to deal with, but not limit to, examples of neutral elastic inclusions. This problem refers to the design of inhomogeneous interfaces between inclusion

and matrix such that the embedded inclusion is "neutral" in the sense that it does not cause any stress disturbance in the surrounding matrix (i.e. the original stress field remains undisturbed). Despite its importance for various problems in the design of composite materials and structures, the general optimization problem of an inhomogeneous interface has received little attention to date (see [114 - 115]).

Hence, the potential gain in studying these various problems, with respect to inhomogeneous imperfect bonding, will significantly improve the understanding and design of composite materials and structures.

References

1. William D. Callister, Jr., Material Science and Engineering An Introduction, Third Edition, John Wiley and Sons (1994)

2. Donald R. Askeland, The Science and Engineering of Materials, Second S.I. Edition, Chapmand and Hall (1990)

3. John David Wolodko, Biaxial Fatigue and Leakage Characteristics of Fiber Reinforced Composite Tubes, Ph.D. Thesis, University of Alberta (1999)

4. T.W. Coyle, H.M. Chan and U.V. Deshmukh, Effects of Heat Treatments in Air on the Microstructure and Mechanical Behavior of the Fiber/Matrix Interface in an Las Glass-Ceramic Matrix-SiC Fiber Composite. *Proceedings of the Second International Conference on Composite Interfaces (ICCI-II)*, Cleveland, Ohio, U.S.A. (1988)

5. I. Verpoest, M. Desaeger and J. Ivens, The Influence of the Fiber-Matrix Interface on Damage Development in Composite Materials. *Proceedings of the Colloquium on Interfaces in Materials, Brussels*, (1988)

6. J.Jenny Yuan, John M. Kennedy and Dan D. Edie, Modeling the Dynamic Response of the Fiber/Matrix Interphase in Continuous Fiber Composite Materials. *Fiber, Matrix and Interface Properties ASTM STP 1290*, C.J. Spragg and L.T. Drzal Eds., American Society for Testing and Materials, (1996) 67 - 83

7. Krishnan Jayaraman and Kenneth L. Reifsnider, Residual Stresses in a Composite with Continuously Varying Young's Modulus in the Fiber/Matrix Interphase. *Journal of Composite Materials*, Vol. 26, No. 6 (1992) 770 - 791

8. C.O. Horgan and A.M. Chan, The Pressurized Hollow Cylinder or Disk Problem for Functionally Graded Isotropic Linearly Elastic Materials. *Journal of Elasticity*, Vol. 55, No. 1 (1999) 43 - 59

9. Z. Hashin, Analysis of Composite Materials - A Survey. ASME, *Journal of Applied Mechanics*, Vol. 50 (1983) 481 - 505

10. Z. Hashin, Composite Materials with Viscoelastic Interphase: Creep and Relaxation. *Mechanics of Materials*, Vol. 11 (1991) 135 - 148

11. Krishnan Jayaraman, Kenneth L. Reifsnider and Robert E. Swain, Elastic and Thermal Effects in the Interphase: Part I. Comments on Characterization Methods. *Journal of Composite Technology and Research*, Vol. 15, No.1 (1993) 3 - 13

12. A.G. Metcalfe, Interaction and Fracture of Titanium - Boron Composites. *Journal of Composite Materials*, Vol. 1 (1967) 356 - 365

13. M.R. Piggot, A. Sandai, P.S. Chua and D. Andison, Mechanical Interactions in the Interphasial Region of Fibre Reinforced Thermosets. *Composite Interfaces*, H. Ishida and J.L. Koenig, Eds. North-Holland, Amsterdam (1986)

14. J.A. Nairn, Thermoelastic Analysis of Residual Stresses in Unidirectional High Performance Composites. *Polymer Composites*, Vol. 6 (1985) 123 - 130

15. P.S. Theocaris, On the Evaluation of Adhesion Between Phases in Fiber Composites. *Colloid and Polymer Science*, Vol. 262 (1984) 929 - 938

16. M. Vedula, R.N. Pangborn and R.A. Queeney, Modifications of Residual Thermal Stress in a Metal - Matrix Composite with the use of a Tailored Interfacial Region. *Composites*, Vol. 19 (1988) 133 - 137

17. G.P. Tandon and N.J. Pagano, A Study of Fiber - Matrix Interfacial Modeling. *Proceedings of the Fourth Japan-U.S. Conference on Composite Materials*, Technomic Publishing Co. Lancaster, PA. (1988) 191 - 200

18. N.J. Pagano and G.P. Tandon, Elastic Response of Multidirectional Coated-Fiber Composites. *Composite Science and Technology*, Vol. 31 (1988) 273 - 293

19. Y. Benveniste, G.J. Dvorak and T. Chen, Stress Fields in Composites with Coated Inclusions. *Mechanics of Materials*, Vol. 7 (1989) 305 - 317

20. H.A. Luo and G.J. Weng, On Eshelby's S-Tensor in a Three-Phase Cylindrically Concentric Solid and the Elastic Moduli of Fiber-Reinforced Composites. *Mechanics of Materials*, Vol. 8 (1989) 77 - 88

21. N.R. Sottos, R.L. McCullough and S.I. Guceri, Thermal Stresses due to Property Gradients at the Fiber/Matrix Interface. *Mechanics of Composite Materials and Structures*, J.N. Reddy and J.L. Teply Eds. American Society of Mechanical Engineers, New York (1989) 11 - 20

22. S.M. Arnold, V.K. Arya and M.M. Melis, Elastic/Plastic Analysis of Advanced Composites Investigating the Use of the Compliant Layer Concept in Reducing Residual Stresses Resulting from Processing. *NASA TM* - 103204 (1990)

23. J.J. Caruso, C.C. Chamis and H.C. Brown, Parametric Studies to Determine the Effect of Compliant Layers on Metal Matrix Composite Systems. *NASA TM* - 102465 (1990)

24. K.H. Lo, R.W. Schmitz and W.G. Gottenberg, Determination of Flexible Interlayer Thickness for Fiber Reinforced Composites. *Proceedings of the Materials Research Society Symposium*, Vol. 170 (1990) 55 - 58

25. N.J. Pagano and G.P. Tandon, Thermo-Elastic Model for Multidirectional Coated Fiber Composites: Traction Formulation. *Composite Science and Technology*, Vol. 38 (1991) 247 - 269

26. K. Jayaramn, Z. Gao and K.L. Reifsnider, Stress Fields in Continuous Fiber Composites with Interphasial Property Gradients. *Proceedings of the Sixth Technical Conference of the American Society for Composites*, Technomic Publishing Co. Lancaster, PA. (1991) 759 - 768

27. K. Jayaramn, and K.L. Reifsnider, Local Stress Fields in a Unidirectional Fiber-Reinforced Composite with a Non-homogeneous Interphase Region: Formulation. *Advanced Composites Letters*, Vol. 1 (1992) 54 - 57

28. David D. Robertson and Shankar Mall, Fiber-Matrix Interphase Effects upon Transverse Behavior in Metal-Matrix Composites, *Journal of Composite Research and Technology*, Vol. 14, No. 1 (1992) 3 - 11

29. P.S. Theocaris, The Elastic Moduli of the Mesophase as Defined by Diffusion Process. *Journal of Reinforced Plastics and Composites*, Vol. 11 (1992) 537 - 551

30. A.M. Wass, Effect of Interphase on Compressive Strength of Unidirectional Composites. *ASME, Journal of Applied Mechanics*, Vol. 59 (1992) S183 - S188

31. I. Jasiůk and M.W. Kouider, The Effect of an Inhomogeneous Interphase on the Elastic Constants of Transversely Isotropic Composites. *Mechanics of Materials*, Vol. 15 (1993) 53 - 63

32. Krishnan Jayaraman, Kenneth L. Reifsnider and Robert E. Swain, Elastic and Thermal Effects in the Interphase: Part II. Comments on Modeling Studies. *Journal of Composite Technology and Research*, Vol. 15, No. 1 (1993) 14 - 22

33. M.P. Lutz and R.W. Zimmerman, Effect of the Interphase Zone on the Bulk Modulus of a Particulate Composite. *ASME, Journal of Applied Mechanics*, Vol. 63 (1996) 855 - 861

34. C.Q Ru, Effect of Interphase Layers on Thermal Stresses within an Elliptical Inclusion. *Journal of Applied Physics*, Vol. 84, No. 9 (1998) 4872 - 4879

35. C.Q. Ru, P. Schiavone and A. Mioduchowski, Uniformity of Stresses within a Three-Phase Elliptic Inclusion in Anti-Plane Shear. *Journal of Elasticity*, Vol. 52 (1999) 121 - 128

36. C.Q. Ru, Three-Phase Elliptical Inclusions with Internal Uniform Hydrostatic Stresses. *Journal of the Mechanics and Physics of Solids*, Vol. 47 (1999) 259 - 273

37. L.J. Broutman and B.D. Agarwal, A Theoretical Study of the Effect of an Interfacial Layer on the Properties of Composites. *Polymer Engineering and Science*, Vol. 14, No.8 (1974) 581 - 588

38. B.D. Agarwal and R.K. Bansal, Effect of an Interfacial Layer on the Properties of Fibrous Composites: A Theoretical Analysis. *Fibre Science and Technology*, Vol. 12 (1979) 149 - 158

39. Y.J. Liu, N. Xu and J.F. Luo, Modeling of Interphases in Fiber-Reinforced Composites Under Transverse Loading Using the Boundary Element Method. *Journal of Applied Mechanics*, Vol. 67 (2000) 41 - 49

40. J.D. Achenbach and H. Zhu, Effect of Interfacial Zone on Mechanical Behavior and Failure of Fiber-Reinforced Composites. *Journal of the Mechanics and Physics of Solids*, Vol. 37, No. 3 (1989) 381 - 393

41. Jacob Aboudi, Damage in Composites - Modeling of Imperfect Bonding. *Composite Science and Technology*, Vol. 28 (1987) 103 - 128

42. Y. Benveniste, On the Effect of Debonding on the Overall Behavior of Composite Materials. *Mechanics of Materials*, Vol. 3 (1984) 349 - 358

43. Y. Benveniste, The Effective Mechanical Behavior of Composite Materials with Imperfect Contact between the Constituents. *Mechanics of Materials*, Vol. 4 (1985) 197 - 208

44. A.K. Mal and S.K. Bose, Dynamic Elastic Moduli of a Suspension of Imperfectly Bonded Spheres. *Proc. Cambridge Phil. Soc.*, Vol. 76 (1974) 587 - 599

45. J.P. Jones and J.S. Whittier, Waves at a Flexibly Bonded Interface. *Journal of Applied Mechanics*, Vol. 34 (1967) 905 - 909

46. F. Ghahremani, Effect of Grain Boundary Sliding on Anelasticity of Polycrystals. *International Journal of Solids and Structures*, Vol. 16 (1980) 825 - 845

47. F. Lene and D. Leguillon, Homogenized Constitutive Law for a Partially Cohesive Composite Material. *International Journal of Solids and Structures*, Vol. 18 (1982) 443 - 458

48. P.S. Steif and S.F. Hoysan, An Energy Method for Calculating the Stiffness of Aligned Short-Fiber Composites. *Mechanics of Materials*, Vol. 6 (1987) 197 - 210

49. Y. Tong and I. Jasiuk, The Effect of Interface on the Mechanical Properties of Composites. *Interfaces in Polymer, Ceramic and Metal Matrix Composites*, Elsevier Science Publishing Co. (1988)

50. Z. Hashin, Thermoelastic Properties of Fiber Composites with Imperfect Interface. *Mechanics of Materials*, Vol. 8 (1990) 333 - 348

51. J.D. Achenbach and H Zhu, Effect of Interphases on Micro and Macromechanical Behavior of Hexagonal-Array Fiber Composites. *ASME, Journal of Applied Mechanics*, Vol. 57 (1990) 956 - 963

52. Z. Hashin, The Spherical Inclusion with Imperfect Interface. *ASME, Journal of Applied Mechanics*, Vol. 58 (1991) 444 - 449

53. J.D. Achenbach and H. Zhu, Radial Matrix Cracking and Interphase Failure in Transversely Loaded Fiber Composites. *Mechanics of Materials*, Vol. 11 (1991) 347 - 356

54. Autar K. Kaw and Vishnu G. Das, Crack in an Imperfect Interface in Composites. *Mechanics of Materials*, Vol. 11 (1991) 295 - 322

55. Alan J. Levy, The Debonding of Elastic Inclusions and Inhomogeneities. *Journal of the Mechanics and Physics of Solids*, Vol. 39, No. 4 (1991) 477 - 505

56. M.F. Thorpe and I. Jasiuk, New Results in the Theory of Elasticity for Two-Dimensional Composites. *Proc. R. Soc.* A438 (1992) 531 - 544

57. I. Jasiuk, T. Chen and M.F. Thorpe, Elastic Moduli of Composites with Sliding Inclusions. *Journal of Mechanics and Physics of Solids*, Vol. 40 (1992) 373 - 391

58. Z. Hashin, Extremum Principles for Elastic Heterogenous Media with Imperfect Interfaces and their Applications to Bounding of Effective Moduli. *Journal of the Mechanics and Physics of Solids*, Vol. 40 (1992) 767 - 781

59. Sukky Jun and Iwona Jasiuk, Elastic Moduli of Two-Dimensional Composites with Sliding Inclusions - A Comparison of Effective Medium Theories. *International Journal of Solids and Structures*, Vol. 30, No. 18 (1993) 2501 - 2523

60. Jianmin Qu, Eshelby Tensor for an Elastic Inclusion with Slightly Weakened Interface. *ASME, Journal of Applied Mechanics*, Vol. 60 (1993) 1048 - 1050

61. J. Qu, The Effect of Slightly Weakened Interfaces on the Overall Elastic Properties of Composite Materials. *Mechanics of Materials*, Vol. 14 269 - 281

62. R. Lipton and B. Vernescu, Variational Methods, Size Effects and Extremal Microstructure for Elastic Composites with Imperfect Interface. *Mathematical Models and Methods in Applied Sciences*. Vol. 5 (1995) 1139 - 1173

63. Zhanjun Gao, A Circular Inclusion with Imperfect Interface: Eshelby's Tensor and Related Problems. *ASME, Journal of Applied Mechanics*, Vol. 62 (1995) 860 - 866

64. Z. Zhong and S.A. Meguid, On the Eigenstrain Problem of a Spherical Inclusion with an Imperfectly Bonded Interface. *ASME, Journal of Applied Mechanics*, Vol. 63 (1996) 877 - 883

65. D. Bigoni, M. Ortiz and A. Needleman, Effect of Interfacial Compliance on Bifurcation of a Layered Bonded to a Substrate. *International Journal of Solids and Structures*, Vol. 34 (1997) 4305 - 4326

66. N. Tullini, M. Savoia and C.O. Horgan, End Effects in Multilayered Orthotropic Strips with Imperfect Bonding. *Mechanics of Materials*, Vol. 26 (1997) 23 - 34

67. N. Tullini, M. Savoia and C.O. Horgan, End Effects for Anti-plane Shear Deformation of Periodically Laminated Strips with Imperfect Bonding. *Journal of Elasticity*, Vol. 55 (1998) 227 - 244

68. D. Bigoni, S.K. Serkov, M. Valentini and A.B. Movchan, Asymptotic Models of Dilute Composites with Imperfectly Bonded Inclusions. *International Journal of Solids and Structures*, Vol. 35, No. 24 (1998) 3239 - 3258

69. Hongnian Shen, An Elliptic Inclusion with Imperfect Inhomogeneous Interface Embedded in an Infinite Elastic Medium, Ph.D. Thesis, University of Alberta (2000)

70. M. Gosz, B. Moran and J.D. Achenbach, Load-Dependent Constitutive Response of Fiber Composites with Compliant Interphases. *Journal of the Mechanics and Physics of Solids*, Vol. 40, No. 8 (1992) 1789 - 1803

71. H.S. Choi and J.D. Achenbach, Stress States at Neighboring Fibers Induced by Single-Fiber Interphase Defects. *International Journal of Solids and Structures*, Vol. 32, No. 11 (1995) 1555 - 1570

72. J.D. Eshelby, The Determination of the Elastic Field of an Ellipsoidal Inclusion and Related Problems. *Proc. Roy. Soc. London Ser.* A 241 (1957) 376 - 396

73. J.D. Eshelby, The Elastic Field Outside and Ellipsoidal Inclusion. *Proc. Roy. Soc. London Ser.* A 252 (1959) 561 - 569

74. G.P. Sendeckyj, Elastic Inclusion Problems in Plane Elastostatics. *International Journal of Solids and Structures*, Vol. 6 (1970) 1535 - 1543R.M

75. S.X. Gong and S.A. Meguid, On the Elastic Fields of an Elliptical Inhomogeneity under Plane Deformation. *Proc. R. Soc. Lond.* A443 (1993) 457 - 471

76. S.X. Gong, A Unified Treatment of the Elastic Elliptical Inclusion under Anitplane Shear. *Archive of Applied Mechanics*, Vol. 65 (1995) 55 - 64

77. C.Q. Ru and P. Schiavone, On the Elliptic Inclusion in Anti-Plane Shear. *Mathematics and Mechanics of Solids*, Vol. 1 (1996) 327 - 333

78. G.P. Tandon and N.J. Pagano, Effective Thermoelastic Moduli of a Unidirectional Fiber Composite Containing Interfacial Arc Microcracks. *ASME, Journal of Applied Mechanics*, Vol. 63 (1996) 210 - 217

79. C.Q. Ru and P. Schiavone, A Circular Inclusion with Circumferentially Inhomogeneous Interface in Antiplane Shear. *Proc. Roy. Soc. Lond.* A453 (1997) 2551 - 2572

80. C.Q. Ru. A Circular Inclusion with Circumferentially Inhomogeneous Sliding Interface in Plane Elastostatics. *ASME, Journal of Applied Mechanics*, Vol.65 (1998) 30 - 38

81. L.J. Sudak, C.Q. Ru, P. Schiavone and A. Mioduchowski, Plane Deformation of a Circular Inclusion with Inhomogeneous Imperfect Interface. *17th Canadian Conference of Applied Mechanics (CANCAM)*, (1999) McMaster University, Hamilton, Ontario, Canada

82. L.J. Sudak, C.Q. Ru, P. Schiavone and A. Mioduchowski, A Circular Inclusion with Inhomogeneously Imperfect Interface in Plane Elasticity. *Journal of Elasticity*, Vol. 55 (1999) 19 - 41

83. L.J. Sudak, On a Circular Inclusion with Imperfect Interface in Plane Elasticity. *Mathematics and Mechanics of Solids* (In Press)

84. L.J. Sudak, C.Q. Ru, P. Schiavone and A. Mioduchowski, A Circular Inclusion with Circumferentially Inhomogeneous Non-Slip Interface in Plane Elasticity (Submitted for Publication)

85. R. Hill, A Self-Consistent Mechanics of Composite Materials. *Journal of the Mechanics and Physics of Solids*, Vol. 13 (1965) 213 - 222

86. R.M. Christenson and K.H. Lo, Solutions for Effective Shear Properties in Three Phase Sphere and Cylinder Models. *Journal of the Mechanics and Physics of Solids*, Vol. 27 (1979) 315 - 330

87. R.M. Christenson, A Critical Evaluation for a Class of Micromechanics Models. *Journal of the Mechanics and Physics of Solids.* Vol. 38, No. 3 (1990) 379 - 404

88. Jacob Aboudi, Mechanics of Composite Materials: A Unified Micromechanical Approach, Elsevier Science Publishers (1991)

89. S. Nemat-Nasser and M. Hori, Micromechanics: Overall Properties of Heterogeneous Materials, North-Holland, New York (1993)

90. Y. Huang and K.X. Hu, A Generalized Self-Consistent Mechanics Method for Solids Containing Elliptical Inclusions. *ASME, Journal of Applied Mechanics*, Vol. 62 (1995) 566 - 572

91. Marek-Jerzy Pindera, Jacob Aboudi and Steven M. Arnold, Limitations of the Uncoupled, RVE-based Micromechanical Approach in the Analysis of Functionally Graded Composites. *Mechanics of Materials*, Vol. 20 (1995) 77 - 94

92. Jiang Y. Li, On Micromechanics Approximations for the Effective Thermoelastic Moduli of Multi-phase Composite Materials. *Mechanics of Materials*, Vol. 31 (1999) 149 - 159

93. G. Siboni and Y. Benveniste, A Micromechanics Model for the Effective Thermomechanical Behavior of Multiphase Composite Media. *Mechanics of Materials*, Vol. 11 (1991) 107 - 122

94. W. Huang, S.I. Rokhlin, Generalized Self-Consistent Model for Composites with Functionally Graded and Multilayered Interphases. Transfer Matrix Approach. *Mechanics of Materials*, Vol. 22 (1996) 219 - 247

95. J.P. Collier, M.B. Mayor, J.C. Chae, V.A. Surprenant, H.P. Surprenant and L.A. Dauphinais, Macroscopic and Microscopic Evidence of Prosthetic Fixation with Porous Coated Materials. *Clin. Orthop. Rel. Res.*, Vol.235 (1988) 173 - 180

96. C.R. Bragdon, M. Jasty, T. Haire, W. Maloney and W.H. Harris, Porous Coated Femoral Components can Loosen Despite Extensive Bone Ingrowth: Observations on Retrieved Components. *Transactions of the 37th Annual Meeting of the Orthopaedic Research Society*, (1991) Anaheim, CA.

97. A.M. Sadegh, G.M. Luo and S.C. Cowin, Bone Ingrowth: An Application of the Boundary Element Method to Bone Remodeling at the Implant Interface. *Journal of Biomechanics*, Vol. 26, No. 2 (1993) 167 - 182

98. Gangming Luo, Ali M. Sadegh, Harold Alexander, William Jaffe, David Scott and Stephen C. Cowin, The Effect of Surface Roughness on the Stress Adaptation of Trabecular Architecture Around a Cylindrical Implant. *Journal of Biomechanics*, Vol. 32 (1999) 275 - 284

99. Stig Hansson and Michael Norton, The Relation Between Surface Roughness and Interfacial Shear Strength for Bone-Anchored Implants. A Mathematical Model. *Journal of biomechanics*, Vol. 32 (1999) 829 - 836

100. B. Van Rietbergen, R. Huiskes, H. Weinans. D.R. Sumner, T.M. Turner and J.O. Galante, The Mechanism of Bone Remodeling and Resorption Around Press-Fitted THA Stems. *Journal of Biomechanics*, Vol. 26 (1993) 369 - 382

101. H. Weinans, R. Huiskes and H.J. Grootenboer, Effects of Fit and Bonding Characteristics of Femoral Stems on Adaptive Bone Remodeling. *ASME, Journal of Biomechanical Engineering*, Vol. 116 (1994) 393 - 400

102. R. Huiskes, The Differing Stress Patterns of Press-Fit, Ingrown and Cemented Femoral Stems. *Clin. Orthop.*, Vol. 261 (1990)

103. H.M. Tensi, H. Gese and P. Ascherl, Non-linear Three-Dimensional Finite Element Analysis of a Cementless Hip Endoprosthesis. *J. Eng. Medicine (Proc. Instn. Mech. Engrs. H)*, Vol. 203 (1989) 215 - 222

104. J.H. Kuiper and R. Huiskes, Mathematical Optimization of Elastic Properties: Application to Cementless Hip Stem Design. *ASME, Journal of Biomechanical Engineering, Vol. 119 (1997) 166 - 174*

105. S.D. Cook, K.A. Thomas and R.J. Haddad Jr., Histologic Analysis of Retrieved Human Porous-Coated Total Joint Components. *Clin. Orthop. Rel. Res.*, Vol. 234 (1988) 90 - 101

106. A.F. Mak, L.M. Keer, S.H. Chen and J.L. Lewis, A No-Slip Interface Crack. *ASME, Journal of Applied Mechanics*, Vol. 47 (1980) 347 - 350

107. A.F. Mak and L.M. Keer, A No-Slip Edge Crack on a Bimaterial Interface. *ASME, Journal of Applied Mechanics*, Vol. 47 (1980) 816 - 820

108. J.P. Clech, L.M. Keer and J.L. Lewis, A Model of Tension and Compression Cracks with Cohesive Zone at a Bone Cement Interface. *ASME, Journal of Biomechanical Engineering*, Vol. 107 (1985) 175 - 182

109. L.J. Sudak, C.Q. Ru, P. Schiavone and A. Mioduchowski, Inhomogeneous Non-Slipping Interfacial Shear Stresses around Implant - Bone Interface (In Preparation)

110. N.I. Muskhelishvili, Some Basic Problems of the Mathematical Theory of Elasticity, Groningen: Noordhoff (1963)

111. C.Q. Ru, Interface Design of Neutral Elastic Inclusions. *International Journal of Solids and Structures*, Vol. 35, No. 7-8 (1998) 559 - 572

112. R.V. Churchill and J.W. Brown, Complex Variables and Applications, 5^{th} Edition, McGraw Hill (1990)

113. R.L. Reis, A.M. Cunha, M.J. Bevis and W.A. Kaplan, Oriented Composites meet tough Orthopedic Demands. *Modern Plastics*, Vol. 76, Issue 5, ISSN: 00268275 (1999)

114. Y. Benveniste and T.Miloh, Neutral Inhomogeneities in Conduction Phenomena. *Journal of the Mechanics and Physics of Solids*, Vol. 47 (1999) 1873 - 1892

115. F. Krasucki and S. Lenci, Analysis of Interfaces of Variable Stiffness. *International Journal of Solids and Structures*, Vol. 37 (2000) 3619 - 3632

116. C. Constanda, A Mathematical Analysis of Bending of Plates with Transverse Shear Deformation. Longman Scientific & Technical, Harlow (1990)

117. A.H. England, Complex Variable Methods in Elasticity, Wiley - Interscience, London (1971)

118. I.S. Gradshteyn and I.M. Ryzhik, Table of Integrals Series and Products. Academic Press, (1965)

APPENDIX A

Derivation of Equation 3.24 and 3.25

In view of (3.12) and (3.14), respectively, the expression $\dfrac{\delta_o}{z\left[1+f\left(z\right)\right]}$ is rewritten as follows:

$$\frac{\delta_o}{z\left[1+f\left(z\right)\right]}=\frac{\delta_o}{R\left(\dfrac{z}{R}\right)\left[1+f\left(z\right)\right]}. \tag{A1}$$

Multiplying the numerator and denominator of (A1) by $\left(\dfrac{z}{R}\right)^{s-1}$, and noting that the functional form describing inhomogeneous interface damage is given by $f\left(z\right)=\dfrac{b_s}{2}\left(\dfrac{z^s}{R^s}+\dfrac{R^s}{z^s}\right)$ yields the following

$$\frac{R\delta_o}{z\left[1+f\left(z\right)\right]}=\frac{\left(\dfrac{z}{R}\right)^{s-1}\delta_o}{\left(\dfrac{z}{R}\right)^{s}+\dfrac{b_s}{2}\left(\dfrac{z}{R}\right)^{2s}+\dfrac{b_s}{2}}. \tag{A2}$$

Multiplying the numerator and denominator of (A2) by $\dfrac{2}{b_s}$ gives

$$\frac{R\delta_o}{z\left[1+f\left(z\right)\right]}=\frac{\delta_o\left(\dfrac{2}{b_s}\right)\left(\dfrac{z}{R}\right)^{s-1}}{\left(\dfrac{z}{R}\right)^{2s}+\dfrac{2}{b_s}\left(\dfrac{z}{R}\right)^{s}+1}. \tag{A3}$$

It has been shown in Chapter 3 that

$$-\frac{2}{b_s}=\frac{1+\rho^{*2}}{\rho^*},$$

then with this condition (A3) is rewritten as follows

$$\frac{R\delta_o}{z\left[1+f\left(z\right)\right]}=\frac{-\delta_o\left(\frac{1+\rho^{*2}}{\rho^*}\right)\left(\frac{z}{R}\right)^{s-1}}{\left(\frac{z}{R}\right)^{2s}-\left(\frac{1+\rho^{*2}}{\rho^*}\right)\left(\frac{z}{R}\right)^{s}+1}. \tag{A4}$$

Since the denominator of (A4) is a product of factors yields the following

$$\frac{R\delta_o}{z\left[1+f\left(z\right)\right]}=\frac{-\delta_o\left(\frac{1+\rho^{*2}}{\rho^*}\right)\left(\frac{z}{R}\right)^{s-1}}{\left[\left(\frac{z}{R}\right)^{s}-\rho^*\right]\left[\left(\frac{z}{R}\right)^{s}-\frac{1}{\rho^*}\right]}. \tag{A5}$$

Now, using the technique of partial fractions, the right hand side of (A5) is rewritten as

$$\frac{-\delta_o\left(\frac{1+\rho^{*2}}{\rho^*}\right)\left(\frac{z}{R}\right)^{s-1}}{\left[\left(\frac{z}{R}\right)^{s}-\rho^*\right]\left[\left(\frac{z}{R}\right)^{s}-\frac{1}{\rho^*}\right]}=\frac{A\left(\frac{z}{R}\right)^{s-1}+B}{\left[\left(\frac{z}{R}\right)^{s}-\rho^*\right]}+\frac{C\left(\frac{z}{R}\right)^{s-1}+D}{\left[\left(\frac{z}{R}\right)^{s}-\frac{1}{\rho^*}\right]}, \tag{A6}$$

where A, B, C, and D are constants that must be determined. Expanding the right hand side of (A6) and writing it in the standard form for polynomials, we obtain

$$-\delta_o\left(\frac{1+\rho^{*2}}{\rho^*}\right)\left(\frac{z}{R}\right)^{s-1}=(A+C)\left(\frac{z}{R}\right)^{2s-1}+\left(-\frac{A}{\rho^*}-C\rho^*\right)\left(\frac{z}{R}\right)^{s-1}+$$
$$(B+D)\left(\frac{z}{R}\right)^{s}-\frac{B}{\rho^*}-D\rho^*, \tag{A7}$$

and since the polynomials in (A7) are equal, so their coefficients must also be

equal. Hence, we have

$$\begin{aligned} A &= -\delta_o \left(\frac{1+\rho^{*2}}{\rho^{*2}-1} \right), \\ B &= 0, \\ C &= \delta_o \left(\frac{1+\rho^{*2}}{\rho^{*2}-1} \right), \\ D &= 0. \end{aligned} \tag{A8}$$

Therefore, substituting the values of (A8) into (A6), (A5) becomes

$$\begin{aligned} \frac{R\delta_o}{z\left[1+f\left(z\right)\right]} &= \frac{-\delta_o \left(\frac{1+\rho^{*2}}{\rho^{*2}-1} \right) \left(\frac{z}{R} \right)^{s-1}}{\left[\left(\frac{z}{R} \right)^{s} - \rho^{*} \right]} + \frac{\delta_o \left(\frac{1+\rho^{*2}}{\rho^{*2}-1} \right) \left(\frac{z}{R} \right)^{s-1}}{\left[\left(\frac{z}{R} \right)^{s} - \frac{1}{\rho^{*}} \right]} \\ &= \frac{-\lambda \left(\frac{z}{R} \right)^{s-1}}{\left[\left(\frac{z}{R} \right)^{s} - \rho^{*} \right]} + \frac{\lambda \left(\frac{z}{R} \right)^{s-1}}{\left[\left(\frac{z}{R} \right)^{s} - \frac{1}{\rho^{*}} \right]}, \end{aligned} \tag{A9}$$

where $\lambda = -\delta_o \left(\frac{1+\rho^{*2}}{1-\rho^{*2}} \right) < 0.$

This completes the derivation of condition (3.24).

The derivation of equation of (3.25) follows a similar pattern as above. To this end, we have

$$\frac{1}{1+f\left(z\right)} = \frac{1}{1+\frac{b_s}{2}\left(\frac{z}{R} \right)^{s} + \frac{b_s}{2}\left(\frac{R}{z} \right)^{s}}. \tag{A10}$$

Multiplying the numerator and denominator of (A10) by $\frac{2}{b_s}\left(\frac{z}{R}\right)^s$ gives

$$\begin{aligned}\frac{1}{1+f(z)} &= \frac{\frac{2}{b_s}\left(\frac{z}{R}\right)^s}{\left(\frac{z}{R}\right)^{2s}+\frac{2}{b_s}\left(\frac{z}{R}\right)^s+1} \\ &= \frac{\frac{2}{b_s}\left(\frac{z}{R}\right)^s}{\left(\frac{z}{R}\right)^{2s}-\left(\frac{1+\rho^{*2}}{\rho^*}\right)\left(\frac{z}{R}\right)^s+1} \\ &= \frac{\frac{2}{b_s}\left(\frac{z}{R}\right)^s}{\left[\left(\frac{z}{R}\right)^s-\rho^*\right]\left[\left(\frac{z}{R}\right)^s-\frac{1}{\rho^*}\right]}.\end{aligned} \tag{A11}$$

This completes the derivation of equation (3.25).

APPENDIX B

Derivation of Equation 3.26 and 3.27

The exact closed-form solutions for Φ_I and Φ_M are given symbolically by conditions (3.16) and (3.17), respectively. In order to solve these equations explicitly, one must evaluate the given integrals according to a class of inhomogeneous imperfect interface (i.e. what is the functional form describing the circumferential variation in damage along the interface). In this work, the inhomogeneous interface imperfections are given by $f(z) = \frac{b_s}{2}\left(\frac{z^s}{R^s} + \frac{R^s}{z^s}\right)$. To this end, the integral $R\delta_o \int \frac{dz}{z\left[1+f(z)\right]}$ in conjunction with (3.24) gives

$$R\delta_o \int \frac{dz}{z\left[1+f(z)\right]} = -\lambda \int \frac{\left(\frac{z}{R}\right)^{s-1}}{\left[\left(\frac{z}{R}\right)^s - \rho^*\right]} dz + \lambda \int \frac{\left(\frac{z}{R}\right)^{s-1}}{\left[\left(\frac{z}{R}\right)^s - \frac{1}{\rho^*}\right]} dz. \qquad \text{(B1)}$$

Making the substitution $u = \left(\frac{z}{R}\right)^s - \rho^*$ and $v = \left(\frac{z}{R}\right)^s - \frac{1}{\rho^*}$ allows (B1) to be evaluated. Thus, the solution of (B1) is given by

$$\delta_o \int \frac{dz}{z\left[1+f(z)\right]} = -\frac{\lambda}{s}\log\left[\left(\frac{z}{R}\right)^s - \rho^*\right] + \frac{\lambda}{s}\log\left[\left(\frac{z}{R}\right)^s - \frac{1}{\rho^*}\right]. \qquad \text{(B2)}$$

Therefore, in view of (3.16), the expression for $Q(z)$ becomes

$$Q(z) = \delta_o \beta \int \frac{dz}{z\,[1+f(z)]} = -\beta\frac{\lambda}{s}\log\left[\left(\frac{z}{R}\right)^s - \rho^*\right] + \beta\frac{\lambda}{s}\log\left[\left(\frac{z}{R}\right)^s - \frac{1}{\rho^*}\right]$$
$$= \log\left\{\left[\left(\frac{z}{R}\right)^s - \rho^*\right]^{-\frac{\lambda\beta}{s}}\left[\left(\frac{z}{R}\right)^s - \frac{1}{\rho^*}\right]^{\frac{\lambda\beta}{s}}\right\}. \qquad \text{(B3)}$$

Also, in view of (3.25), the expression for $C(z)$ becomes

$$C(z) = \int_{z_1}^{z} \frac{F(z)}{1+f(z)} e^{Q(z)} dz + C_o$$
$$= \int_{z_1}^{z} F(z) \frac{\left(\frac{2}{b_s}\right)\left(\frac{z}{R}\right)^s \left[\left(\frac{z}{R}\right)^s - \rho^*\right]^{-\frac{\lambda\beta}{s}} \left[\left(\frac{z}{R}\right)^s - \frac{1}{\rho^*}\right]^{\frac{\lambda\beta}{s}}}{\left[\left(\frac{z}{R}\right)^s - \rho^*\right]\left[\left(\frac{z}{R}\right)^s - \frac{1}{\rho^*}\right]} dz + C_o \qquad \text{(B4)}$$
$$= \int_{z_1}^{z} F(z)\left(\frac{2}{b_s}\right)\left(\frac{z}{R}\right)^s \left[\left(\frac{z}{R}\right)^s - \rho^*\right]^{-\left(\frac{\lambda\beta}{s}+1\right)} \left[\left(\frac{z}{R}\right)^s - \frac{1}{\rho^*}\right]^{\frac{\lambda\beta}{s}-1} dz + C_o.$$

Therefore, using (B3) and (B4), the solution for Φ_I is

$$\Phi_I(z) = \left(\frac{2}{b_s}\right)\left[\left(\frac{z}{R}\right)^s - \rho^*\right]^{\frac{\lambda\beta}{s}} \left[\left(\frac{z}{R}\right)^s - \frac{1}{\rho^*}\right]^{-\frac{\lambda\beta}{s}} \times$$
$$\int_{z_1}^{z} F(z)\left(\frac{z}{R}\right)^s \left[\left(\frac{z}{R}\right)^s - \rho^*\right]^{-\left(\frac{\lambda\beta}{s}+1\right)} \left[\left(\frac{z}{R}\right)^s - \frac{1}{\rho^*}\right]^{\frac{\lambda\beta}{s}-1} dz + \qquad \text{(B5)}$$
$$C_o\left[\left(\frac{z}{R}\right)^s - \rho^*\right]^{\frac{\lambda\beta}{s}} \left[\left(\frac{z}{R}\right)^s - \frac{1}{\rho^*}\right]^{-\frac{\lambda\beta}{s}}, \quad z \in D_I.$$

Note that in (B5) the integrand has branch points at $z = R\rho_k (k = 1, 2, ..., s)$. Accordingly, branch cuts are made from each of the s branch points of the multi-valued function appearing in (B5) with each branch cut being parallel to the real

axis, and since $\lambda < 0$ and $\beta > 0$ the integral in (B5) is a weakly singular kernel and is convergent at each branch point (see [110], [116] or [117] for details). In addition, to guarantee that Φ_I is bounded at $z = R\rho_1$, it must be that $C_o = 0$. Hence, with these results, we arrive at solution for Φ_I

$$\Phi_I(z) = \left(\frac{2}{b_s}\right)\left[\left(\frac{z}{R}\right)^s - \rho^*\right]^{\frac{\lambda\beta}{s}}\left[\left(\frac{z}{R}\right)^s - \frac{1}{\rho^*}\right]^{-\frac{\lambda\beta}{s}} \times$$
$$\int_{R\rho_1}^{z} F(t)\left(\frac{t}{R}\right)^s\left[\left(\frac{t}{R}\right)^s - \rho^*\right]^{-\left(\frac{\lambda\beta}{s}+1\right)}\left[\left(\frac{t}{R}\right)^s - \frac{1}{\rho^*}\right]^{\frac{\lambda\beta}{s}-1} dt, \quad z \in D_I. \qquad \text{(B6)}$$

This completes the derivation for the stress potential, $\Phi_I(z)$, (i.e. equation (3.26)) inside the circular inclusion.

The derivation for the stress potential, $\Phi_M(z)$, (i.e. equation (3.27)) outside the inclusion follows a similar pattern to what is shown above. In view of (3.17) and (B2), the expression $P(z)$ takes the form

$$P(z) = -\delta_o \int \frac{dz}{z\left[1 + f(z)\right]} = \frac{\lambda}{s}\log\left[\left(\frac{z}{R}\right)^s - \rho^*\right] - \frac{\lambda}{s}\log\left[\left(\frac{z}{R}\right)^s - \frac{1}{\rho^*}\right]$$
$$= \log\left\{\left[\left(\frac{z}{R}\right)^s - \rho^*\right]^{\frac{\lambda}{s}}\left[\left(\frac{z}{R}\right)^s - \frac{1}{\rho^*}\right]^{-\frac{\lambda}{s}}\right\}. \qquad \text{(B7)}$$

Also, in view of (3.25), the expression for $H(z)$ becomes

$$H(z) = \int_{z_M}^{z} \frac{G(z)}{[1+f(z)]} e^{P(z)} dz + H_o$$

$$= \int_{z_M}^{z} G(z) \left(\frac{2}{b_s}\right) \left(\frac{z}{R}\right)^s \frac{\left[\left(\frac{z}{R}\right)^s - \rho^*\right]^{\frac{\lambda}{s}} \left[\left(\frac{z}{R}\right)^s - \frac{1}{\rho^*}\right]^{-\frac{\lambda}{s}}}{\left[\left(\frac{z}{R}\right)^s - \rho^*\right] \left[\left(\frac{z}{R}\right)^s - \frac{1}{\rho^*}\right]} dz + H_o \qquad \text{(B8)}$$

$$= \int_{z_M}^{z} G(z) \left(\frac{2}{b_s}\right) \left(\frac{z}{R}\right)^s \left[\left(\frac{z}{R}\right)^s - \rho^*\right]^{\frac{\lambda}{s}-1} \left[\left(\frac{z}{R}\right)^s - \frac{1}{\rho^*}\right]^{-\left(\frac{\lambda}{s}+1\right)} dz + H_o$$

Therefore, using (B7) and (B8) the solution for Φ_M is

$$\Phi_M(z) = \left(\frac{2}{b_s}\right) \left[\left(\frac{z}{R}\right)^s - \rho^*\right]^{-\frac{\lambda}{s}} \left[\left(\frac{z}{R}\right)^s - \frac{1}{\rho^*}\right]^{\frac{\lambda}{s}} \times$$

$$\int_{z_M}^{z} G(z) \left(\frac{z}{R}\right)^s \left[\left(\frac{z}{R}\right)^s - \rho^*\right]^{\frac{\lambda}{s}-1} \left[\left(\frac{z}{R}\right)^s - \frac{1}{\rho^*}\right]^{-\left(\frac{\lambda}{s}+1\right)} dz + \qquad \text{(B9)}$$

$$H_o \left[\left(\frac{z}{R}\right)^s - \rho^*\right]^{-\frac{\lambda}{s}} \left[\left(\frac{z}{R}\right)^s - \frac{1}{\rho^*}\right]^{\frac{\lambda}{s}}, \quad z \in D_M.$$

Note that in (B9) the integrand has branch points at $z = \frac{R}{\rho_k} (k = 1, 2, ..., s)$. Accordingly, branch cuts are made from each of the s branch points of the multi-valued function appearing in (B9) with each branch cut being parallel to the real axis, and since $\lambda < 0$ the integral in (B9) is a weakly singular kernel and is convergent at each branch point (see [110], [116] or [117] for details). In addition, to guarantee that Φ_M is bounded at $z = \frac{R}{\rho_1}$, it must be that $H_o = 0$. Hence, with

these results, we arrive at solution for Φ_M

$$\Phi_M(z) = \left(\frac{2}{b_s}\right)\left[\left(\frac{z}{R}\right)^s - \rho^*\right]^{-\frac{\lambda}{s}}\left[\left(\frac{z}{R}\right)^s - \frac{1}{\rho^*}\right]^{\frac{\lambda}{s}} \times$$

$$\int_{R/\rho_1}^{z} G(t)\left(\frac{t}{R}\right)^s\left[\left(\frac{t}{R}\right)^s - \rho^*\right]^{\frac{\lambda}{s}-1}\left[\left(\frac{t}{R}\right)^s - \frac{1}{\rho^*}\right]^{-\left(\frac{\lambda}{s}+1\right)} dz, \quad z \in D_M. \qquad \text{(B10)}$$

This completes the derivation for the stress potential, $\Phi_M(z)$, (i.e. equation (3.27)) in the matrix.

APPENDIX C

Derivation of Homogeneous Coefficients for the Case s = 1

To determine the homogeneous coefficients X_1 and A_1, for the case corresponding to the functional form of the inhomogeneous spring - layer interface given by the circumferential number $s = 1$, the circumferential inhomogeneous interface parameter (ρ^*) must be zero (i.e. by selecting $\rho^* = 0$, this corresponds to a homogeneous imperfect interface). To this end, let us consider the coefficient X_1 first. Note that in the expression for the coefficient X_1 (i.e. condition (4.7)) the natural logarithm can be rewritten in the form of an infinite sum (see [118] for details)

i.e.

$$\ln\left(\frac{1}{1-\rho^{*2}}\right) = \rho^{*2} + \frac{1}{2}\rho^{*4} + \text{ higher order terms of } \rho^*, \quad \rho^{*4} < 1. \tag{C1}$$

Note that since $\rho^* = 0$, the higher order terms appearing in (C1) can be neglected and condition (4.7) can be rewritten as

$$X_1\rho^{*4} + \overline{X_1}\left[\frac{1}{2}\rho^{*4} + \frac{\delta_o\eta}{2}\rho^{*4} + \frac{1}{2}\rho^{*6}\right] = \left[A\delta_o(1+\eta) - \frac{2\delta_o\varepsilon_1}{\frac{\kappa_M}{\mu_M} + \frac{1}{\mu_I}}\right] \times \left[\frac{1}{2}\rho^{*4} + \rho^{*6} + \frac{1}{2}\rho^{*8}\right]. \tag{C2}$$

Multiplying (C2) by ρ^{*-4} and noting that $\rho^* = 0$ yields the following

$$2X_1 + \overline{X_1}\,(1 + \delta_o\eta) = \left[A\delta_o\,(1+\eta) - \frac{2\delta_o\varepsilon_1}{\dfrac{\kappa_M}{\mu_M} + \dfrac{1}{\mu_I}}\right]. \tag{C3}$$

Clearly, (C3) is a real quantity, therefore, $\mathrm{Im}\,[X_1] = 0$ and as such the value of X_1 is

$$X_1\,(3 + \delta_o\eta) = A\delta_o\,(1+\eta) - \frac{2\delta_o\varepsilon_1}{\dfrac{\kappa_M}{\mu_M} + \dfrac{1}{\mu_I}}. \tag{C4}$$

Note that $\delta_o = \dfrac{1-\rho^{*2}}{1+\rho^{*2}}$.

Hence, for the purposes of examining the effects of the circumferential inhomogeneity of an imperfect interface on the average mean stress induced within the circular inclusion, under otherwise identical conditions and no eigenstrains, the coefficient X_1 takes the form

$$X_1 = \frac{A\,(1-\rho^{*2})\,(1+\eta)}{3 + \eta + \rho^{*2}\,(3-\eta)}. \tag{C5}$$

Unlike in the previous analysis where the homogeneous coefficient X_1 is obtained from an explicit expression of X_1 (i.e. condition (4.7)), the determination of the homogeneous coefficient A_1 requires the knowledge of stress potential $\Phi_M\,(z)$, specifically, we require the coefficient corresponding to the power of z^{-1}. This can be seen by considering the series expansion for $\Phi_M(z)$ given by condition (2.5).

To begin with, let us rewrite the logarithmic term appearing in (4.9) in the form of an infinite sum, specifically,

$$\left[\frac{\frac{z}{R}-\rho^*}{\frac{z}{R}-\frac{1}{\rho^*}}\right]\log\left[\frac{1-\rho^{*2}}{1-\frac{R}{z}\rho^*}\right]=\left[\frac{1-\frac{R}{z}\rho^*}{1-\frac{R}{z}\frac{1}{\rho^*}}\right]\left[\log\left(1-\rho^{*2}\right)-\log\left(1-\frac{R}{z}\rho^*\right)\right],$$

$$=\left[\frac{1-\frac{R}{z}\rho^*}{1-\frac{R}{z}\frac{1}{\rho^*}}\right]\left[\log\left(1-\rho^{*2}\right)+\frac{R}{z}\rho^*+\frac{1}{2}\left(\frac{R}{z}\right)^2\rho^{*2}+\right.$$

$$\left.\text{higher order terms of }\left(\frac{R}{z}\right)\rho^*\right]. \qquad \text{(C6)}$$

Multiplying the numerator and denominator of (C6) by $1+\frac{R}{z}\frac{1}{\rho^*}$ and selecting the coefficient that corresponds to the power z^{-1} gives

$$R\rho^*+R\left(\frac{1-\rho^{*2}}{\rho^*}\right)\ln(1-\rho^{*2}). \qquad \text{(C7)}$$

In addition, the term

$$\frac{\overline{B}R}{\left(\frac{z}{R}-\frac{1}{\rho^*}\right)}\left[\frac{R}{z\rho^*}-\frac{\rho^*\left(\frac{z}{R}-\rho^*\right)}{1-\rho^{*2}}\right]=\overline{B}R\left[\frac{R(1-\rho^{*2})-z\rho^{*2}\left(\frac{z}{R}-\rho^*\right)}{z\rho^*\left(1-\rho^{*2}\right)\left(\frac{z}{R}-\frac{1}{\rho^*}\right)}\right],$$

$$=\overline{B}R\left[\frac{\frac{R^2}{z}(1-\rho^{*2})-z\rho^{*2}\left(1-\frac{R}{z}\rho^*\right)}{z\rho^*\left(1-\rho^{*2}\right)\left(1-\frac{R}{z}\frac{1}{\rho^*}\right)}\right]. \qquad \text{(C8)}$$

Multiplying the numerator and denominator of (C8) by $\left(1+\frac{R}{z}\frac{1}{\rho^*}\right)\frac{1}{z}$ gives

$$\overline{B}R\frac{\left[\left(\frac{R}{z}\right)^2\left(1-\rho^{*2}\right)\left(1+\frac{R}{z\rho^*}\right)-\rho^{*2}\left[1+\frac{R}{z\rho^*}-\frac{R}{z}\rho^*-\left(\frac{R}{z}\right)^2\right]\right]}{\rho^*\left(1-\rho^{*2}\right)\left[1-\left(\frac{R}{z}\right)^2\right]},$$

and by selecting the coefficient corresponding to the power z^{-1} yields the desired expression

$$-\overline{B}R^2. \tag{C9}$$

Hence, in view of (4.7), (C7) and (C9) the coefficient A_1, which is the coefficient of the power z^{-1}, is given by

$$A_1=\frac{\overline{B}R^2}{\rho^{*2}}\left[(1+\eta)\left(1-\rho^{*2}\right)-\rho^{*2}\right]+\frac{\overline{B}R^2}{\rho^{*4}}(1+\eta)\left(1-\rho^{*2}\right)^2\ln\left(1-\rho^{*2}\right)+$$
$$\frac{2R^2\left(1-\rho^{*2}\right)(\varepsilon_2+i\varepsilon_3)}{\left(\frac{\kappa_M}{\mu_M}+\frac{1}{\mu_I}\right)}\left[\frac{\rho^{*2}+\left(1-\rho^{*2}\right)\ln\left(1-\rho^{*2}\right)}{\rho^{*4}}\right]. \tag{C10}$$

Note that the coefficient A_1 given in (C10) corresponds to the inhomogeneous imperfect interface. If $\rho^* = 0$ (i.e. corresponding homogeneous condition) then A_1 is identical to that given by [80].

To get the coefficient A_1 corresponding to the homogeneous imperfect interface the inhomogeneous interface parameter ρ^* must be chosen to be zero. Therefore, for the purposes of examining the effects of the circumferential inhomogeneity

of an imperfect interface on the average mean stress induced within the circular inclusion, under otherwise identical conditions and no eigenstrains, the coefficient A_1 takes the form

$$\frac{\overline{A_1}}{R^2} = B\left(\frac{\delta_o \eta - 1}{\delta_o + 1}\right), \tag{C11}$$

where the parameter δ_o is defined as before.

This completes the derivations for the homogeneous coefficients X_1 and A_1, for the case corresponding to the functional form of the inhomogeneous spring - layer interface given by the circumferential number $s = 1$, respectively.

APPENDIX D

Derivation of Homogeneous Coefficients for the Case s = 2

To determine the homogeneous coefficients X_1 and A_1, for the case corresponding to the functional form of the inhomogeneous spring - layer interface given by the circumferential number $s = 2$, the circumferential inhomogeneous interface parameter (ρ^*) must be zero (i.e. by selecting $\rho^* = 0$, this corresponds to a homogeneous imperfect interface). To this end, let us consider the expressions given in (4.32), and let us rewrite the natural logarithm in the form of an infinite sum (see [118] for details)

$$\ln\left[\frac{1+\rho^*}{1-\rho^*}\right] = 2\rho^* + \frac{2}{3}\rho^{*3} + \text{ higher order terms of } \rho^*, \quad \rho^{*2} < 1. \tag{D1}$$

Since $\rho^* = 0$ the higher order terms can be neglected, and in view of the expression for the coefficient X_1 (i.e. condition (4.30)), the expressions in (4.32) can be rewritten as

$$\begin{aligned}\left(\frac{b_2}{2}\right)\left(\frac{I_{10}}{I_{12}}\right) &= \left(\frac{b_2}{2}\right)\left[\frac{12\rho^* - 4\rho^{*3} - 2\rho^{*5}}{4\rho^{*2} + 2\rho^{*4}}\right], \\ &= -\left(\frac{1}{1+\rho^{*2}}\right)\left[\frac{6 - 2\rho^{*2} - \rho^{*4}}{2+\rho^{*2}}\right], \\ &= -3 \text{ as } \rho^* = 0,\end{aligned} \tag{D2}$$

and

$$\left(\frac{b_2}{2}\right)\left(\frac{I_{14}}{I_{12}}\right) = \frac{1}{\rho^*}\left(\frac{b_2}{2}\right)\left[\frac{3\rho^{*2}}{2+\rho^{*2}}\right],$$
$$= \left(\frac{b_2}{2}\right)\left[\frac{3\rho^*}{2+\rho^{*2}}\right], \tag{D3}$$
$$= 0 \text{ as } \rho^* = 0,$$

and

$$\left(\frac{b_2}{2}\right)\left(\frac{M_{10}}{M_{12}}\right) = \frac{1}{\rho^*}\left(\frac{b_2}{2}\right)\left[\frac{2\rho^{*2}+\rho^{*4}}{6-2\rho^{*2}-\rho^{*4}}\right],$$
$$\left(\frac{b_2}{2}\right)\left[\frac{2\rho^*+\rho^{*3}}{6-2\rho^{*2}-\rho^{*4}}\right], \tag{D4}$$
$$= 0 \text{ as } \rho^* = 0,$$

and

$$\left(\frac{b_2}{2}\right)\left(\frac{M_{14}}{M_{12}}\right) = \left(\frac{b_2}{2}\right)\left[\frac{6\rho^{*2}-2-2\rho^{*4}-\rho^{*6}}{2\rho^*-\left(\frac{2}{3}\right)\rho^{*3}-\left(\frac{1}{3}\right)\rho^{*5}}\right],$$
$$= -\left(\frac{1}{1+\rho^{*2}}\right)\left[\frac{6\rho^{*2}-2-2\rho^{*4}-\rho^{*6}}{2-\left(\frac{2}{3}\right)\rho^{*2}-\left(\frac{1}{3}\right)\rho^{*4}}\right], \tag{D5}$$
$$= -1 \text{ as } \rho^* = 0,$$

and

$$\left(\frac{b_2}{2}\right)\left(\frac{M_{1-2}}{M_{12}}\right) = \frac{1}{\rho^{*2}}\left(\frac{b_2}{2}\right)\left[\frac{6\rho^* - 4\rho^{*3} - 6\rho^*\left(1-\rho^{*2}\right) - 2\rho^{*3}\left(1-\rho^{*2}\right)}{4\rho^* - \left(\frac{4}{3}\right)\rho^{*3} - \left(\frac{2}{3}\right)\rho^{*5}}\right],$$

$$= \left(\frac{b_2}{2}\right)\left[\frac{3\rho^{*2}}{6 - 2\rho^{*2} - \rho^{*4}}\right], \qquad \text{(D6)}$$

$$= 0 \text{ as } \rho^* = 0.$$

Note that in the above calculations the term $\left(\frac{b_2}{2}\right) = -\frac{\rho^*}{1+\rho^{*2}}$.

Hence, with conditions (D2 - D6), the expression for the coefficient X_1 reduces to the following

$$X_1\left(4+\delta_o\eta\right) = A\left(2+\delta_o\eta\right) - \frac{2\delta_o\varepsilon_1}{\left(\frac{\kappa_M}{\mu_M}+\frac{1}{\mu_I}\right)},$$

$$\delta_0 = 2\left(\frac{1-\rho^{*2}}{1+\rho^{*2}}\right). \qquad \text{(D7)}$$

With regards to the coefficient A_1, (4.31) can be written into the following form

$$A_1 = AR^2\left[\frac{M_{14}}{M_{12}} + \frac{2}{b_2}\left(1-\delta_o\right)\right] + \overline{B}R^2\left(\frac{M_{1-2}}{M_{12}}\right) + R^2\left[\overline{B}\left(1-\delta_o\eta\right) - \frac{2\delta_o\left(\varepsilon_2+i\varepsilon_3\right)}{\left(\frac{\kappa_M}{\mu_M}+\frac{1}{\mu_I}\right)}\right] \times$$

$$\left(\frac{2}{b_2}\right)\left(\frac{M_{10}}{M_{12}}\right) - R^2\left(\frac{M_{10}}{M_{12}}\right)\left(X_1 + \overline{X_1} - A\right). \qquad \text{(D8)}$$

Therefore, to obtain the homogeneous coefficient A_1, note the following

$$\left[\frac{M_{14}}{M_{12}} + \frac{2}{b_2}\left(1-\delta_o\right)\right] = \left[\frac{6\rho^{*2} - 2 - 2\rho^{*4} - \rho^{*6}}{2\rho^* - \left(\frac{2}{3}\right)\rho^{*3} - \left(\frac{1}{3}\right)\rho^{*5}}\right] - \frac{1}{\rho^*}\left[-1 + 3\rho^{*2}\right],$$

$$= 0 \text{ as } \rho^* = 0,$$

and

$$\left(\frac{2}{b_2}\right)\left(\frac{M_{10}}{M_{12}}\right) = \left(\frac{2}{b_2}\right)\left[\frac{2\rho^* + \rho^{*3}}{6 - 2\rho^{*2} - \rho^{*4}}\right],$$
$$= -\left(\frac{1+\rho^{*2}}{\rho^*}\right)\left[\frac{\rho^*(2+\rho^{*2})}{6 - 2\rho^{*2} - \rho^{*4}}\right],$$
$$= -\frac{1}{3} \text{ as } \rho^* = 0.$$

Therefore, with the above notes, (D8) reduces to the following homogeneous results

$$A_1 = -\frac{\overline{B}R^2}{3}(1 - \delta_o\eta) + \frac{2\delta_o(\varepsilon_2 + i\varepsilon_3)}{3\left(\frac{\kappa_M}{\mu_M} + \frac{1}{\mu_I}\right)}R^2,$$
$$\delta_0 = 2\left(\frac{1-\rho^{*2}}{1+\rho^{*2}}\right). \qquad \text{(D9)}$$

This completes the derivations for the homogeneous coefficients X_1 and A_1, for the case corresponding to the functional form of the inhomogeneous spring - layer interface given by the circumferential number $s = 2$, respectively.

APPENDIX E

Derivation of Equation (5.9)

The goal in deriving equation (5.9) is to eliminate the stress potential $\Phi_M(z)$, and rewrite the normal interface condition in terms of $\Phi_I(z)$. Therefore, to begin with, the normal component of the traction across the material interface is required. This is obtained from Muskhelishvili's results. Therefore, from $(2.1)_3$ we have

$$\sigma_r - i\sigma_{r\theta} = \Phi'(z) + \overline{\Phi'(z)} - e^{2i\theta}\left[\overline{z}\Phi''(z) + \Psi'(z)\right],$$

and by taking the complex conjugate of the above and adding the two results gives the desired expression for the normal component of the traction in the following form

$$2\sigma_r = 2\left[\Phi'(z) + \overline{\Phi'(z)}\right] - \overline{z}e^{2i\theta}\Phi''(z) - e^{2i\theta}\Psi'(z) - ze^{-2i\theta}\overline{\Phi''(z)} - e^{-2i\theta}\overline{\Psi'(z)}, \quad z \in \Gamma. \tag{E1}$$

The next step involves multiplying equation (5.4) by $\frac{z}{R}$ and subsequently taking the derivative with respect to the variable z. This yields

$$\frac{1}{4}\left[\frac{\kappa_M}{\mu_M}+\frac{1}{\mu_I}\right]\Phi_M'(z)+\frac{1}{2}\left[\frac{\kappa_I}{\mu_I}+\frac{1}{\mu_M}\right]\frac{z}{R^2}\overline{\Phi_I}\left(\frac{R^2}{z}\right)-\frac{1}{4}\left[\frac{\kappa_I}{\mu_I}+\frac{1}{\mu_M}\right]\overline{\Phi_I'}\left(\frac{R^2}{z}\right)-$$
$$\frac{1}{4\mu_I}\overline{B}\left(\frac{R}{z}\right)^2+\frac{1}{4\mu_M}\overline{B}\left(\frac{R}{z}\right)^2+\frac{1}{2}\left(\frac{R}{z}\right)^2(\varepsilon_2+i\varepsilon_3)-\frac{1}{4}A\left[\frac{\kappa_M}{\mu_M}+\frac{1}{\mu_I}\right]-$$
$$\frac{1}{4}\overline{X_1}\left[\frac{\kappa_I}{\mu_I}+\frac{1}{\mu_M}\right]=0,\quad z\in D_M,$$

which when solved for Φ_M' gives

$$\Phi_M'(z)=\beta\overline{\Phi_I'}\left(\frac{R^2}{z}\right)-2\beta\frac{z}{R^2}\overline{\Phi_I}\left(\frac{R^2}{z}\right)-\overline{B}\left(\frac{R}{z}\right)^2\eta-\frac{2(\varepsilon_2+i\varepsilon_3)}{\left[\frac{\kappa_M}{\mu_M}+\frac{1}{\mu_I}\right]}\left(\frac{R}{z}\right)^2$$
$$+A+\beta\overline{X_1},\quad z\in D_M \tag{E2}$$

where the parameters β and η take the following forms, respectively

$$\beta=\frac{\left[\frac{\kappa_I}{\mu_I}+\frac{1}{\mu_M}\right]}{\left[\frac{\kappa_M}{\mu_M}+\frac{1}{\mu_I}\right]}>0,\qquad \eta=\frac{\frac{1}{\mu_M}-\frac{1}{\mu_I}}{\left[\frac{\kappa_M}{\mu_M}+\frac{1}{\mu_I}\right]}. \tag{D3}$$

Substituting (E2) into $(2.10)_1$ and then taking the derivative with respect to the variable z gives

$$\Psi_M'(z)=B+(\beta-1)\left(\frac{R}{z}\right)^2\overline{\Phi_I'}\left(\frac{R^2}{z}\right)-2\beta\frac{1}{z}\overline{\Phi_I}\left(\frac{R^2}{z}\right)-\overline{B}\left(\frac{R}{z}\right)^4\eta-\frac{R^2}{z}\Phi_M''(z)$$
$$-\frac{2(\varepsilon_2+i\varepsilon_3)}{\left[\frac{\kappa_M}{\mu_M}+\frac{1}{\mu_I}\right]}\left(\frac{R}{z}\right)^4+(A+\beta\overline{X_1})\left(\frac{R}{z}\right)^2-\left(A+\frac{B_1}{R^2}-\overline{X_1}\right)\left(\frac{R}{z}\right)^2,\quad z\in D_M. \tag{E4}$$

Now, by substituting (E2) and (E4) into (E1) and noting that on the inclusion - matrix boundary $z\bar{z} = R^2$ and $z = \mathrm{Re}^{i\theta}$ the expression for the normal component of the traction across the material interface is given by

$$\sigma_r = \left(\frac{1+\beta}{2}\right)\overline{\Phi_I'}\left(\frac{R^2}{z}\right) - \beta\left(\frac{z}{R^2}\right)\overline{\Phi_I}\left(\frac{R^2}{z}\right) - \frac{\overline{B}}{2}(1+\eta)\left(\frac{R}{z}\right)^2 - \frac{(\varepsilon_2 - i\varepsilon_3)}{\left[\frac{\kappa_M}{\mu_M} + \frac{1}{\mu_I}\right]}\left(\frac{z}{R}\right)^2 + \frac{1}{2}\left(A + \beta\overline{X_1}\right) + \frac{1}{2}\left(A + \frac{B_1}{R^2} - \overline{X_1}\right) + \left(\frac{1+\beta}{2}\right)\Phi_I'(z) - \frac{\beta}{z}\Phi_I(z) - \frac{B}{2}(1+\eta)\left(\frac{z}{R}\right)^2 - \frac{(\varepsilon_2 + i\varepsilon_3)}{\left[\frac{\kappa_M}{\mu_M} + \frac{1}{\mu_I}\right]}\left(\frac{R}{z}\right)^2 + \frac{1}{2}(A + \beta X_1) + \frac{1}{2}\left(A + \frac{B_1}{R^2} - X_1\right), \quad z \in \Gamma. \tag{E5}$$

Having derived the expression for the normal component of traction, implies that the left hand side of (5.7) is known. However, the right hand side, specifically the jump in the displacement across the inclusion - matrix boundary is not known. Therefore, in view of $(2.1)_1$, the jump in the displacement is written as follows

$$\begin{aligned} \|u_r - iu_\theta\| &= (u_r - iu_\theta)_M - (u_r - iu_\theta)_I, \\ &= \frac{e^{i\theta}}{2\mu_M}\left[\kappa_M\overline{\Phi_M(z)} - \bar{z}\Phi_M'(z) - \Psi_M(z)\right] - \\ &\quad \frac{e^{i\theta}}{2\mu_I}\left[\kappa_I\overline{\Phi_I(z)} - \bar{z}\Phi_I'(z) - \Psi_I(z)\right], \quad z \in \Gamma. \end{aligned} \tag{E6}$$

Clearly, in order to solve (E6) requires a knowledge of $\overline{\Phi_M}$, Φ_M', Ψ_M and Ψ_I. So then, as before, multiply (5.4) by $\frac{z}{R}$. Then, by taking the complex conjugate and

solving for $\overline{\Phi_M(z)}$ yields

$$\overline{\Phi_M(z)} = B\eta\frac{R^2}{\bar{z}} + A\bar{z} + \beta X_1\bar{z} + \frac{2(\varepsilon_2 - i\varepsilon_3)}{\left[\frac{\kappa_M}{\mu_M} + \frac{1}{\mu_I}\right]}\left(\frac{R^2}{\bar{z}}\right) + \left[\frac{\frac{C_1}{\mu_M} - \frac{C_2}{\mu_I}}{\frac{\kappa_M}{\mu_M} + \frac{1}{\mu_I}}\right] - \beta\left(\frac{\bar{z}}{R}\right)^2\Phi_I\left(\frac{R^2}{\bar{z}}\right), \quad z \in D_M. \tag{E7}$$

The expressions for $\Psi_M(z)$ and $\Psi_I(z)$ are obtained form conditions (2.10). Therefore, in view of (E2), the expression for Ψ_M is rewritten as

$$\Psi_M(z) = Bz + \frac{AR^2 + B_1 - \overline{X_1}R^2}{z} - \beta\frac{R^2}{z}\overline{\Phi_I'}\left(\frac{R^2}{z}\right) + 2\beta\overline{\Phi_I}\left(\frac{R^2}{z}\right) + \overline{B}\eta\frac{R^4}{z^3} + \frac{2(\varepsilon_2 + i\varepsilon_3)}{\left[\frac{\kappa_M}{\mu_M} + \frac{1}{\mu_I}\right]}\left(\frac{R^4}{z^3}\right) - (A + \beta\overline{X_1})\left(\frac{R^2}{z}\right) + \overline{\Phi_I}\left(\frac{R^2}{z}\right) + C_1, \quad z \in D_M. \tag{E8}$$

However, in order to solve for $\Psi_I(z)$, an expression for $\overline{\Phi_M}\left(\frac{R^2}{z}\right)$ is required. Therefore, multiplying (5.4) by $4\frac{R}{z}$ yields

$$\overline{\Phi_M}\left(\frac{R^2}{z}\right) + \beta\left(\frac{R}{z}\right)^2\Phi_I(z) + \frac{1}{z}\left[\frac{Bz^2 + AR^2 + B_1 - \overline{X_1}R^2 + C_2z}{\mu_I\left(\frac{\kappa_M}{\mu_M} + \frac{1}{\mu_I}\right)}\right] - \frac{1}{z}AR^2$$

$$-\beta\overline{X_1}\left(\frac{R^2}{z}\right) - \frac{1}{z}\left[\frac{Bz^2 + AR^2 + B_1 - \overline{X_1}R^2 + C_1z}{\mu_M\left(\frac{\kappa_M}{\mu_M} + \frac{1}{\mu_I}\right)}\right] + \left(A + \frac{B_1}{R^2} - X_1\right)\eta\left(\frac{R^2}{z}\right)$$

$$-\frac{2(\varepsilon_2 - i\varepsilon_3)}{\left[\frac{\kappa_M}{\mu_M} + \frac{1}{\mu_I}\right]}z = 0, \quad z \in D_I,$$

and solving for $\overline{\Phi_M}\left(\frac{R^2}{z}\right)$ gives

$$\overline{\Phi_M}\left(\frac{R^2}{z}\right) = B\eta z + \left[A + \frac{B_1}{R^2} - \overline{X_1}\right]\eta\left(\frac{R^2}{z}\right) + \left[\frac{\frac{C_1}{\mu_M} - \frac{C_2}{\mu_I}}{\frac{\kappa_M}{\mu_M} + \frac{1}{\mu_I}}\right] + \left(A + \beta\overline{X_1}\right)\left(\frac{R^2}{z}\right)$$
$$+ \frac{2(\varepsilon_2 - i\varepsilon_3)}{\left[\frac{\kappa_M}{\mu_M} + \frac{1}{\mu_I}\right]} z - \left(A + \frac{B_1}{R^2} - X_1\right)\eta\left(\frac{R^2}{z}\right) - \beta\left(\frac{R}{z}\right)^2 \Phi_I(z), \quad z \in D_I. \quad \text{(E9)}$$

Substituting (E9) into $(2.10)_2$ yields the expression for Ψ_I as

$$\Psi_I(z) = (1+\eta)\,Bz + (1+\eta)\left[A + \frac{B_1}{R^2} - \overline{X_1}\right]\left(\frac{R^2}{z}\right) + \left[\frac{\frac{C_1}{\mu_M} - \frac{C_2}{\mu_I}}{\frac{\kappa_M}{\mu_M} + \frac{1}{\mu_I}}\right] +$$
$$\left(A + \beta\overline{X_1}\right)\left(\frac{R^2}{z}\right) + \frac{2(\varepsilon_2 - i\varepsilon_3)}{\left[\frac{\kappa_M}{\mu_M} + \frac{1}{\mu_I}\right]} z - \left(A + \frac{B_1}{R^2} - X_1\right)\eta\left(\frac{R^2}{z}\right) - \frac{R^2}{z}\Phi_I'(z)$$
$$-\beta\left(\frac{R}{z}\right)^2 \Phi_I(z) + C_2, \quad z \in D_I. \quad \text{(E10)}$$

Substituting (E2), (E7), (E8) and (E10) into (E6) and noting that on the inclusion - matrix boundary $z\bar{z} = R^2$ and $z = \mathrm{Re}^{i\theta}$ the jump in the displacement vector takes the form

$$\|u_r - iu_\theta\| = \frac{z}{2R\mu_M}\left\{ Bz\left(\kappa_M\eta - 1\right) + \kappa_M\left(A + \beta X_1\right)\frac{R^2}{z} + \frac{2\kappa_M\left(\varepsilon_2 - i\varepsilon_3\right)}{\left[\dfrac{\kappa_M}{\mu_M} + \dfrac{1}{\mu_I}\right]}z - \right.$$

$$\left. \kappa_M\beta\left(\frac{R}{z}\right)^2\Phi_I(z) + \kappa_M\left[\frac{\dfrac{C_1}{\mu_M} - \dfrac{C_2}{\mu_I}}{\dfrac{\kappa_M}{\mu_M} + \dfrac{1}{\mu_I}}\right] - \left(A + \frac{B_1}{R^2} - \overline{X_1}\right)\left(\frac{R^2}{z}\right) - \overline{\Phi_I}\left(\frac{R^2}{z}\right) - C_1\right\}$$

$$-\frac{z}{2R\mu_I}\left\{\kappa_I\overline{\Phi_I}\left(\frac{R^2}{z}\right) - Bz\left(\eta + 1\right) - \left(1 + \eta\right)\left[A + \frac{B_1}{R^2} - \overline{X_1}\right]\left(\frac{R^2}{z}\right) - \right.$$

$$\left(A + \beta\overline{X_1}\right)\left(\frac{R^2}{z}\right) - \left[\frac{\dfrac{C_1}{\mu_M} - \dfrac{C_2}{\mu_I}}{\dfrac{\kappa_M}{\mu_M} + \dfrac{1}{\mu_I}}\right] - \frac{2\left(\varepsilon_2 - i\varepsilon_3\right)}{\left[\dfrac{\kappa_M}{\mu_M} + \dfrac{1}{\mu_I}\right]}z + \left(A + \frac{B_1}{R^2} - X_1\right)\eta\left(\frac{R^2}{z}\right) +$$

$$\left.\beta\left(\frac{R}{z}\right)^2\Phi_I(z) - C_2\right\}, \quad z \in \Gamma. \tag{E11}$$

Therefore, substituting the normal traction component (E5), the jump in the displacement vector (E11) and the stress-free displacement component (5.8) into condition (5.7), and using the first compatibility condition (5.6) yields

$$\left(\frac{1+\beta}{2}\right)\overline{\Phi_I}'\left(\frac{R^2}{z}\right)-\beta\frac{z}{R^2}\overline{\Phi}\left(\frac{R^2}{z}\right)-\frac{\overline{B}R^2}{2z^2}(1+\eta)-\frac{z^2(\varepsilon_2-i\varepsilon_3)}{R^2\left(\frac{\kappa_M}{\mu_M}+\frac{1}{\mu_I}\right)}+\frac{1}{2}\left(A+\beta\overline{X_1}\right)$$

$$+\frac{1}{2}(A+\beta X_1)+\left(\frac{1+\beta}{2}\right)\Phi_I'(z)-\frac{\beta}{z}\Phi_I(z)-\frac{Bz^2}{2R^2}(1+\eta)-\frac{R^2(\varepsilon_2+i\varepsilon_3)}{z^2\left(\frac{\kappa_M}{\mu_M}+\frac{1}{\mu_I}\right)}$$

$$+\frac{1}{2}\left(A+\frac{B_1}{R^2}-\overline{X_1}\right)=\frac{m(\theta)R}{2}\left(\frac{\kappa_M}{\mu_M}+\frac{1}{\mu_I}\right)\left\{-\frac{\beta}{z}\Phi_I(z)-\beta\frac{z}{R^2}\overline{\Phi_I}\left(\frac{R^2}{z}\right)+\right.$$

$$\frac{1}{2}\left(A+\beta\overline{X_1}\right)+\frac{1}{2}(A+\beta X_1)-\frac{\eta}{2}\left(A+\frac{B_1}{R^2}-X_1\right)-$$

$$\left.\frac{\eta}{2}\left(A+\frac{B_1}{R^2}-\overline{X_1}\right)-\frac{2\varepsilon_1}{\left(\frac{\kappa_M}{\mu_M}+\frac{1}{\mu_I}\right)}\right\},\quad z\in\Gamma. \tag{E12}$$

Hence, condition (E12) shows the normal displacement interface condition given in terms of the stress potential $\Phi_I(z)$. This completes the proof of equation (5.9).